

UV/Vis and CD Spectral Studies of the
Interaction between Pinacyanol Chloride and
Alginates, γ -Cyclodextrin, and Aerosol-OT

Der Fakultät für Naturwissenschaften
der Universität Duisburg-Essen
(Standort Duisburg)

zur Erlangung des akademischen Grades eines
Doktors der Naturwissenschaften

genehmigte Dissertation von

Sa'ib Al-khouri

aus

Irbid, Jordanien

Tag der mündlichen Prüfung: 10.04.2003

Die vorliegende Arbeit entstand in der Zeit vom 1. September 1999 bis 20. Januar 2003 in der Fakultät für Naturwissenschaften an der Gerhard-Mercator-Universität – Gesamthochschule Duisburg (Deutschland) unter Betreuung von Herrn Prof. Volker Buß.

Referent: Prof. Dr. V. Buß

Korreferent: Prof. em. Dr. D. Döpp

ACKNOWLEDGEMENT

It is my great pleasure to thank my supervisor Prof. Dr. V. Buss for giving me the chance to work in this topic, the full supervision, the fruitful guidance, and for the continual support through this work.

I wish to express my gratitude to Prof. em. Dr. D. Döpp for writing the 2nd referee's report.

I would also like to express my sincere gratitude to all my colleagues in the department of theoretical chemistry, who have contributed their time, helpful discussion and friendly atmosphere to the successful completion of the work and preparation of my thesis: Julia Hufen, Robert Knierim, Dr. Klaus Kolster, Dr. Guido Nuding, Daniel Richter, Nicole Richter, Marko Schreiber, Oliver Weingart, and Dr. Edgar Zimmermann.

I thank Natascha Schürks in the research group of Prof. Dr. C. Mayer for her kind help and the purified alginate samples. I thank also Wassef Sekhaneh in the research group of Prof. Dr. W. Veeman for his encouragement and kind help when it was needed.

My thanks also go to all members of the group of researchers (physical chemistry of bio-film) for the useful discussions, which took place in the context of the meetings of group of researchers supervised by Prof. Dr. H.-C. Flemming.

I thank the catholic academic foreign-service (KAAD) and German research council (DFG) in Bonn for their support of this work.

To father, sisters, and brothers my sincere gratitude and appreciation for their support and encouragement over the years of my study.

My special thanks and appreciation to my wife and my children for their encouragement and patience to complete this work during our stay in Germany.

To the loving memory of my mother

Contents

1 Preface	1
2 Introduction	
2.1 Cyanine dyes.....	4
2.1.1 Structure and classification.....	4
2.1.2 Molecular aggregation of cyanine dyes.....	6
2.1.3 Pinacyanol chloride.....	10
2.2 Polysaccharides.....	12
2.2.1 Classifications.....	12
2.2.2 Structure.....	13
2.2.3 Alginates.....	15
2.2.3.1 History, nomenclature, properties and applications	16
2.2.3.2 Molecular structure and conformations.....	18
2.2.3.3 Calcium alginate and the “egg-box model”	19
2.2.3.4 Alginates and circular dichroism.....	22
2.2.3.5 Induced Circular Dichroism in Alginate-Dye Systems.....	23
2.2.4 Cyclodextrins.....	25
2.2.4.1 Discovery and Nomenclature.....	25
2.2.4.2 Structural Features.....	26
2.2.4.3 Solubility in Polar solvents.....	27
2.2.4.4 Cyclodextrin inclusion complexes.....	27
2.2.4.4.1 Stoichiometric ratios and driving force.....	28
2.2.4.4.2 Methods of detecting the inclusion process.....	28
2.2.4.5 Practical use of cyclodextrins.....	29
2.2.4.6 Cyclodextrin derivatives.....	30
2.2.4.7 Cyclodextrins and induced circular dichroism.....	30
2.2.4.8 Cyanine dye complexes.....	31
2.3 Surfactants.....	32
2.3.1 Properties and classification.....	32
2.3.2 Aggregation of surfactants.....	34
2.3.2.1 Formation of micelles.....	35
2.3.2.2 The critical micellar concentration (cmc).....	37
2.3.3 Surfactant – dye interactions.....	39

3 Theoretical background

3.1 UV/Vis spectrophotometry.....	41
3.2 Circular dichroism spectroscopy.....	44
3.2.1 Principle of the measurement.....	44
3.2.2 The rotational strength.....	47
3.2.3 Induced circular dichroism.....	48
3.2.4 Exciton coupling and exciton chirality.....	49
3.2.5 Coupled oscillator model for the calculation of spectral properties of exciton-split chromophores.....	52

4 Results and discussion

4.1 Pinacyanol chloride solutions.....	55
4.1.1 Pinacyanol chloride in aqueous solution with 7.5% v/v ethanol.....	55
4.1.2 Pinacyanol chloride spectra in ethanol.....	57
4.1.3 Pinacyanol chloride spectra with different concentrations of ethanol	58
4.1.4 Derivative spectra.....	59
4.1.5 Peak height measurements.....	62
4.1.6 Analysis of the spectra using PeakFit.....	62
4.1.7 Thermodynamic considerations.....	67
4.1.8 Discussion.....	70
4.2 The inclusion of pinacyanol chloride by cyclodextrins.....	73
4.2.1 Interaction with γ -cyclodextrin - UV/Vis spectra.....	73
4.2.1.1 The fourth derivative of the visible spectra.....	74
4.2.2 Interaction with γ -cyclodextrin - Circular dichroism spectra.....	75
4.2.3 The dipole strength of pinacyanol chloride.....	77
4.2.4 Modelling the pinacyanol aggregation with OSCI	78
4.2.5 Calculating the twist angle of pinacyanol chloride in γ -cyclodextrin.....	80
4.2.6 Discussion.....	81
4.3 Interaction of pinacyanol chloride with alginates.....	83
4.3.1 Manuacol-LHF; characterization by CD	83
4.3.2 Aggregation of pinacyanol chloride with Manuacol-LHF.....	83
4.3.2.1 UV/Vis and CD spectra.....	83
4.3.2.2 Job's Method for determination of stoichiometry.....	85
4.3.2.3 Conductometric titration.....	87

4.3.2.4 Effect of ethanol on the spectra.....	88
4.3.2.5 Temperature effect on the spectra.....	90
4.3.2.6 Effect of pH on the spectra.....	91
4.3.2.7 Effect of divalent cations on the spectra.....	92
4.3.3 Mannuronate rich alginate; characterization by CD.....	94
4.3.4 Aggregation of pinacyanol chloride with mannuronate rich alginate.....	94
4.3.5 Guluronate rich alginate; characterization by CD.....	95
4.3.6 Aggregation of pinacyanol chloride with guluronate rich alginate.....	96
4.3.7 SG81- alginate; characterization by CD.....	96
4.3.8 Aggregation of pinacyanol chloride with SG81- Alginate.....	97
4.3.9 Discussion.....	98
4.4 Complex formation of Pinacyanol chloride with Aerosol-OT.....	101
4.4.1 UV/Vis and CD spectra in aqueous solutions.....	101
4.4.2 Effect of ethanol on the surfactant spectra.....	103
4.4.3 Temperature effect.....	104
4.4.4 Discussion.....	105
5 Summary / Zusammenfassung	
5.1 Summary.....	107
5.2 Zusammenfassung.	109
6 Experimental	
6.1 Materials and solvents used.....	111
6.2 Instruments used.....	111
6.3 Glassware, tool and methods.....	112
7 References.....	113

1 Preface

CD spectroscopy is a modified form of absorbance spectrophotometry, in which the difference in absorbance between left and right circular polarized beams of light that pass through a sample is measured as a function of wavelength. For the method to be applicable, the sample has to be optically active, *i.e.* it has to contain elements of chirality, and this distinguishes CD from absorbance. However, even an optically active medium can be CD “silent”, if there is no absorbance in the spectrally accessible wavelength range.

Almost all biological macromolecules are chiral, and many are CD active, which widens the range of application in the study of natural products. Proteins, polynucleotides, and carbohydrates are intrinsically CD active; however, the chromophores absorb in the UV and some (carbohydrates in particular) absorb only in the far UV. In spite of the extreme difficulties that are inherent in measuring CD in that spectral range, a number of studies have been published in which CD data have been used to interpret the secondary and tertiary structures of these macromolecules in aqueous solution. The chirality inherent in these large molecules has been exploited in experiments where activity was induced into CD inactive molecules by either substitution or by molecular complexation. For carbohydrates, for example, CD spectra that originate from exciton coupling between absorbing aromatic substituents have been used to interpret the anomeric forms of linkages and the local stereochemistry between neighboring diols in monomeric repeat units. Molecular association reactions are most familiar, and especially those involving small molecules (“guests”) which fit into the chiral interior of cyclodextrin oligomers (“hosts”).

The interaction of biopolymers with dyes has been investigated by many researchers from the viewpoints of physiology, biochemistry, and physical chemistry. These investigations have been made mainly using spectroscopic techniques, since the interaction can be studied in detail even when the dye concentration is very low. The electronic spectra of biopolymer-dye systems often differ from those of free dyes in a number of ways. In the biopolymer-dye systems, the dyes may lose absorption intensity (hypochromism), change the absorption maxima (metachromasy), display new bands, and under certain conditions become optically active. The last property is the most significant, and derives from the fact that biopolymers are in general chiral. A symmetric chromophore having a plane or center of symmetry becomes optically active when placed in the asymmetric field of another chiral molecule. This effect is known as induced optical activity or induced circular dichroism (ICD). The advantage of studying the binding of achiral dye molecules to a chiral substrate is that the extrinsic CD

activity is observed in the experimentally convenient and readily accessible visible spectral range. The conformational rearrangement of the dye, as it adapts to the chiral field imposed upon it by association with the biopolymer molecule, will generate an extrinsic CD spectrum that will reveal information about the structure of the host/guest complex in solution. Putting it in another way, structural information about the host can be obtained without needing to solve the experimental problems that are associated with making CD measurements in the far-UV.

Polysaccharides can have various types of conformation in solution. Conformational and anomeric changes are often connected with physiological activities. So far, only the optical rotatory dispersion (ORD) of polysaccharides could be measured in general, and CD studies were possible in those cases where other chromophores were present in their molecules. Alternatively, the ICD of dyes bound to the saccharides through ionic coupling or hydrophobic interaction has been measured for analyzing conformational changes in solution but with many problems remaining.

The literature concerning the CD of saccharides has been less documented than those of proteins and nucleic acids, because of the difficulty of measuring CD in the vacuum UV. The ICD of dyes bound to saccharides through ionic coupling or hydrophobic interaction may remain a conflicting problem due to the non-covalent bonding between the dye and the saccharide. Also, there may be a general lack of detailed information about the dye itself with respect to self aggregation as a function of concentration, solvent and temperature. In the present work, the interaction of pinacyanol chloride with algae and bacterial alginates (natural anionic copolymers polysaccharide), with cyclodextrins and with surfactants is reported. Special emphasis is placed on the process of self aggregation of pinacyanol chloride by studying its behaviour in aqueous solution using special methods (like derivative spectroscopy) and programs to analyze the results. The knowledge about the dye probe itself (its transition dipole length and the type of aggregation) helps to explain the spectral results of the ICD measurements after complexation with alginate, cyclodextrin or surfactant.

The main objective of this work is to show how induced circular dichroism (ICD) measurements can lead to stereochemical information about complexes involving biological macromolecules. The study of modified alginates complexes with dyes using visible absorption and CD spectroscopy has stimulated our interest to examine the types of conformational structures of alginates in solutions under different experimental conditions in view of important recent applications.

The organization of this work is as follows. The introduction into the chemistry of the main components making up the complexes will be followed by a theoretical section providing the background of the spectroscopic methods used in this study. The central part is the presentation and discussion of the experimental results and the theoretical models derived for the different complexes. There will be an english and a german summary, an experimental part and a list of references.

2. Introduction

2.1 Cyanine dyes

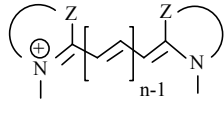
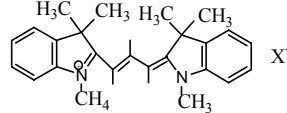
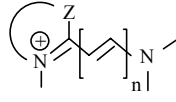
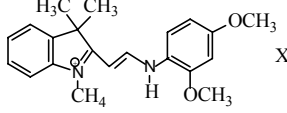
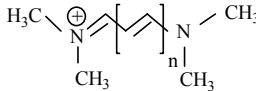
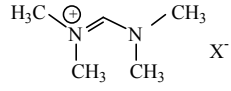
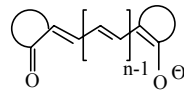
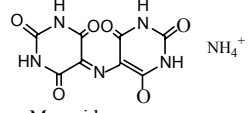
Cyanine dyes were added as a new class of dyes to the supply of commercial dyestuffs with the synthesis of the first polymethine dye (“cyanine”) by C. Williams in 1856.¹ Cyanine dyes are characterized by their intense and sharp absorption bands in the UV-visible region, usually between 225 and 735 nm, with narrow half-band widths of typically ~ 25 nm. Cyanine dyes did not become commercial dyes for coloration purposes immediately after their discovery, since they are prone to decolorization by light and acid. One of the most important applications of cyanine dyes is their use as spectral sensitizers for silver halide micro-crystals in photographic films, since their absorption spectra are easily shifted by chemical substitution and by aggregation.^{2, 3} Cyanine dyes have been used extensively to probe biological systems, such as the helical structure of DNA, through the measurement of induced circular dichroism (ICD) spectra.⁴ The chiral environment of anionic polysaccharides and cyclodextrins has been investigated through measurement of induced CD spectra with different types of cyanine dyes.^{5, 6}

2.1.1 Structure and classification

Cyanine dyes are cationic dyes typically consisting of two nitrogen containing heterocyclic ring systems, which terminate a chain of conjugated double bonds. One of the nitrogen atoms is positively charged and is linked by the chain consisting of an odd number of carbon atoms to the other nitrogen. The absorption of visible light in a cyanine dye is mainly determined by the sequence of methine groups (- CH =), which are normally in the *E* or *trans* configuration. The carbon atoms of the methine chain can be substituted by hetero atoms (“azacyanines”), and they can carry other groups than hydrogen; they can also be parts of carbocyclic or heterocyclic ring systems.¹

Extensive conjugation of the methine chain leads to the long wavelength absorption maxima and large molar absorptivities typical for cyanine dyes. Bond lengths, which can be determined by x-ray analysis, indicate that the positive charge on the nitrogen atom is significantly delocalised along the chain extending to the opposite heterocycle, which can result in the case of symmetrically substituted cyanine dyes in a structure in which the two end groups carry the same amount of (half a) positive charge.⁷ Though the preferred

Table 2.1. Classification of polymethine dyes. ¹

Group name	General formula	Example
Cyanine		 Astraphloxine FF
Hemicyanine		 Maxilon Yellow 5G
Streptocyanine		 Amidinium salt
Oxonol		 Murexide

2.1.2 Molecular aggregation of cyanine dyes

Cyanine dyes have a natural tendency to aggregate spontaneously in solution when their concentration is increased or the temperature is lowered. Aggregation is promoted in the presence of polyelectrolytes, such as polyphosphates, or biological macromolecules, which influence or even control the formation of dye aggregates, generally by non-bonding reversible interactions. Various mechanisms have been suggested to explain the forces holding dye molecules together in solution; these include intermolecular van der Waals-like attractive forces between the molecules, ¹⁴ hydrogen bonding with the solvent, ¹⁵ or coordination with metal ions. ^{14, 15} The aggregation behaviour of cyanine dyes has been extensively investigated by studying the photophysical and photochemical properties of these aggregates, which result from the strong dispersion forces associated with the high polarizability of the chromophoric chains. When dye molecules aggregate the absorption spectra are distinctly different compared to the monomeric species; also, the Lambert-Beer law is no longer obeyed. From the spectral shifts caused by aggregation, various aggregation types of dyes have been proposed. H-type aggregates are formed when the dye molecules arrange themselves face-to-face in a near vertical stack. For those aggregates the allowed absorption band is observed at higher energy than the monomer absorption band. The shift of this band depends on the

number of monomers in the aggregate, increasing and approaching a limiting value for the infinite aggregate (“H-band”).¹⁶ J-aggregates are formed when the dye molecules arrange into a slanted stack, and the observed absorption maximum shifts to longer wavelength (lower energy), with broad bands in general, but narrow, intense excitonic absorption bands are also possible.¹⁷

The commercially most important cyanine dyes, which are used for spectral sensitization in photographic emulsions aggregate on silver halide micro-crystals with red-shifted absorption spectra indicating J-aggregation.^{18, 19} The relationship between the relative orientation of chromophores and the spectral shifts of a dye aggregate has been explained in terms of molecular exciton theory.²⁰⁻²² According to this theory, the dye molecules are treated as point dipoles. Interaction of the transition dipoles splits the excited state of the dye aggregate into levels according to the number of monomers in the aggregate. For a dimer aggregate, two levels result (Figure 2.2) with energies and intensities according to the geometry-dependent interaction term.²³

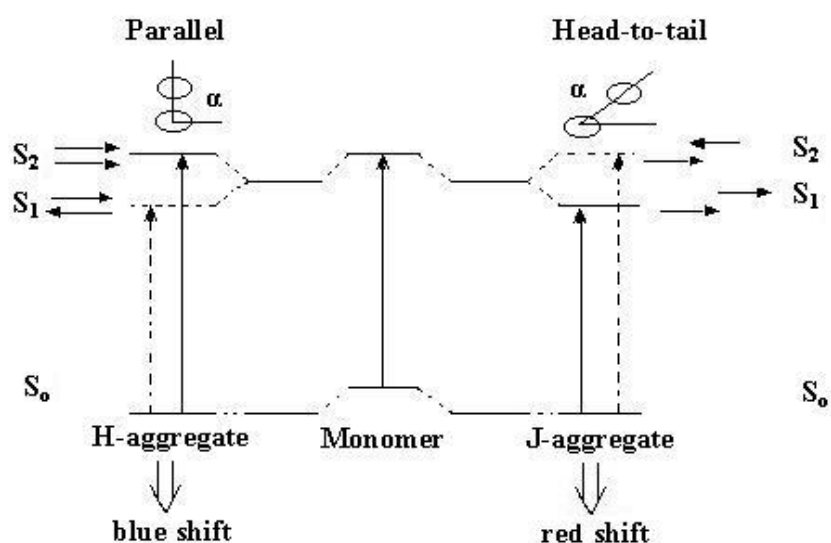


Fig. 2.2. Schematic diagram of the relationship between the chromophore arrangements and spectral shifts based on molecular exciton theory (adopted from ref. 23).

The angle between the line of centers of a column of dye molecules and the long axis of any one of the parallel molecules (Figure 2.2) is called the “angle of slippage”, α . Large molecular slippage (*i.e.* $\alpha > \sim 32^\circ$) results in a bathochromic shift (J-aggregate), while small slippage ($\alpha < \sim 32^\circ$) results in a hypochromic shift (H-aggregate).²⁴ The exciton model is

probably unsuitable for prediction of orbital energy levels of a dye aggregate, since it is valid only when the interaction between orbitals of constituent molecules is negligible.²⁵ Extensive studies on J- and H-aggregates lead to the proposal that these aggregates exist as a one-dimensional assembly in solution that could be in a brickwork-, ladder-, or staircase-type of arrangement (Figure 2.3).²⁴



Fig. 2.3 Schematic representation of one-dimensional cyanine dye aggregates on a solid surface or in solution.²⁴

There are several factors affecting the tendency of a dye to aggregate, namely the structure of the dye, but also the environment, such as the polarity of solvent and the pH, the presence of electrolytes (ionic strength) and the temperature. Cyanine dyes have a high tendency to aggregate, while merocyanine and oxonol dyes generally do not. Due to its high dielectric constant water reduces the repulsive forces between the charged dye molecules, Also, the disruption of the regular hydrogen-bonded water structure by the dye molecules tends to favor larger aggregates instead of monomers, these make water to be the most favorable solvent for dye aggregation. The addition of inorganic salts increases the dielectric constant of a solvent and facilitates aggregation. Organic solvents like alcohols reduce the dielectric constant and inhibit aggregation. In most solvents, reducing the temperature favors aggregation.^{16, 25}

The definitive dye aggregate structures have never been determined directly at the molecular level and remain the subject of much speculation and controversy.²⁵ Many different, often conflicting solution aggregate models have been proposed largely on the basis of indirect evidence. This includes, for example, theoretical approximations of aggregate wavelength shifts in response to intermolecular orientations,²⁰ electron microscopy of H-aggregates formed in solution²⁶ in addition to IR and NMR spectroscopy and measurements of dielectric polarization.

Marchetti *et al.*²⁷ have observed deviations from the Lambert-Beer law accompanied by distinct spectral shifts relative to the monomer or M-band for 1,1'-diethyl-2,2'-cyanine

chloride. They attributed this to the formation of dye dimers, oligomers, and n-mers (Figure 2.4). A blue shifted band with loss of intensity was termed a D-band and ascribed to dimeric species. The third band or shoulder on the high-energy side of the D-band with a loss of intensity corresponds to the H-band. ¹⁶ M-, D-, and H-bands are quite common in all classes of dyes, while red-shifted J-bands are observed only for photographic cyanine dyes.

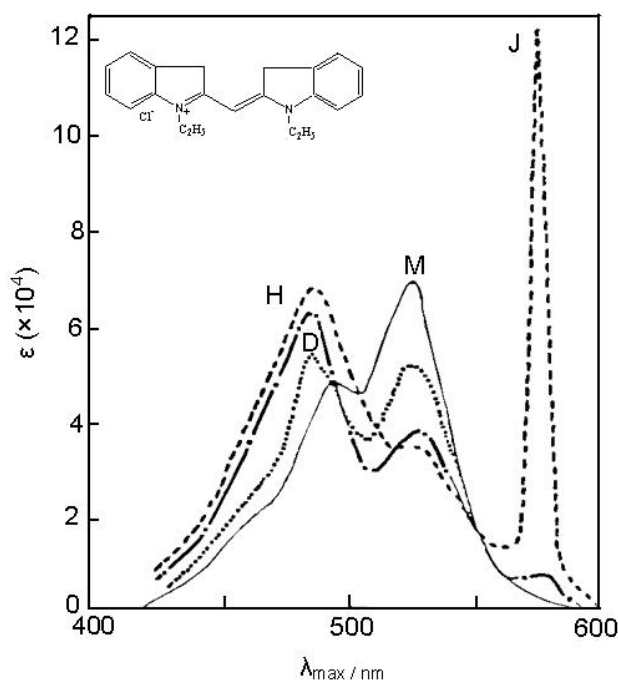


Fig. 2.4. The different shapes of visible absorption spectra of 1,1'-diethyl-2,2'-cyanine chloride solutions at room temperature. M, D, H, and J correspond respectively to monomer, dimer, H-aggregate and J-aggregate forms of the dye. (adopted from ref. 19, there is no mention in the reference about concentration values).

With the sensitivity of aggregation to external factors, and the ease with which quantitative UV/Vis-spectroscopy is performed, cyanine and merocyanine dyes present perfect probes for studying various microenvironments. ³⁰ Cyanine dyes have been used extensively as sensors for the examination of polypeptide β -sheet structures in solution and in thin films. ²⁸ Several near-infrared absorbing carbocyanine dyes containing different functional groups have been employed as fluorescent probes for the study of DNA, lipids, peptides, and proteins. ²⁹ To study the interaction between membranes and surfactants, probes such as cyanine dyes are used for exploiting the application of detergents in biotechnology, such as to activate, extract, and purify intrinsic enzymes.

2.1.3 Pinacyanol chloride

Pinacyanol chloride (1,1'-diethyl-2,2'-carbocyanine chloride, Figure 2.5) is a symmetric trimethinecyanine dye, a class of dyes, which are important sensitizers in photography. Pinacyanol has been used to determine spectrophotometrically the critical micellar concentration (cmc) of surfactants.^{31, 32} Because of its solvatochromic behavior, it can be used as an indicator of solvent polarity.³³ The dye is of particular interest in heterogeneous media due to its ability to form H- and J- type aggregates.³⁴

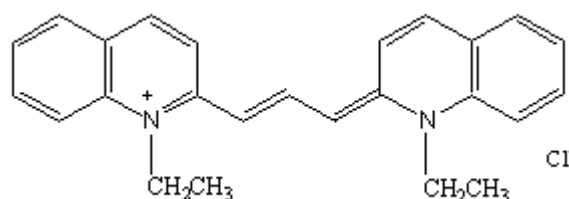


Fig. 2.5. Pinacyanol chloride, 1,1'-diethyl-2,2'-carbocyanine chloride.

Different theoretical methods have been applied to explain the spectral characteristics of pinacyanol chloride. Kuhn³⁵ has modified his famous particle-in-a-box model for the π -electrons in the dye in order to deal with the two nitrogen atoms, which represent a substantial disruption of the conjugated π -system. He proposed that these atoms can be treated as the terminating walls of the box. Then the absorption wavelength depends on the number of bonds between the nitrogen atoms. There are six such bonds in pinacyanol and eight π -electrons (six from the polymethine chain and two from the neutral nitrogen atom). With this information, the absorption wavelength of pinacyanol can be calculated from the length of the carbon chain between the two nitrogen atoms. In accordance with the particle-in-the-box model Kuhn treated the 8 π -electrons of the molecule as standing waves whose wavelengths was adjusted such that the walls of the box coincided with nodes and the condition for standing waves was satisfied.

In the more popular molecular orbital treatment the π -orbitals of the polymethine chain of pinacyanol are formed from the side-by-side overlap of atomic π -orbitals (Figure 2.6). With increasing energies these orbitals have an increasing number of nodes. Typical for these odd-numbered π -electron systems is the central non-bonding molecular orbital in which there is a node at every other carbon atom. There are even more nodes in the anti-bonding MO's. Applying the Pauli-principle, the 8 π -electrons of the polymethine chain are distributed

pairwise into the four energy-lowest π -orbitals, which makes the non-bonding orbital the highest occupied molecular orbital or HOMO in the electronic ground state.

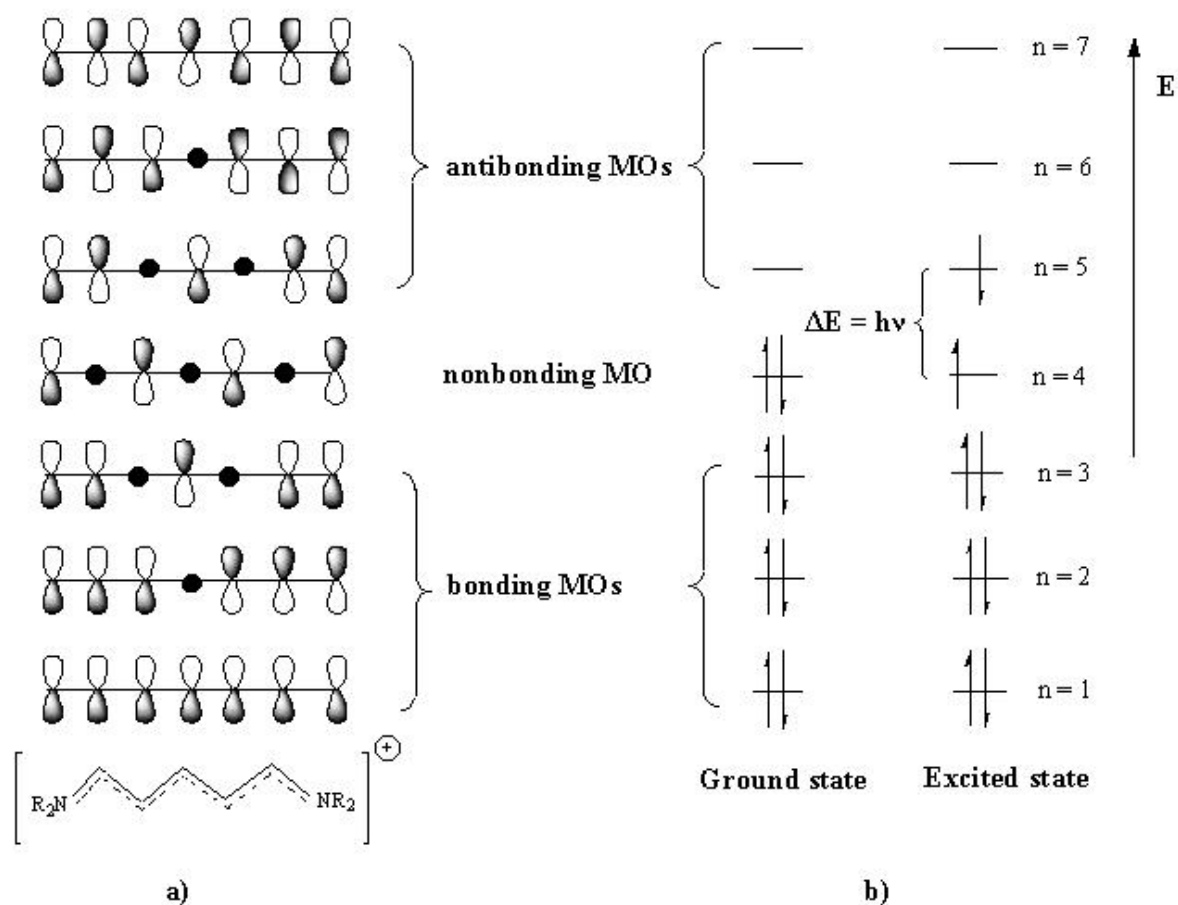


Fig. 2.6. a) Schematic representation of the molecular orbitals (MO's) of the polymethine chain of pinacyanol as linear combination of atomic orbitals. b) Qualitative MO diagram of pinacyanol with electron occupation of the ground and first excited state.

Absorption of light quanta of appropriate energy promotes an electron from the highest occupied to the lowest unoccupied molecular orbital (LUMO). This electronic excitation corresponds at the same time to the most intense and longest wavelength absorption. Excitations from lower occupied into higher empty energy levels involve more energy and thus will occur at shorter wavelengths, usually in the ultraviolet region of the electromagnetic spectrum. These energies and intensities can be interpreted in terms of three different theoretical models of increasing sophistication *viz.* the particle-in-a-box model, semi-empirical molecular orbital theory, and *ab initio* methods.^{36,37}

2.2 Polysaccharides

Polysaccharides are natural macromolecules occurring in all living organisms. They constitute the largest and structurally the most diversified groups of natural compounds with use either as an energy source (starches and glycogens in plants and animals, respectively), or as structural units in the morphology of living material (cellulose and chitin in plants and in the shells of insects, crabs etc., respectively).^{38, 39}

2.2.1 Classifications

Polysaccharides are classified on the basis of their main monosaccharide components and the sequences and linkages between them, as well as the anomeric configuration of linkages, the ring size (pyranose or furanose), the absolute configuration of asymmetric centers (D or L) and any other substituents present. The most stable geometry of a polysaccharide will be the one which satisfies both the intra- and intermolecular minimum energy criterion.⁴⁰ Figure 2.7 shows the atom numbering of two monosaccharides units (a pyranose and a furanose), in which the notation used confirms with that for specifying polynucleotide conformation.⁴¹ Figure 2.8 shows some sugar units that are constituents of some common polysaccharides. Only few of these monosaccharides play a role in context of this study.

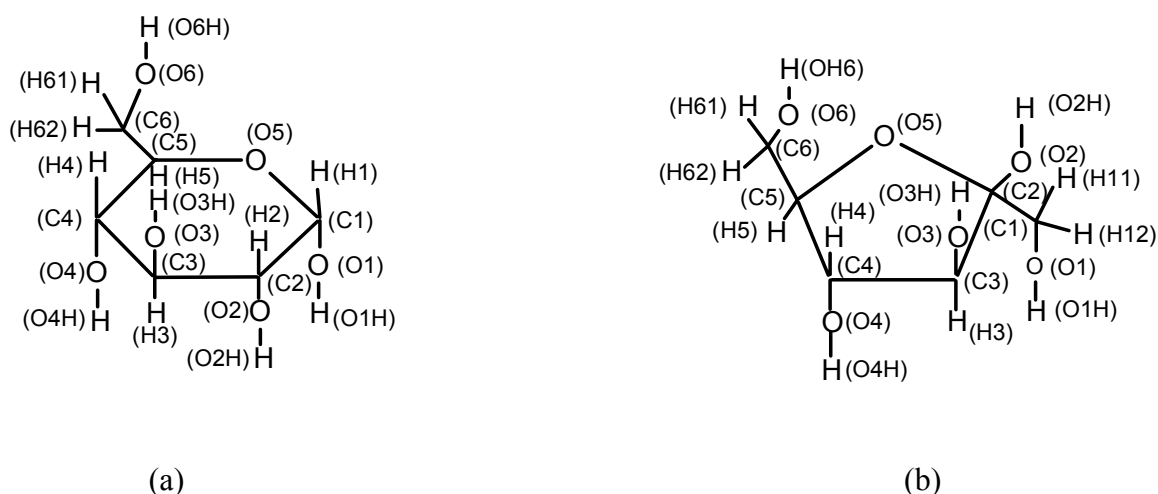


Fig. 2.7. Atomic numbering of a hexapyranose (a) and a hexafuranose (b).

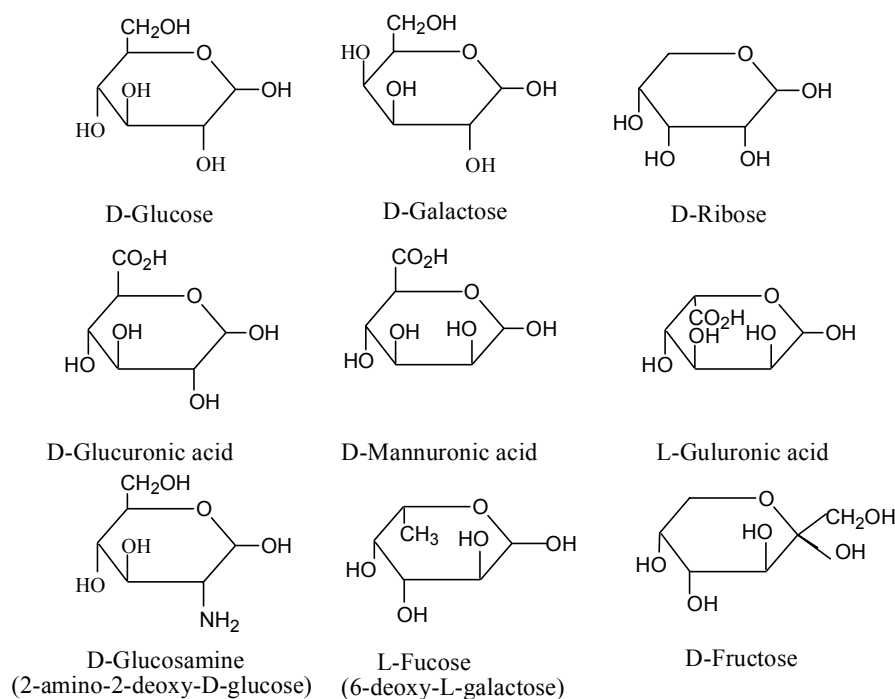


Fig. 2.8. Some monosaccharides, which are the building units of polysaccharides.

2.2.2 Structure

The geometry of the monosaccharides is not planar as suggested by the structural formula, but is derived from the chair conformation of the alicyclic cyclohexane. There are two chair conformations, which are important in polysaccharide conformational analysis. They are designated 4C_1 and 1C_4 , respectively, (Figure 2.9) to indicate the disposition of groups above and below the plane of the ring, which are energetically most favourable.³⁹

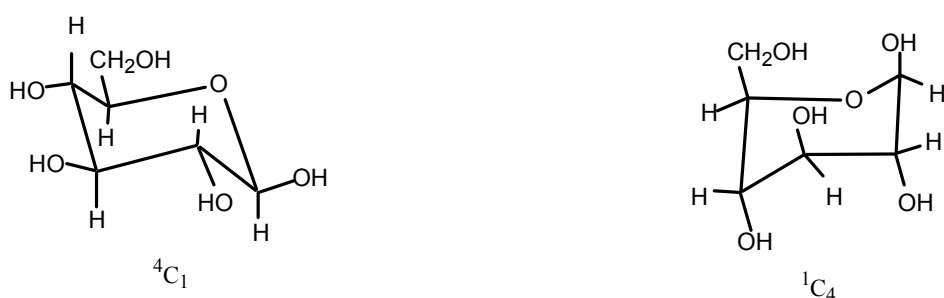


Fig. 2.9. The two pyranose ring conformations illustrated for β -D-glucose. C stands for chair conformation.

All macromolecular carbohydrates have definite three-dimensional structures, and the four aspects of these structures (primary, secondary, tertiary, and quaternary structure) have essentially the same meaning for carbohydrates as for proteins and other biopolymers.³⁸ The primary structure indicates the sequence of monosaccharide residues as a linear chain. In the secondary structure the spatial relationship between the nearest neighbour sugar rings is specified. The geometry of the sugar ring as an individual unit of a polysaccharide is essentially rigid, but the relative orientations of component residues (*i.e.* rotation about the glycosidic linkage) determines the overall conformation of the polysaccharide. Two rotational angles are required to define the glycosidic bond between two carbohydrate residues, A and B, except for (1,6) linked polysaccharides, which require three angles (Figure 2.10). ϕ is the dihedral angle between the C1-O5 and the glycosidic O-C4' bonds, while ψ is the corresponding angle between the glycosidic C1-O and the C4'-C5' bonds. Finally, ω corresponds to the dihedral angle between the glycosidic O-C6' and the C5'-O5' bonds.³⁹

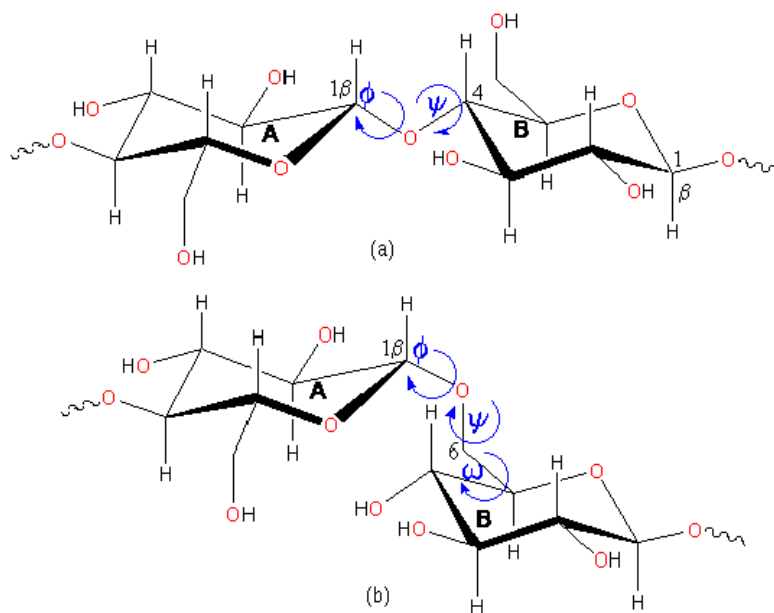


Fig. 2.10. Rotation of individual residues about the glycosidic linkage (interresidue linkage), illustrated for the glucose homopolymers in (a) pyranose and (b) furanose (adopted from ref. 40).

The tertiary structure is formed from the repeating sequences in the primary structures of polysaccharides, which lead to regular patterns in secondary structures and then to sterically regular gross conformations aided by favourable noncovalent interactions between some groups that are found in the repeating sequences like hydroxyl, amino, carboxyl, etc. groups. Irregularities in primary and secondary structures and large branched structures inhibit tertiary

structure formation. The presence of ionic species in polysaccharide solution can cause changes in the tertiary structure; for example, charged polysaccharides can form stable, tertiary structures by incorporation of counterions within the tertiary structure. Figure 2.11 shows different types of tertiary structures formed from homopolysaccharides.³⁸

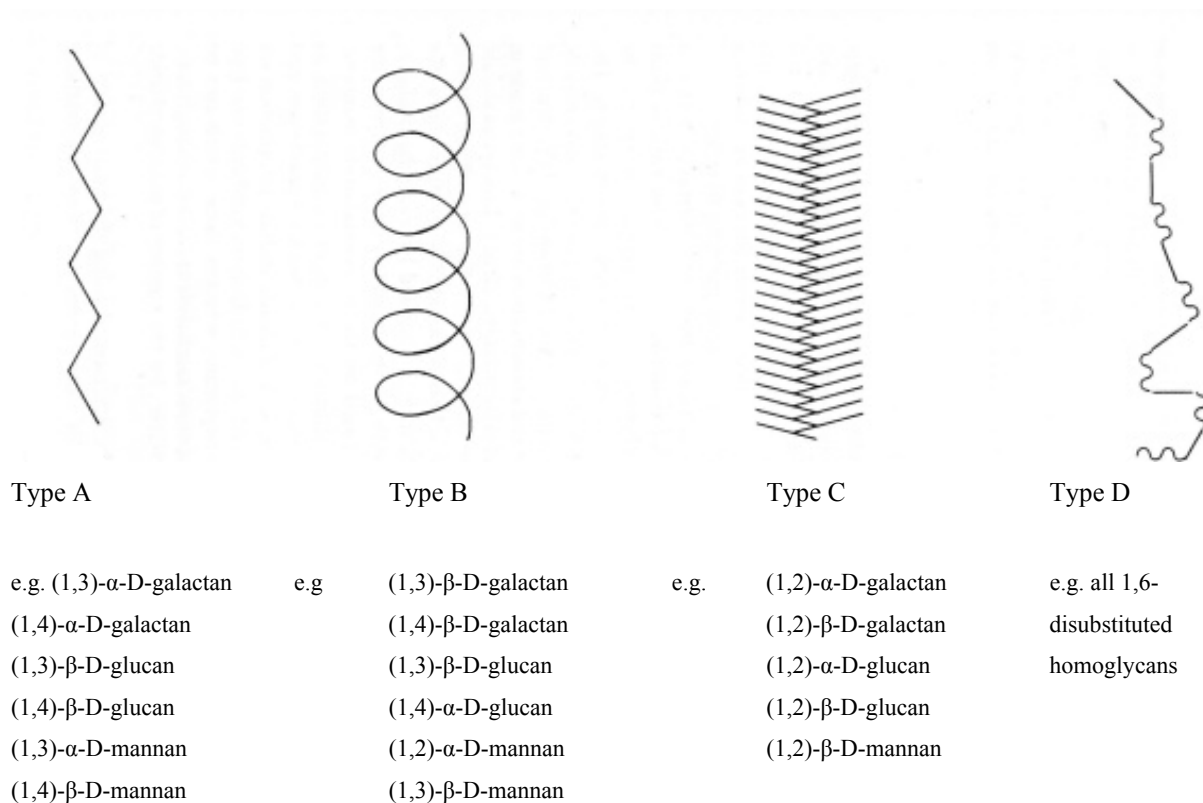


Fig. 2.11. Types of tertiary structures found in homopolysaccharides. Type A, extended ribbon; Type B, flexible helix; Type C, crumpled ribbon; Type D, flexible coil (adopted from ref. 38).

The quaternary structure in polysaccharide is the result of non-covalent aggregation of a number of polysaccharide chains. Aggregation can be between like or unlike molecules, as *e.g.* the interaction between identical chains in cellulose and the interaction between xanthan helices with the unsubstituted regions of the backbone of galactomannans.³⁸

2.2.3 Alginates

Alginates were first isolated from seaweeds over a century ago and are now one of the most well established hydrocolloids in the market. They cover a wide range of application in the food and industrial sector, a result of their two basic functions, viz. the thickening and the gelling of water. Alginates are the major structures of the cell wall of various types of brown

seaweeds (*phaeophyceae*), of which they comprise up to 40% of the total dry matter. ⁴² Called algal alginate, they give both strength and flexibility to the algal tissue and prevent desiccation of the seaweed when exposed to air, for example at low tide. ³⁸ Another source of alginate with the same basic structure as algal alginate is that produced by certain bacteria, such as *Azetobacter vinelandii*. ⁴³

Alginates contain two different monosaccharide residues, β -D-mannuronate (M for short) and α -L-guluronate blocks (G for short), linked randomly by β -1,4 and α -1,4 glycosidic bonds (Figure 2.12). The presence of carboxyl groups renders these polymers highly ionic. Sodium alginates are commercially produced alginates, used primarily for their ability to form a gel in contact with most divalent cations. This property has been widely used in the food and drink industry as well as in the pharmaceutical sector. Other alginates available contain potassium, ammonium, or calcium. ⁴⁴

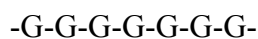


Fig. 2.12. Molecular structures of D-mannuronate and L-guluronate.

2.2.3.1 History, nomenclature, properties and applications

Alginic acid was discovered in 1883 by E. C. Stanford, a british pharmacist who called it algin. ⁴⁵ In seaweeds, algin is present as a mixed salt of sodium, potassium, calcium and magnesium, with the exact composition varying with algal species. After the discovery by Stanford, the name algin has been applied to alginic acid and all alginates, which derive from alginic acid. Production of alginates on an industrial scale began in California in the 1930s. ⁴⁵ Originally, alginates were produced for the manufacture of canned food used at sea.

Alginates are linear and may be prepared in a wide range of average molecular weights (50 to 100 000 residues), in which three distinct types of segments are present (see below): ³⁸



Each type may contain either one of the two monosaccharide residues, or approximately equal quantities of both, which may be distributed randomly or show some alternating sequence.⁴⁶

The proportion of these blocks depends on the species of seaweed, the condition of growth and the part of plant from which the alginate was derived (stalk or leaf of the seaweeds). In addition to that it has been reported that the content of L-guluronate increases as the tissue gets older and tougher.⁴⁷ The number and length of the blocks is very important as these factors determine the physical properties of alginates. These properties can be changed according to the extraction conditions from the algal species used. Examples of common algal species used to produce alginates are *Ascophyllum nodosum*, *Ecklonia maxima*, or various species of *Laminaria* and *Lessonia*.³⁸

Alginic acid is insoluble in water but swells on contact with aqueous solutions. The water-soluble forms of the product are made by neutralizing alginic acid to give the appropriate soluble salt forms, mostly the sodium and potassium salts. These monovalent salts are the varieties of algin that are most commonly used as thickeners. Multivalent ions such as calcium, lead, and chromium react more strongly with alginates in solution causing them to precipitate from solution. This phenomenon, referred to as ion exchange, is responsible for the ability of alginates to selectively remove metal ions from solutions and to form fibres, films and gels. Calcium is the most commonly used gelling agent, and it is also used to form insoluble alginate filaments and films. The gelling is thermally not reversible, and its rigidity increases with increasing ratio of L-guluronic to D-mannuronic acid.⁴⁵ The acidic solutions, which are the source of hydronium ions, if present in high concentration, behave like multivalent ions and cause alginate to precipitate.

Alginates dissolve in hot and cold water to give solutions with a wide range of unusually high apparent viscosities, even at 1% solute concentrations, due to their high molecular weight and rigid structure.³⁸ The viscosity increases logarithmically in accordance with an increase in concentration. Addition of water-miscible solvents such as alcohols, glycols, or acetone, increases viscosity and reaching a certain concentration the alginate will precipitate.³⁸

Alginates are very friendly to use and consume, because they are natural, sustainable, renewable, of vegetable and not animal origin. They are non-calorific and wholly safe by all known tests. The various alkali solutions of alginate are tasteless and almost colourless.⁴⁸ Alginates are used extensively in food products, pharmaceuticals and cosmetics and for a wide range of other industrial applications, for example in controlling viscosity in sauces and syrups, to improve pouring and handling properties in liquid detergent and shampoos, to

retard phase separation and ice crystal growth in ice-cream, or to produce a semi-solid product with good spreading properties in ointments.³⁸

2.2.3.2 Molecular structure and conformations

Alginates are linear unbranched polyelectrolyte copolymers containing β -(1,4)-linked D-mannuronate (M) and α -(1,4)-linked L-gulonate (G) residues.⁴⁹ D-mannuronate is 4C_1 with diequatorial links and L-gulonate is 1C_4 with diaxial links between the residues (Figure 2.13). Bacterial alginates are, in contrast to algal alginates, O-acetylated in some of the 2 and/or 3 positions of the D-mannuronate residues. Acetyl groups in bacterial alginate confer the resistance to enzymes and greatly reduce the ion binding capacity.⁵⁰ In sodium alginate, the sodium cations are understood to be bound to the carboxylate groups in the alginate residues.

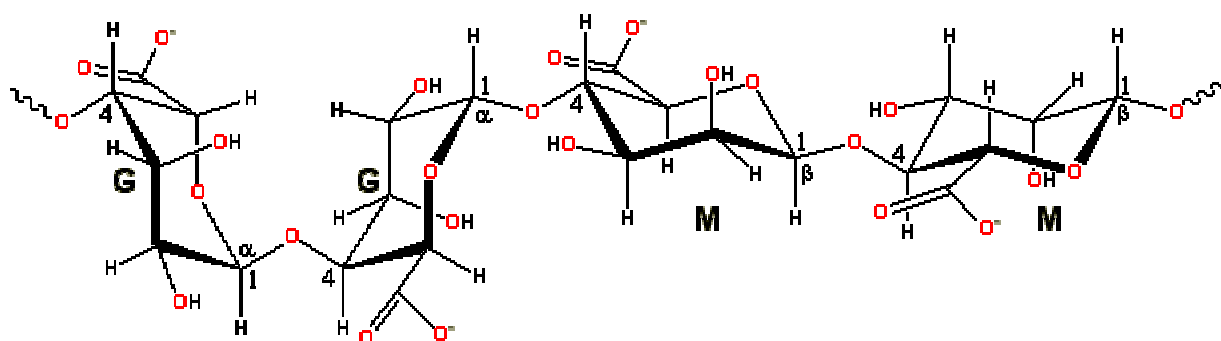


Fig. 2.13. Glycosidic bonds between β -(1,4)-linked D-mannuronate (M) and α -(1,4)-linked L-gulonate (G) residues in the polymer chain of alginate (adopted from ref. 51).

Poly β -(1,4)-linked D-mannuronate tends to form a 3-fold left-handed helix (Figure 2.14) with weak intramolecular hydrogen bonding between the hydrogen of the hydroxyl group in the 3-position (*i.e.* O3H) and the ring oxygen of the subsequent residues (*i.e.* O5). Poly α -(1,4)-linked L-gulonate forms more rigid 2-fold screw helical chains by intramolecular hydrogen bonding between the carboxyl group and the hydroxyl group in the 2-position (*i.e.* O2H) of the prior residues and weaker hydrogen bonding with the hydroxyl group in the 3-position (*i.e.* O3H) of the subsequent residues. Alternating poly α -(1,4)-linked L-gulonate- β -(1,4)-linked D-mannuronate contains both equatorial-axial and axial-equatorial links and the conformation is disordered. In this dissimilar conformation there are hydrogen bonds between the carboxyl group on the mannuronate and the hydroxyl groups in the 2- and the 3-positions

form similar junctions, but with marked differences in the strength of binding. ⁵³ Mg²⁺ does not promote gelation. ⁵⁴

The gelation process in alginates (or in pectins, which are another similar type of ionic polysaccharides composed of galacturonate residues) results from specific and strong interactions between divalent ions and blocks of guluronate, but not mannuronate residues (Figure 2.15). The guluronate blocks are better disposed to chelate the divalent ions, because a spatial arrangement between adjacent blocks forms a cavity lined with carboxylate and other oxygen atoms, which is suitable to complex the divalent cations. ³⁹ Therefore, the gel strength in alginate is related to the level of L-guluronate present, ⁵⁶ in which the divalent ions lie in cavities on alignment of two guluronate chain sections. ^{38, 56}

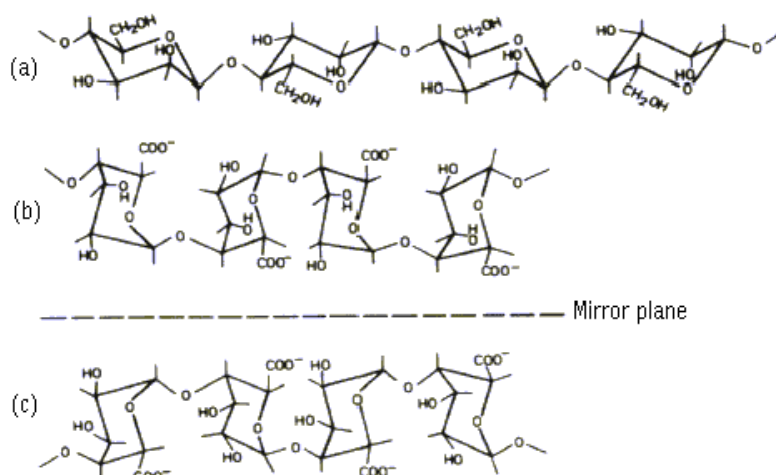


Fig. 2.15. Schematic drawings of (a) polymannuronate (b) polyguluronate in alginate, and (c) polygalacturonate in pectin (adopted from ref. 39).

This conformation of calcium alginate is known as the “egg-box”, a model structure which was proposed to explain the location of the Ca²⁺ ions, predominantly within the G-block. ⁵⁷ In this model, two 2-fold helical poly-guluronate chains are packed with the calcium ions located between them (Figure 2.16). The box is proposed to contain 10 oxygen atoms from the guluronate chains involved in the coordination of the calcium ions. Six oxygen atoms can interact directly with the calcium ion present in the box, these are the hydroxyl group on C2 and C3, and a carboxylate oxygen of the subsequent residue. The other four oxygen atoms are from the (1,4)-O linkages and one ring oxygen by each chain, but slightly further away. The chains are stabilized by hydrogen bonding between the other carboxylate oxygen and two hydroxyl groups on the subsequent residues. ⁴⁶

The low gel strength in some alginate is probably due to the instability between the two chains (intermolecular bonds). For example, *P. aeruginosa* alginate does not form a gel with Ca^{2+} though it contains 4 - 40 % guluronate, but it does so in the acidic form.⁵⁸ Probably the distribution of cations is not regular to allow the association of two polysaccharide chains.

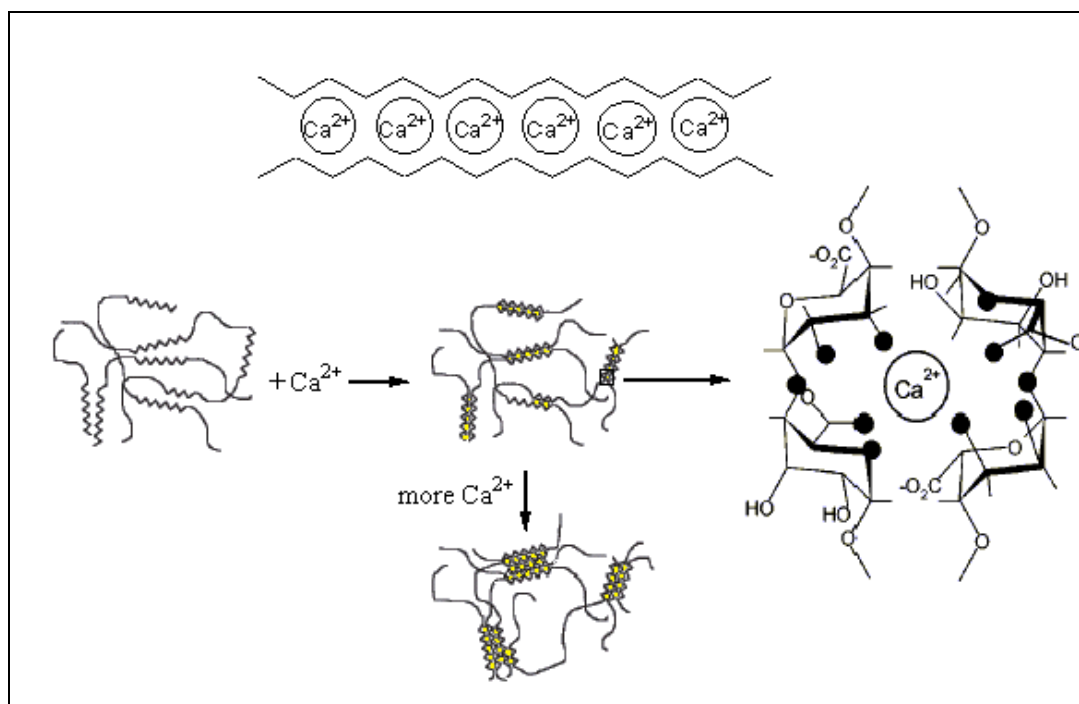


Fig. 2.16. The “egg box model” for the interaction between Ca^{2+} and poly-guluronate. Dark circles represent the oxygen atoms involved in the coordination of calcium ion (adopted from ref. 56).

The diequatorial linkage in poly-mannuronate leads to a much flatter structure with cavities too shallow for cations to occupy. This would explain the inability of such chains to complex except at higher ion concentrations.⁵⁷

When the chain in the “egg box model” has 3-fold screw symmetry, a three-dimensional structure is more likely than the simplified model. Chains with 2-fold screw symmetry are closer to form sheet-like aggregates, but may also associate in the third dimension. The chains of alternating mannuronate having integral screw symmetry (mainly 4-fold) do not offer suitable sites for complexation.⁵⁷

X-ray emission spectra were obtained to investigate the spatial distribution of calcium ions in alginate. Evidence was found for an inhomogeneous distribution of calcium ions between

the surface and the core of the gel spheres being highest at the surface and lower in the gel interior.⁵⁹

2.2.3.4 Alginates and circular dichroism

In solution, carbohydrate polymers often exist as disordered coils, either extended or collapsed, but helical structures also occur, with a wide range of residual value along the helix axis. Short-chain carbohydrates can be flexible or relatively rigid. From conformational analysis supported by circular dichroism (CD) evidence, the absolute conformation can be extracted, and polymer coils can be distinguished from helices, or flexible oligomers from rigid oligomers. Because carbohydrates are saturated oxocarbon compounds in their simplest form, there are special experimental problems in their circular CD analysis. The simple pyranose rings contain only ether chromophores, and electronic transitions occur at wavelengths shorter than 200 nm. CD spectra in this range are not easily accessible, and until recently required special prototype instruments.⁶⁰ Stevens *et al*⁶¹ found that the CD bands in the 180 – 190 nm, 164 – 177 nm, and 145 – 160 nm regions depend on the absolute conformation of glycosidic linkages of the α - and β -(1,3), -(1,4), and -(1,6) types, respectively.

When the carbohydrates carry unsaturated substituents, it is in general possible to find CD absorption bands at wavelengths longer than 200 nm. Among the most common substituents of this kind are acetamido and uronic acid moieties. Both groups have characteristic $n\pi^*$ and $\pi\pi^*$ transitions, which makes it possible to observe the CD at wavelengths of 180 nm or longer. Alginates have carboxylate as the intrinsic chromophore and hence exhibit circular dichroism around 210 nm corresponding to the $n\pi^*$ transition of the COO^- group.⁵ The three types of block sequences present in alginates show very different CD behaviour, the spectrum of poly-L-guluronate being entirely negative, whereas that of poly-D-mannuronate has a strong positive band and mixed sequences show intermediate behaviour. Spectra of intact alginates show a peak at ~ 200 nm, and a trough at ~ 215 nm (Figure 2.17), with relative magnitudes varying with composition.⁶² The ratio of peak height to trough depth varies almost linearly with the ratio of mannuronate to guluronate residues. From the following two simple linear equations (2.1 and 2.2) the % mannuronate in alginate can be calculated:⁶²

$$\text{mannuronate/guluronate} \approx 2.0 (\text{peak/trough}) \quad \text{if peak/trough} < 1 \quad (2.1)$$

$$\% \text{ mannuronate} \approx 27 (\text{peak/trough}) + 40 \quad \text{if peak/trough} > 1 \quad (2.2)$$

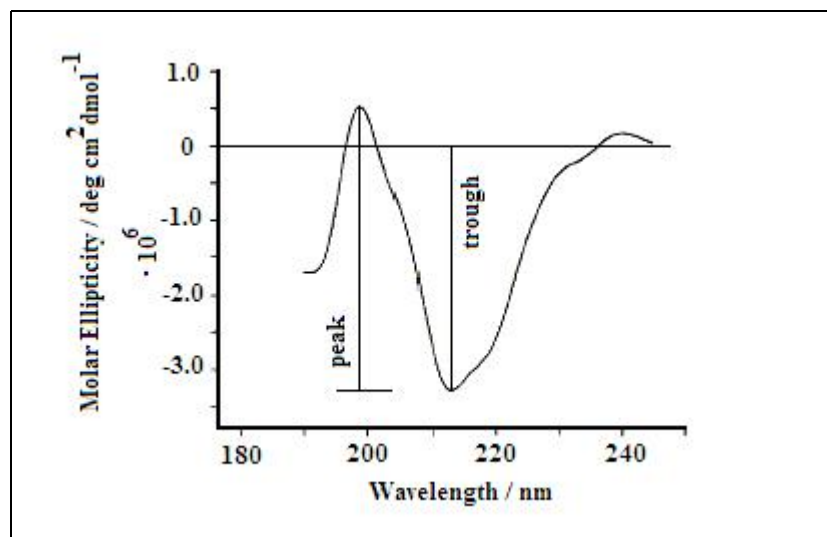


Fig. 2.17. Circular dichroism spectrum of an alginate. The sample concentration is 0.8 mg/ml (pH 7.0), and the path length is 2 mm. The relative content of mannuronate residues calculated for this sample was 71 % (adopted from ref. 63).

This method is not destructive, and reliable estimates of alginates composition can be obtained from less than 1 mg. The CD spectrum of mixed blocks are not identical to that of an equal molar mixture of the two types of homopolymeric block, indicating that CD behaviour is sensitive to the nature of adjacent residues in the polymer chain. The method gives good agreement with the previous analyses of the same samples by hydrolysis and NMR-spectroscopy.⁶²

2.2.3.5 Induced Circular Dichroism in Alginate-Dye Systems

As mentioned before monosaccharides, oligosaccharides, and polysaccharides have electronic transitions in wavelength regions shorter than 200 nm. Commercially available CD spectrometers are currently limited to make measurements with wavelengths above 190 nm, since atmospheric dioxygen begins to absorb strongly at wavelengths shorter than 180 nm. It is now possible to measure the CD of polysaccharides directly, even when the sample absorbs below 180 nm,^{61, 64} but with experimental problems that are associated with measurements in the far UV-region, in which evacuated CD spectrometer equipped with a MgF₂ polarizer and CaF₂ quarter-wave retarder is necessary.⁶⁴ The use of induced circular dichroism (ICD) of dyes bound to the carbohydrate for predicting conformational changes and anomeric changes in solution has been emphasized.⁶⁴ ICD is the result of specific interactions between the polysaccharide residues and the dye molecules with conformational rearrangement of the dye,

as it adapts to the chiral field in the carbohydrate molecule. This interaction will generate an extrinsic CD spectrum that will reveal information about the structure of the polysaccharide in solution in a way that is quite analogous to the application of the exciton coupling models.⁶⁵ This method has the advantage that there is no need to solve the experimental problems associated with far-UV measurements.

Natural anionic polysaccharides are well known chromotropes containing more than one kind of substituted sugar residue, such as heparin, hyaluronic acid, and chondroitin sulfate.⁶⁶ However, the formation of dye-alginate complexes has not received very detailed treatment in the past. Seely and Hart⁶⁶ have studied the interaction between methylene blue and some types of sodium alginate by absorption and circular dichroism spectroscopy at high polymer to dye ratios. They obtained different types of spectra when they added methylene blue to certain samples of sodium alginate, due to aggregation of the dye molecules as a result of their interaction with alginate, but at any sensible polymer to dye ratio there was no induced dichroism. Seely and Hart in their study tried to distinguish the varieties of UV and CD absorption of the dye, and relate the different modes of dye aggregation to the different kinds of alginate segments, poly(Man), poly(Gul), and poly(Gul-Man).

Pal and Mandel⁵ have studied the ICD of the same dye, methylene blue (MB), in addition to other dyes, acridine orange (AO), 1,9-dimethylmethyleneblue (DMMB), and pinacyanol (PCYN) in potassium alginate, which was prepared from alginic acid (from *Macrocystis-pyrifera*). However, these researchers used in their study a reasonable polymer – dye ratio, because they felt that it was safer to work at this lower ratio, and also in order to avoid the risk of observing CD absorption caused by a trace impurity in the polymer samples. Under this condition, alginate does not induce CD in MB, in agreement with the observation by Seely and Hart. Pal and Mandel also noted that MB and AO exhibit weak metachromasia and no induced dichroism at any sensible polymer to dye ratio. As for the other dyes strong dichroism was observed with potassium alginate and strong induced blue shifts (up to 125nm) of the maximum in the visible spectra. From the CD spectra ($1.2 \cdot 10^{-4}$ and $8.4 \cdot 10^{-4}$ M) in the absence of dye it was concluded that potassium alginate shows no conformational change associated with a change in concentration. The CD spectrum with DMMB (polysaccharide to dye ratio of 70) was also identical except for the shallow trough around 300 nm, which was assigned to the UV band of the dye.

These results indicate that potassium alginate has a rather stable conformation, which is not appreciably perturbed either by dilution or by the dye. With respect to PCYN, Pal and Mandel observed that this dye shows broad and multiply banded metachromasia induced by

potassium alginate, with peaks around 483, 590, and 635 nm; the shape of the metachromatic spectrum does not significantly change upon increasing the polysaccharide to dye ratio from 1 to 10.

2.2.4 Cyclodextrins

There are many reasons that make the cyclodextrins one of the most important among all the host type macromolecules, which have the ability to complex guest molecules without forming a covalent bond. They are produced in tons from natural precursors by relatively simple enzymes conversion and can be modified chemically for different tasks. Cyclodextrins appear to pose no risk when used together with nutrients. Molecular encapsulation using cyclodextrins is already widely utilized in many industrial products, technologies, and analytical methods, and as ingredients for drugs, food, or cosmetics.

2.2.4.1 Discovery and Nomenclature

In 1891, Villiers⁶⁷ isolated about 3 g of a crystalline substance from 1000 g starch by digesting starch with a particular enzyme (*Bacillus macrons*), and determined its composition as $(C_6H_{10}O_5)_2 \cdot 3H_2O$. This new compound was named “cellulosine” because it was resistant against acidic hydrolysis and did not show reducing properties. Villiers observed two distinct types of “cellulosines”, which were later referred to a α - and β - cyclodextrins. In 1903, Schardinger⁶⁸ described the properties of crystalline dextrans that seemed to be identical with the “cellulosines” of Villiers. In all his experiments, the major crystalline product was the so-called α -dextrin. He found the iodine reaction suitable to distinguish between the α - and β -dextrans.⁶⁹ In 1936, Freudenberg and co-workers postulated the cyclic structure of the crystalline Schardinger dextrans⁷⁰ and in 1948, they discovered γ -dextrin and elucidated its structure.⁷¹ Three years later Cramer, in his concept of the “cavity in solution”, developed a model for the complexing ability of the cyclodextrins, which was widely accepted in 1957.⁷² For a long time, the most common and commercially available cyclodextrins were α -cyclodextrin (cyclohexaamylose), β -cyclodextrin (cycloheptaamylose), and γ -cyclodextrin (cyclooctaamylose), which are referred to as α -CD, β -CD, and γ -CD respectively. The larger cyclodextrins (δ -, ϵ -CD etc.), which were observed by French⁷² in the early 1950s, are not regular cylinder shaped structures. They have collapsed, and their real cavity is even smaller than in γ -CD.

2.2.4.2 Structural Features

Cyclodextrins are macrocyclic oligosacchrides, formed by α -1,4-linked glucopyranose subunits, and appear like toroidal macro rings with a cavity in the center (Figure 2.18).⁷³ Crystal structure analyses of cyclodextrins have proven that all glucose residues in the ring possess the thermodynamically favoured 4C_1 chair conformation with all substitutions in the equatorial position. The external surface of a cyclodextrin contains secondary hydroxyl groups situated on one of the two rims of the ring, whereas primary hydroxyl groups are placed on the other rim. The inner surface of the cavity is lined by the hydrogen atoms and ether-like oxygen.⁷⁴ The overall appearance of a cyclodextrin molecule is less that of a ring, but rather of a truncated cone with the wide “open” side formed by secondary hydroxyl groups, whereas the primary hydroxyl groups are located on the narrower “closed” side. The cavity diameters (maximum values) are 5.3, 6.5, and 8.3 Å for α -CD, β -CD, and γ -CD respectively. Table 2.2 summarizes the most important structural features of α -, β -, and γ -cyclodextrin.

Table 2.2. Structural and some physical features of α -, β -, and γ -cyclodextrin.^{75, 76}

	α	β	γ
Number of glucose units	6	7	8
Molecular weight (g/mol)	972	1135	1297
Solubility in water (g/100ml)	14.5	1.85	23.2
$[\alpha]_D$ at 25 °C	150 ± 0.5	162.5 ± 0.5	177.4 ± 0.5
Cavity diameter, Å	4.7 - 5.3	6.0 - 6.5	7.5 - 8.3
Height of torus, Å	7.9 ± 0.1	7.9 ± 0.1	7.9 ± 0.1
Approx. volume of cavity, Å ³	174	262	427
Crystal water, wt %	10.2	13.2 - 14.5	8.13 - 17.7
Hydrolysis by <i>A.oryzae</i> α -amylase	negligible	slow	rapid

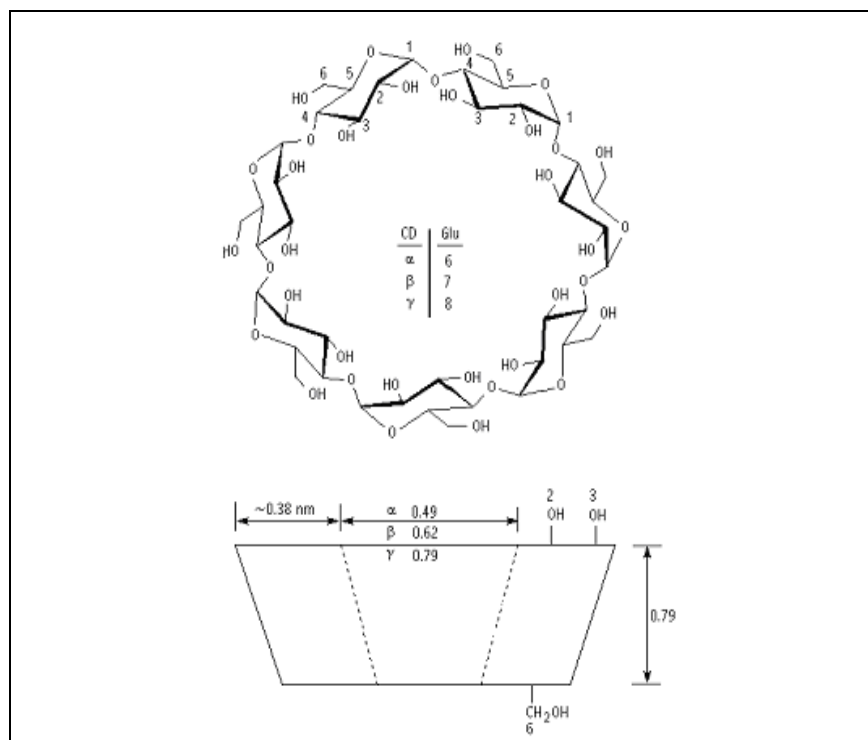


Fig. 2.18. Structure of β-CD (top) and approximate geometric dimensions of α-, β-, and γ-CD (bottom) (adopted from ref. 77).

2.2.4.3 Solubility in Polar solvents

Because of the presence of many hydroxyl groups, cyclodextrins are soluble in polar solvents.⁷⁸ Studies of cyclodextrin chemistry have therefore mostly been performed in aqueous media. Of the three common cyclodextrins β-CD has the lowest water solubility (see Table 2.2); this is possibly due to intramolecular hydrogen bond formation between the C2-OH group of one glucopyranoside unit with the C3-OH group of the adjacent glucopyranose. In β-CD, a complete secondary belt is formed by these hydrogen bonds; thus the β-CD molecule presents a rather rigid structure. The hydrogen bond belt is incomplete in the α-CD molecule, because one glucopyranose unit is in a distorted position. Consequently, instead of the six possible hydrogen bonds, only four can be established fully. γ-CD has a non-coplanar, more flexible structure; therefore, it is the most soluble of the three cyclodextrins.⁷⁵

2.2.4.4 Cyclodextrin inclusion complexes

In contrast to the hydrophilic outer lining, the inner surface of cyclodextrins is hydrophobic. In an aqueous solution, the internal cavity of a cyclodextrin is filled with water

molecules which are energetically unstable (polar - nonpolar interaction), and are readily displaced by appropriate “guest molecules” which are less polar than water.⁷³ In this way, aqueous solutions of cyclodextrins can form complexes with a wide range of solid, liquid, and even gaseous guest molecules.⁷⁹ Cyclodextrins can also form inclusion compounds in the solid state.⁸⁰ These cyclodextrin complexes have found academic as well as commercial interest.

2.2.4.4.1 Stoichiometric ratios and driving force

There is a wide variety of guest molecules forming inclusion complexes with cyclodextrins, ranging from dyes,⁸¹⁻⁸⁴ drugs,⁸⁵ small anions,⁸⁶ carboxylic acids,⁸⁷ to alcohols.⁸⁸ Such substrates usually form inclusion complexes with 1:1 host: guest stoichiometries; however, other stoichiometries have been reported^{83, 84, 89} the most common being 1:2. The ratio 2:1 and 2:2 have also been found⁹⁰⁻⁹² and even more complicated ones.⁹³

Much of the work on cyclodextrin inclusion complexes has been focused on the determination of the formation constants of such complexes. The two main components for the driving force of inclusion are the repulsive forces between the included water molecules and the nonpolar cyclodextrin cavity on one hand, and between the bulk water and the nonpolar guest molecule, on the other hand. The various published studies on cyclodextrin chemistry indicate that the interaction forces responsible for the formation of the cyclodextrin inclusion complexes are mainly of the type described by van der Waals-forces,⁹⁴ hydrophobic interaction,^{95, 96} strain energy of the macro cyclic ring,⁹⁷ dipolar interaction,⁹⁸ and in some cases by hydrogen bonding.⁹⁹ Covalent bonding is inoperative in the inclusion complexes of cyclodextrins.

2.2.4.4.2 Methods of detecting the inclusion process

By forming an inclusion complex with a guest molecule, a cyclodextrin may change some of the physical and chemical properties of the guest molecule; by these changes the complex formation is recognized and studied. For example, spectrophotometric determinations,^{81, 84} which rely on the difference in absorptivity of the free and complexed substrate; conductance measurements,^{100, 101} which depend on the difference in mobility of the free and complexed ionic substrate.

When achiral guests are inserted into the chiral cyclodextrin cavity, they may become optically active and show strong induced Cotton effects.¹⁰² Sometimes the maximum of the UV absorption is shifted by several nm and fluorescence is strongly enhanced, because the fluorescing molecule is transferred from the aqueous media into a non-polar surrounding.¹⁰³ In NMR spectra, the chemical shifts of the anisotropically shielded atoms may be significantly modified.¹⁰⁴

In most cases the reactivity of the included molecule in cyclodextrin cavity decreases, *i.e.* the guest is stabilized, but in many cases the cyclodextrin behaves as an artificial enzyme, accelerating various reactions and modifying reaction pathways.¹⁰⁵

In the solid state the guest compound is molecularly dispersed in the carbohydrate matrix forming a microcrystalline or amorphous powder. These complexes are effectively protected against any type of reaction, except for the cyclodextrin hydroxyl groups or reaction catalysed by them. The sublimation and volatility of the guest molecules in the solid state are reduced to a very low level. The analysis of x-ray data give the most reliable information about the structure of cyclodextrin complexes.¹⁰⁶

2.2.4.5 Practical use of cyclodextrins

By appropriately orienting the guest molecule inside the cavity cyclodextrins can act as catalysts in chemical reactions such as hydrolysis and oxidation.^{105, 107}

The major part of research papers on cyclodextrins, almost 25 %, deals with their pharmaceutical applications.¹⁰⁸ Many drug molecules are ideal as guest molecules for cyclodextrins, because their polarity, molecular mass, and structure enable them to get included into the cyclodextrin cavity. The inclusion of drugs in cyclodextrins can enhance drug solubility, an important aspect since the majority of drug molecules is poorly soluble in water. Also, complexation retards evaporation and may cover bad taste.⁷⁴ Cyclodextrin can also be used to mask or eliminate unpleasant odours and provide protection against oxidation and proteolysis.¹⁰⁹ Biologically active molecules can be fundamentally modified in their action if administered in an encapsulated molecular form.¹¹⁰

Cyclodextrins are widely used in food, cosmetic, and toiletry production. 70 % of all cyclodextrins produced are used in this field;¹¹¹ at the same time only 7 % of cyclodextrin related research papers are dedicated this field. There are some applications of cyclodextrins in pesticide formulation. The effects that can be obtained in this area are essentially the same as in the drug formulation, *viz.* enhancement of stability, absorption and persistency.⁷⁵

In analytical chemistry cyclodextrins are mainly used in gas chromatography,¹¹¹ high-performance liquid chromatography,¹¹² and capillary zone electrophoresis in order to separate drug molecules, especially chiral isomers. The mechanism of the separation is based on the different binding constants of the isomers with cyclodextrins.^{113,114}

2.2.4.6 Cyclodextrin derivatives

The natural cyclodextrins form the basis for a practically unlimited number of derivatives, because of the many hydroxyl groups (both of the primary and secondary types) in the macromolecule. These groups are the most common reaction sites and have been extensively derivatized. Cyclodextrins are derivatized mainly in order to modify the complex solubility, complex properties (stability constants, guest selectivities), or to introduce groups with specific functions (*e.g.* catalytic). For example, methylated cyclodextrins in general exhibit greater stability than their parent cyclodextrins. Methylation also increases solubility, presumably by affecting the distribution of the hydrogen bond system (as mentioned before). Increased solubility by appropriate substitution is also well exemplified by the hydroxypropyl, acetyl, and sulfopropoxy derivatives.⁷⁶ Among the three main cyclodextrins, β -cyclodextrin is the least soluble in water, which reduces its use both as solubilizing agent and carrier of drugs or other organic compounds; therefore most of the cyclodextrin derivatives known presently are derived from β -cyclodextrin.

Cyclodextrin derivatives might be classified as to type, polarity, and the size of the substituents. The use of cyclodextrin derivatives is limited, because they are usually obtained by complicated syntheses that increase the price of the new products.¹⁰⁸ As for pharmaceutical application, the optimum cyclodextrin derivative used as parental drug carrier should be cheap, highly soluble in water, available in high purity, non-toxic, stable during heat sterilization and storing in aqueous solution, and non reacting with cholesterol and phospholipids (and other cell-membrane compounds). This ideal cyclodextrin derivative does not yet exist.¹⁰⁸

2.2.4.7 Cyclodextrins and induced circular dichroism

Most of the molecules that are used as guest molecules in the inclusion process like cyclodextrins are achiral. In the chiral environment of a cyclodextrin these molecules can exhibit induced circular dichroism (ICD), which is widely applied to obtain important

information about the complex structure. Based on the Kirkwood-Tinoco theory of polarizabilities the following rule was developed for the cyclodextrin environment: ¹⁰² if the transition dipole moment of the guest chromophore is aligned parallel to the axis of symmetry of the cyclodextrin (that is, the rotational axis of the cyclodextrin cavity), then the sign of the ICD Cotton effect for that transition will be positive, whereas if the moment axis is aligned perpendicular to the cavity axis, the ICD sign will be negative. This rule applies to a chromophore that resides inside the cavity; if the chromophore is located outside the cavity, the signs of the ICD are opposite to this. ¹¹⁵ The strength of the ICD may be affected by the cyclodextrin conformational flexibility (deviations from radial symmetry). ¹¹⁶

2.2.4.8 Cyanine dye complexes

The formation of inclusion complexes between organic dyes and cyclodextrins has been the focus of many studies, mostly with emphasis on the thermodynamics and kinetics of the inclusion process. The thermodynamic parameters give a macroscopic picture of the inclusion process while its details are revealed by the kinetic data. The literature on cyclodextrin–dye inclusion complexes has many categories. For example, studies include the binding of cyclodextrins with an organic dye whose structure contains the azo linkage ($-N=N-$). ^{91,117-119} Other type of organic dyes that have been used as suitable guest molecules in the complexation reaction with cyclodextrins are cyanine dyes. Circular dichroism spectroscopy has been used to study the effect of β - and γ -cyclodextrin on the aggregation process of different oxacarbocyanines (DOC, DODC, and DOTC, corresponding to the carbo-, dicarbo-, and tricarbo-cyanine, respectively) at different dye concentrations and temperatures. ⁶ The conclusion of this study, among others, was that DOTC in the presence of β -cyclodextrin forms a dimeric aggregate regardless of temperature and concentration, while with γ -cyclodextrin the n-mer ($n>2$) is formed instead. For DOC the observed aggregate depends on the concentration of the dye; in both β - and γ -cyclodextrin the monomer, dimer and n-mer are observed, though the latter appears only at very low temperature. DODC gives a more complex picture. While for β -cyclodextrin all three species are observed, for γ -cyclodextrin, a temperature and concentration dependent equilibrium between the dimer and the n-mer is found, that is not manifest in the UV at all.

2.3 Surfactants

Surfactants, a contraction of surface-active agents, are organic substances which have the tendency to concentrate at the surface or any interface of a system at low concentration, thereby significantly reducing the amount of work required to expand the interface. (Detergents, a term which is often used interchangeably with surfactant, refers to a combination of surfactants and other substances, organic or inorganic, formulated to enhance functional performance, specifically cleaning). Surfactants are considered amphipathic solutes, with their typical head-to-head / tail-to-tail ordering observed at the surface and also in bulk of the solvent as a result of physical interactions among the molecules. These structures may mimic biological structures, such as enzymes and membranes, which have vital importance in biochemical reactions and play a role in a variety of functions in the life of the cell, respectively. A whole new field of mimetic chemistry has grown around this concept, and colloidal structures formed by surfactants are at the centre of the entire subject.^{120, 121}

2.3.1 Properties and classification

Surfactants have a characteristic molecular structure consisting of a lyophobic group that has very little attraction for the solvent, and a lyophilic group that is strongly attracted by the solvent; this combination is known as an “amphipathic” structure. With reference to the solvent water, the lyophobic (or hydrophobic) group of a surfactant is usually a long-chain hydrocarbon residue, and the lyophilic (or hydrophilic) head group an ionic or highly polar group. In the bulk of the solvent, a surfactant molecule increases the free energy of the system due to the distortion of the solvent liquid structure. In this case less work is needed to bring molecules to the surface, and the surfactant concentrates at the surface. The surfactant is said to be surface-active because it lowers the surface tension γ .

The classification of surfactants depends on the nature of their hydrophilic group, which can be anionic, cationic, neutral, or zwitterionic (amphoteric). Anionic surfactants include carboxylates, sulfonates, sulfates, or phosphates as solubilizing group, cationic surfactants are solubilized by amine and ammonium groups. Ethylene oxide chains and hydroxyl groups are the solubilizing groups in non-ionic surfactants, and zwitterionic surfactants are solubilized by combinations of anionic and cationic solubilizing groups. The hydrophobic part of a surfactant may consist of one or several hydrocarbon chains containing from 8 to 20 carbon atoms; the chains may be saturated or unsaturated, linear or branched and they may contain hetero (oxygen) atoms, aromatic rings, amides, esters, or other functional groups.¹²² Table 2.3

The typical surfactant molecules are composed of a single or double tail connected to a single head group; there are other types of surfactants, which have recently been developed.¹²⁵ Figure 2.19 shows schematically different types of surfactants.

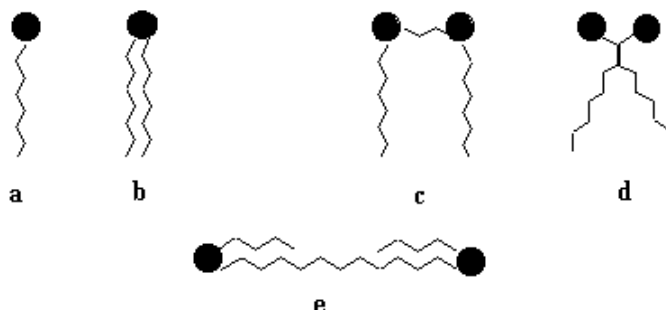


Fig. 2.19. Schematic representation of different types of surfactants: (a) single-tailed (b) double-tailed (c) and (d) gemini and (e) bolaform.

The name gemini (type c and d in figure 2.19) was coined by Menger¹²⁶ and typifies a surfactant that consists of two hydrocarbon tails each attached to a hydrophilic head group, which are connected by a rigid spacer. Gemini surfactants have better solubility in aqueous solution than their monomeric counterparts, and these dimeric surfactants are superior to many conventional surfactants in oil solubilization.¹²⁷ Bolaform surfactants (type e in figure 2.19) consist of two hydrophilic head groups, connected by a long hydrocarbon spacer.¹²⁸ Their tendency to aggregation is usually lower, and aggregation numbers are smaller than those of the monomeric surfactants of which they consist.

2.3.2 Aggregation of surfactants

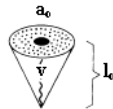

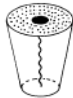

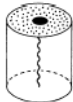
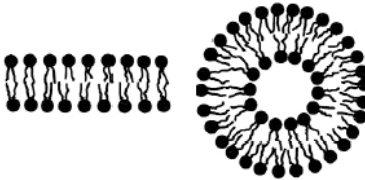


In aqueous solution, surfactants aggregate in different forms, such as spherical micelles, wormlike micelle, bilayer fragments, vesicles, or inverted structures.¹²⁹ The way surfactant molecules aggregate is mainly determined by the attraction between the hydrophilic tails and electrostatic repulsions of the hydrophilic head groups, which are present in the surfactant molecules.

The type of aggregated surfactant can be determined by the packing parameter P as in the following equation:¹³⁰

$$P = \frac{V}{a_o l} \quad (2.3)$$

in which V is the volume of the hydrocarbon part of the surfactant, l is the chain length of alkyl tail, and a_o is the mean cross-sectional head group surface area. A value of P smaller than $1/3$ is indicative of the formation of micelles; P between $1/3$ and $1/2$ indicates the formation of wormlike micelles, whereas surfactants with P between $1/2$ and 1 form vesicles. Inverted structures are formed when P is larger than 1 (see Table 2.4).

Table 2.4 The different types of surfactant aggregation with relation to their shapes (adopted from ref. 130).

Effective molecule	Shape of the surfactant	Packing parameter	Type of aggregation	Schematic structure
	cone	$< 1/3$	spherical micelles	
	truncated cone	$1/3 - 1/2$	wormlike micelles	
	cylinder	$1/2 - 1$	bilayers, vesicles	
	inverted (truncated) cone	> 1	inverted micelles	

2.3.2.1 Formation of micelles

At very low concentration (e.g. 10^{-4} M) many surfactants are soluble in water, forming solutions; if they are ionic, like fatty acid soaps or alkyl sulfate detergents, they will be dissociated as weak or strong electrolytes. As the concentration increases, the adsorption at the air – solution interface becomes stronger. Saturation is reached when the molecules are packed close together, with strong lateral interactions occurring between the hydrophobic chains, which tend to stick up out the water (see Figure 2.20, A and B). When the concentration of surfactant solute in the bulk of solution exceeds a limiting value, the formation of micelles is observed, globular or spheric structures which are organized aggregates of a large number of molecules. In the micelle, the hydrocarbon tails of the

surfactant molecules point toward the center of the sphere and the polar heads towards the water at its surface.¹²⁴ In ionic micelles, the hydrocarbon core is surrounded by a shell that more nearly resembles a concentrated electrolyte solution. It consists of ionic surfactant heads and bound counter-ions in a region called the Stern layer. The hydrocarbon chains occupy a certain volume, which is represented by bars in Figure 2.20, C to E; circles represent the polar head groups, and the dotted region is water

The minimum concentration at which micelles begin to form in the solution is called the critical micellization concentration or cmc.¹²³ Micelle size is expressed as the micellar molecular weight or, more generally, as the aggregation number, *i.e.* the number of monomers making up the micelles. Generally this number is between 20 and 100 for single-chain anionic and cationic surfactants. Large aggregation numbers (> 1000) have been reported for non-ionic micelles, especially when the cloud point is approached.¹²² In these structures the hydrophobic portions of the surfactant molecule associate to form regions from which the solvent (water) is effectively excluded.

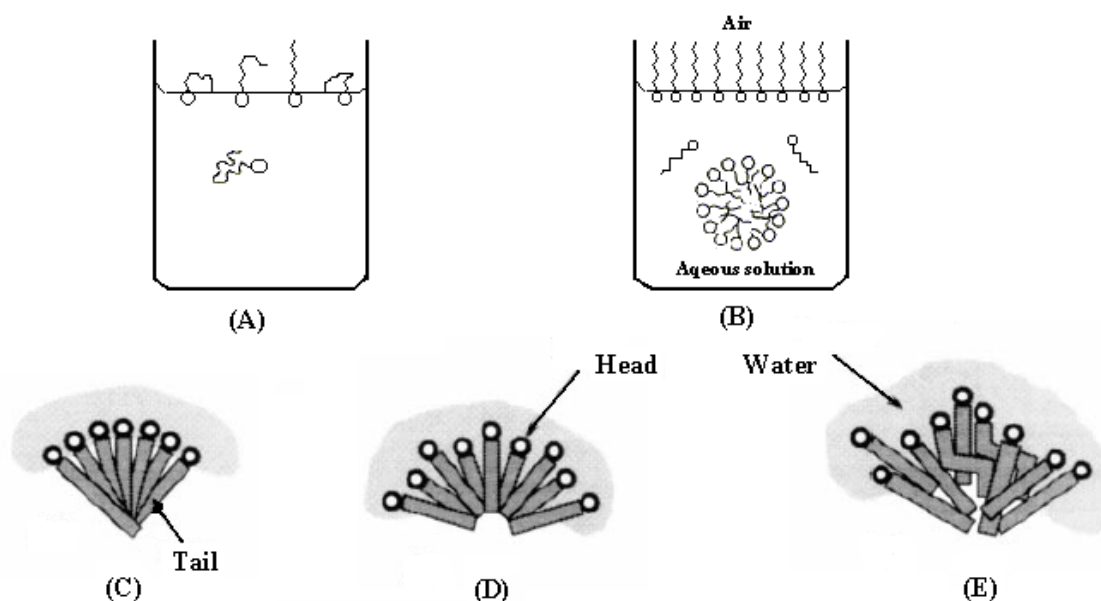


Fig. 2.20 Schematic arrangement of amphiphile molecules at low concentration in water (A), and above the cmc (B).¹²³ Three schematic representations of the structure of an aqueous micelle: (C) tails overlap in the center, (D) water penetrates core, and (E) chain protrusion and bending (adopted from ref. 120 and 124).

The hydrophilic head groups remain on the outer surface to maximize their interaction with water and, in the case of ionic amphiphiles, with the oppositely charged ions (counterions). A significant fraction of the counterions remains strongly bound to the head

groups, so that the lateral repulsive force between those groups is greatly reduced. The precise structure of the micelle depends upon the temperature and concentration but also on the molecular structure: the size of head group, the length and number of hydrocarbon chains, the presence of branches, double bonds or aromatic rings etc are the factors that determine the shape of a micelle. Increasing the concentration of the surfactant leads to the formation of wormlike micelles and, subsequently, liquid crystals.¹²³

2.3.2.2 The critical micellar concentration (cmc)

The cmc is the concentration at which micelles first appear in the solution. Below this critical value, additional surfactant molecules added to the solution remain in monomeric form, and above this, essentially all additional surfactant form micelles. This transition from pre-micellar to micellar solution at the cmc occurs over a narrow concentration range.¹³¹

Surfactant solutions exhibit a striking characteristic when quantitative data of their physical properties are plotted against concentration. Figure 2.21 illustrates this for sodium dodecyl sulfate (Table 2.3). The data for physical properties were taken from the earlier literature (1936 – 1939). Each curve shows a break, an inflection, occurring within a narrow concentration band lying between 0.18 percent and 0.25 percent (0.063 – 0.083 M). Dodecyl sulfate is not unique with respect to these inflections; many data show that each surfactant is characterized by a concentration band to indicate that the inflection at the critical concentration is the beginning of a large-scale colloid formation.¹³²

Among the properties that have been employed to determine the cmc are surface tension, optical turbidity, electric conductivity, osmotic coefficient, density, sound velocity, diffusion, viscosity, solubilization, and NMR chemical shifts.¹²³ Usually, the selected property is plotted against amphiphile concentration; the functions are selected so that the graph resembles as close as possible to a pair of straight lines whose intersection can be taken as the cmc. Conductance measurements, suitable for strong electrolyte amphiphiles, have the advantage that they reach very high precision and are not too difficult to perform.¹²³ The preferred plot for cmc determination is equivalent conductance against the square root of molality, because this has a strictly linear form at high dilution, with a large change as micelles begin to form.

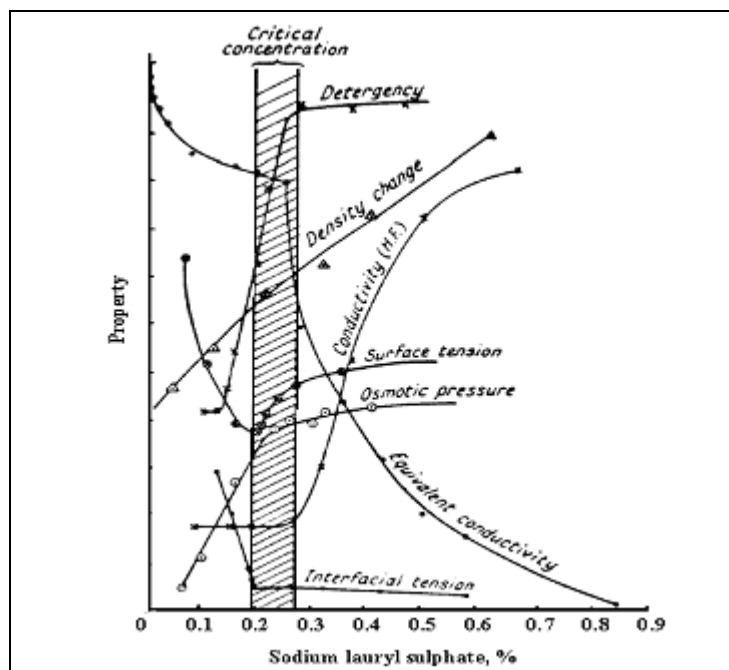
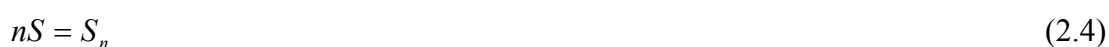


Fig. 2.21. Illustration of the changes in some physical properties that occur in the neighbourhood of the critical micellar concentration (adapted from ref. 132).

The cmc can be used quantitatively as well as qualitatively to determine the average molecular weight and the net charge (if the amphipathic species are ionic) of the micelle.¹²⁰ Factors that are affecting the cmc are the nature of the hydrophilic group and of the counterion, the presence of organic molecules, and the effect of temperature and pressure.¹²³

A low cmc indicates that it is thermodynamically favourable for the hydrophobic domain of the surfactant molecule to leave the aqueous solution, which will result in both an excess concentration at the interface and the formation of micelles. This ability to adsorb at an interface and reduce interfacial tension is of great importance for many processes of technological interest, such as emulsification, foaming, wetting, solubilization, detergency, particle suspensions, and surface coatings.¹³¹

An important point to be considered is the question whether micellization should be viewed in terms of a chemical reaction equilibrium or a phase equilibrium. If the amphipathic species is represented by S , then the clustering process can be described by the reaction



in which S_n is the micelle with a degree of aggregation n . This reaction is reversible, and dilution will shift the equilibrium towards the monomeric surfactant.¹²⁰ The law of mass

action implies that a continuous distribution of species – monomers, dimers, trimers, etc. should be present. Increasing the surface concentration should shift the equilibrium in a reaction as follows to the right,



but the observed transition from monomers to n-mers with $n > 50$ is not expected. Experimentally, large micelles do form sharply at the cmc in aqueous solutions, and to a good approximation the concentration of monomeric surfactant in solution varies little above the cmc. This type of behaviour is typical of a phase equilibrium (equation 2.4). Energetically, some minimum value of n is apparently necessary before the exclusion of hydrophobic tails from the aqueous medium is effective. Once the solution is concentrated enough for aggregates with this critical n value to be formed, any additional surfactant added to the solution goes into the micelle.

In aqueous systems the phase equilibrium model is generally used. Since a degree of approximation is introduced by using the phase equilibrium model to describe micellization, micelles are sometimes called pseudophases.¹²⁰

2.3.3 Surfactant – dye interactions

The solubility of a dye is related to the polarity of solvent in which it is to be dissolved. The addition of surfactant to the aqueous solution of a dye is usually accompanied by structural changes of the dye, which can be noted from spectral measurements. Upon increasing the surfactant concentration, the absorption spectrum of a dye behaves as if the dye molecules were dissolved in a non-polar solvent. Thus, dyes are often used to determine the cmc of surfactants, *e.g.* pinacyanol chloride,¹³³⁻¹³⁵ bromophenol blue,¹³⁶ and pyrene.¹³⁷ It was suggested that, when using charged dyes, its ionic charge should be similar to the charge of surfactant.¹³⁸ The cmc's determined by the dye solubilization method are usually lower than those measured in the absence of dyes indicating that the dye can partly substitute the surfactant molecules. The absorption spectrum of a dye often changes at concentration far below the cmc of the surfactants when the charges of the ionic groups of surfactant and dye are opposite.^{133, 138} For example, methyl orange has been widely studied in this respect.¹³⁸⁻¹⁴¹ This azo dye shows aggregation with the appearance of a new band in its absorption spectrum which is blue shifted by about 80 nm with respect to the absorption band in aqueous

solution. This band is similar to that of the dye in the presence of small amounts of cationic polymers.^{140, 142}

Sodium bis(2-ethylhexyl) sulfosuccinate (sold under the name Aerosol-OT or AOT for short) is a surfactant with two hydrophobic tails (Figure 2.22). This molecule has three asymmetric carbon atoms, one of them adjacent to the sulfonate group, which makes this group optically active and may induce chirality in achiral cationic molecules (e.g. dyes) bound to it. These cations play a major role in the aggregation of anionic surfactants (e.g. Aerosol-OT); even below the cmc cationic dyes may act as mutual counterion to reduce the electrostatic repulsion between the sulfonate

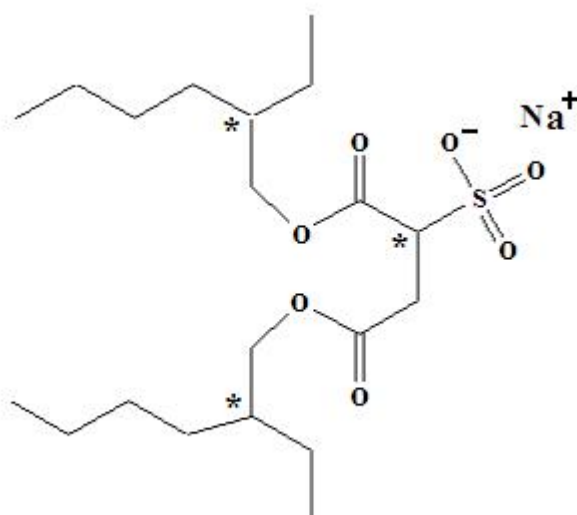


Fig. 2.22. Molecular structure of Sodium bis(2-ethylhexyl) sulfosuccinate (Aerosol-OT). Assymetric carbon atomes are denoted by a star.

Pal and Pal¹⁴³ have shown that Aerosol-OT induces strong dichroism in the cationic dye pinacyanol; this was the first report of the induction of circular dichroism in a cationic dye by Aerosol-OT in dilute aqueous solution, or by any detergent in general. By conductometric titration a 1:1 electrostatic binding between the cationic dye and Aerosol-OT was observed. At this ratio the intensities of the circular dichroism spectral bands are the maximum.

Surfactants can deaggregate cyanine dyes,¹⁴⁵ and in contrast, they can also effect the aggregation of dye, with ion-pairing being a prerequisite for this process.^{146, 147}

3 Theoretical background

3.1 UV / VIS Spectrophotometry

At room temperature most molecules will be in their electronic and vibrational ground states. In ultraviolet and visible (UV/Vis) spectroscopy, a molecule will absorb light and undergoes a transition from the ground to an excited state. This occurs if, in the interaction between the electromagnetic radiation and the molecule, the energy of a quantum of light is equal to the energy difference between the excited and ground states of the molecule. Thus, the following relation has to hold:

$$\Delta E = E_f - E_i = h\nu \quad (3.1)$$

E_f and E_i are the final and initial molecular energy levels in the molecule, h is the Planck constant and ν is the frequency of the light absorbed.

Regardless of the type of transition, not all light of the correct energy is absorbed by a sample of molecules. Empirically, the fraction of light absorbed by a sample follows Beer's law. If I_0 is the intensity of the light entering the sample and I is the intensity of the light emerging from the sample, then

$$\log(I_0/I) = \varepsilon \cdot l \cdot c \quad (3.2)$$

c and l are the concentration and the path length of the sample respectively, ε is the constant of proportionality, also known as the extinction coefficient. The quantity $\log(I_0/I)$ is known as the optical density (OD) or the absorbance (A). Both the absorbance and extinction coefficient depend on the wavelength of the light, *i.e.*

$$A(\lambda) = \varepsilon(\lambda) \cdot l \cdot c \quad (3.3)$$

The extinction coefficient, which characterizes the absorption process, is an empirical measure of the fraction of light absorbed by the molecule as a function of wavelength. By convention, the concentration c is measured in mole/liter and the path length l in centimetres. Since logarithms are unitless, the extinction coefficient has the dimension liter/(mole·cm). For polymers the concentration is calculated per mole of monomeric unit.

During the short time of excitation, the movement of the excited electron creates an instantaneous dipole or polarization of charge called the electric dipole transition moment μ . The intensity of the absorption depends on the size of this electric transition moment, which can be defined quantum-mechanically and computed as a vector quantity (equation 4 and 5) with both a direction (orientation) and a magnitude (intensity) that vary according to the nature of particular transition and the chromophore involved:

$$\vec{\mu} = \langle \Psi_i | \hat{\mu} | \Psi_f \rangle \quad (3.4)$$

$$\hat{\mu} = e \vec{r} \quad (3.5)$$

where Ψ_i and Ψ_f are the wave functions of the initial and the final electronic state. The product of these wavefunctions is the transition density, which is a measure of the shift of the electron density, which follows the excitation. Multiplied by the electric dipole moment operator $\hat{\mu}$ this gives the electric transition moment $\vec{\mu}$.

The magnitude of an absorption band is usually characterized by the maximum value of the extinction coefficient, ϵ_{\max} at the corresponding wavelength λ_{\max} . However, a more quantitative measure is the area A_i under the whole absorption band:

$$A_i = \int_{\nu_1}^{\nu_2} \epsilon(\bar{\nu}) d\bar{\nu} \quad (3.6)$$

This integrated absorption A_i is an experimental measure of an absorption band (see Figure 3.1). It can be approximated using the following relation:

$$A_i = \epsilon_{\max} \cdot N_{1/2} \quad (3.7)$$

where $N_{1/2}$ is the half width (in cm^{-1}) of the absorbance band.

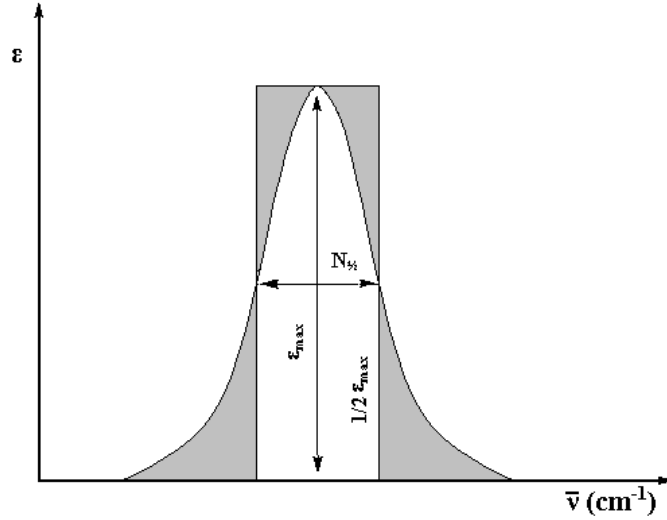


Fig. 3.1. An approximate typical absorption band clarifying how to find its approximate surface.

The intensity of a given UV/Vis transition may also be expressed as the oscillator strength f , a dimensionless quantity with typical values lying between zero and unity. f is defined as:

$$f = \frac{2.303mc^2}{N_o\pi e^2} \int \varepsilon(\bar{\nu})d\bar{\nu} = 4.315 \times 10^{-9} \int \varepsilon(\bar{\nu})d\bar{\nu} \quad (3.8)$$

where $\bar{\nu}$ is the frequency of the light in cm^{-1} , N_o is Avogadro's constant, m and e are the mass and charge of the electron, ε and c have been described earlier. The oscillator strength is proportional to a magnitude called the dipole strength D which is the square of the electric dipole transition moment, $\bar{\mu}$ and can be calculated from the following relation

$$D = |\bar{\mu}|^2 = \frac{f}{\bar{\nu}_{\max}} \cdot \frac{3he^2}{8\pi^2 m_e c} \quad (3.9)$$

where $\bar{\nu}_{\max}$ is the frequency at maximum absorption. Thus D can be evaluated directly as follows:

$$D = |\bar{\mu}|^2 = F \int_{\bar{\nu}_1}^{\bar{\nu}_2} \frac{\varepsilon(\bar{\nu})}{\bar{\nu}} d\bar{\nu} \quad (3.10)$$

With

$$F = \frac{3hc10^3 \ln 10}{8\pi^3 N_o} = 9.184 \times 10^{-39} \quad (3.11)$$

The transition dipole length r can be calculated from the square root of the dipole strength as follows:

$$r = \frac{|\vec{\mu}|}{e} = \frac{\sqrt{D}}{e} \quad (3.12)$$

3.2 Circular dichroism spectroscopy

Circular dichroism (CD) is observed when circularly polarized light passes through an optically active medium, usually a solution of an optically active compound. In such a solution the absorption coefficients of left and right circularly polarized light are slightly different, because they travel through the medium with different velocities. A plot of the difference of the absorption coefficient, $\Delta\varepsilon = \varepsilon_L - \varepsilon_R$, against the frequency ν is called a CD spectrum. There is another effect, which is called optical rotation and results from the fact that left and right circularly polarized light travel at different speeds in an optically active medium, *i.e.* they have different indices of refraction. The difference of the refraction indices, $\Delta n = n_L - n_R$, plotted against the wavelength ν is called an optical rotatory dispersion or ORD spectrum.

Most molecules of biological origin are asymmetric, *i.e.* they contain no element of mirror symmetry. As a result they are not superimposable on their mirror image. Solutions of these molecules are optically active, *i.e.* they show CD and ORD effects. Both effects are highly sensitive to the configuration of the molecule, the mirror image molecule giving a mirror image CD or ORD spectrum. Both methods are thus invaluable in assigning the absolute configuration to a molecule of unknown geometry. The techniques are non-destructive, require only small amounts of material, and are easily applied to molecules in solution.

3.2.1 Principle of the measurement

A CD spectrum is the difference of two absorbance spectra, one measured with left circularly polarized light and the other one with right circularly polarized light:

$$\Delta \varepsilon(\nu) = \varepsilon_L(\nu) - \varepsilon_R(\nu) \quad (3.13)$$

CD spectra can be measured as electronic circular dichroism in the spectral regions where electronic transitions occur, *i.e.* in the UV/Vis regions, or as vibrational circular dichroism in the infrared IR spectral regions. All measurements reported in this study refer to electronic CD. The measured differences $\Delta\varepsilon(\nu)$ are typically $\sim 10^{-5}$ of sample absorbance.

With the usual definition for the extinction coefficient, the following relations hold:

$$\Delta \varepsilon(\nu) = \frac{1}{cl} \Delta A \quad (3.14)$$

$$\Delta A = A_L - A_R = \log_{10} \frac{I_o}{I_L} - \log_{10} \frac{I_o}{I_R} = \log_{10} \frac{I_R}{I_L} \quad (3.15)$$

As seen from relation (3.15), I_o does not appear in this final relation, so there is no need for a reference beam. The instruments are, therefore, of the single-beam type.

Circular dichroism causes another effect, called “ellipticity”. As light enters the cell, the intensities of the two light rays, I_{oL} and I_{oR} , are identical; however, because of the effect of optical rotation, $I_L \neq I_R$ when the rays exit the cell (see Figure 3.2). As a consequence circularly polarized light, after passing an optically active medium like a solution containing optically active matter, is elliptically polarized. The shape of the ellipse is mathematically determined by the angle $\psi = \arctan(b/a)$, in which b and a refer to the lengths of the short and the long axis respectively and ψ is called the *ellipticity* of the sample. For example, an axial ratio of 1:100 will result in an ellipticity of 0.57 degrees. Although the CD instruments measure differential absorbance, they usually plot a CD spectrum in units of ellipticity, θ , in millidegrees, versus λ , rather than ΔA versus λ . The conversion between these two is:

$$\Delta A = \Delta \varepsilon \cdot c \cdot l \quad (3.16)$$

$$= \frac{4\pi\psi(\text{deg})}{180 \ln 10} \quad (3.17)$$

$$= \frac{\psi(m \text{ deg})}{32.982} \quad (3.18)$$

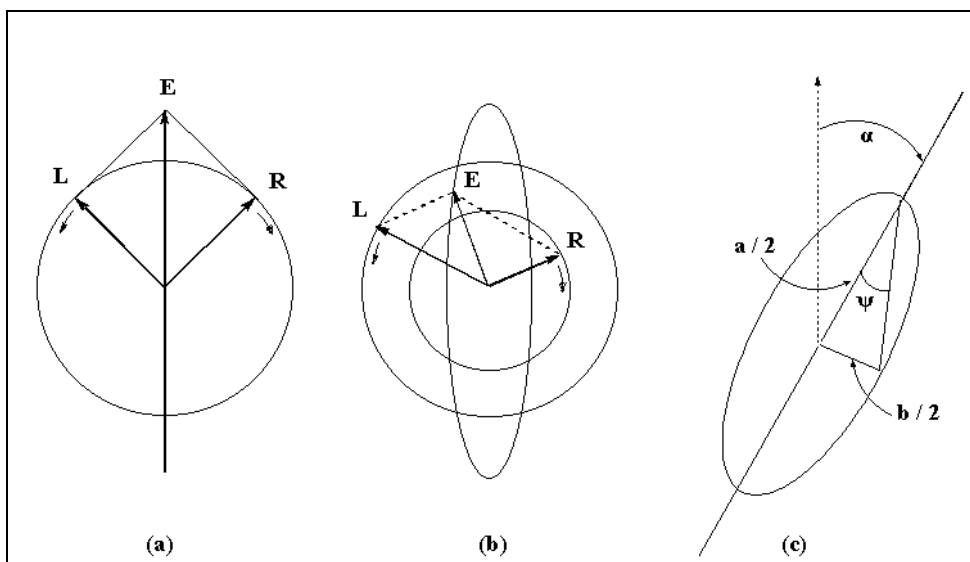


Fig. 3.2. (a) Two circularly polarized light, R and L, with their vector sum, E, always oscillating in the same plane. (b) The right circularly polarized component is less intense (absorbed more) than the left circularly polarized component. The electric light vector now follows an elliptical path, as shown, corresponding to elliptically polarized light. (c) The semi major and semi minor axes of the ellipse form a triangle and the angle opposite the semi minor axis is the angle, Ψ , the ellipticity. The major axis of the ellipse has been rotated through the angle α , which is the effect of optical rotation.

The specific ellipticity $[\psi]$ is defined analogous to the specific rotation:

$$[\psi] = \frac{\psi}{\rho \cdot l} = \frac{100\psi}{c_p \cdot l} \quad (3.19)$$

where ρ is the density in g/cm^3 (if the medium is a chiral liquid), c_p is the concentration in $\text{g}/100\text{cm}^3$ (if the medium is a chiral solution), and l is the cell length in dm.

The molar ellipticity $[\theta]$ is

$$[\theta] = \frac{[\psi]M}{100} \quad (3.20)$$

where M is the molecular weight of the optical active compound. Substituting equations (3.17) and (3.19) into (3.20), one obtains the following expression for the molar ellipticity:

$$[\theta] = 3298 \Delta\varepsilon \quad (3.21)$$

or

$$[\theta] = \frac{\psi}{10 \cdot c \cdot l} \quad (3.22)$$

where $[\theta]$ is in mdeg, c is the molar concentration (mol/l), and l is the cell length in cm. CD spectra are often reported in terms of molar ellipticity, instead of $\Delta\varepsilon$. For interconversion between the two scales one obtains from equations (3.21) and (3.22):

$$\Delta\varepsilon = \frac{\psi \cdot 3.0319 \times 10^{-5}}{c \cdot l} \quad (3.23)$$

3.2.2 The rotational strength R

The dipole strength D is a measure of the strength of an absorption band in UV/Vis spectroscopy. In a similar manner a property called the rotational strength R is defined, which is a measure of the strength of an absorption band in a CD spectrum. Theoretically the rotational strength is calculated as the scalar product of the electric and the magnetic transition moment that results from the excitation of an electron from the state o to the state a :

$$R_{oa} = \mu_{oa} m_{oa} \cos(\mu, m) \quad (3.24)$$

In this equation μ_{oa} and m_{oa} are the magnitudes of the electric and magnetic dipole transition moments, while $\cos(\mu, m)$ is the cosine of the angle between the two vectors. Experimentally the rotational strength is obtained as the integrated area of a CD band multiplied by a conversion factor:

$$R = 0.696 \times 10^{-42} \times 3300 \int \frac{\Delta\varepsilon}{\lambda} \cdot d\lambda \quad (3.25)$$

with R in cgs-units. As an approximation a Gaussian-shaped CD curve is assumed with maximum amplitude by $\Delta\epsilon^{\max}$ at the wavelength λ^{\max} , which yields the following equation:

$$R = 0.696 \times 10^{-42} \sqrt{\pi} \times 3300 (\Delta\epsilon^{\max}) (\Delta\lambda / \lambda^{\max}) \quad (3.26)$$

where $\Delta\lambda$ is the half-width (in nm) at $1/e$ times the height ($0.368\Delta\epsilon^{\max}$), e is the base of the natural logarithm, equal 2.71 (Figure 3.3).

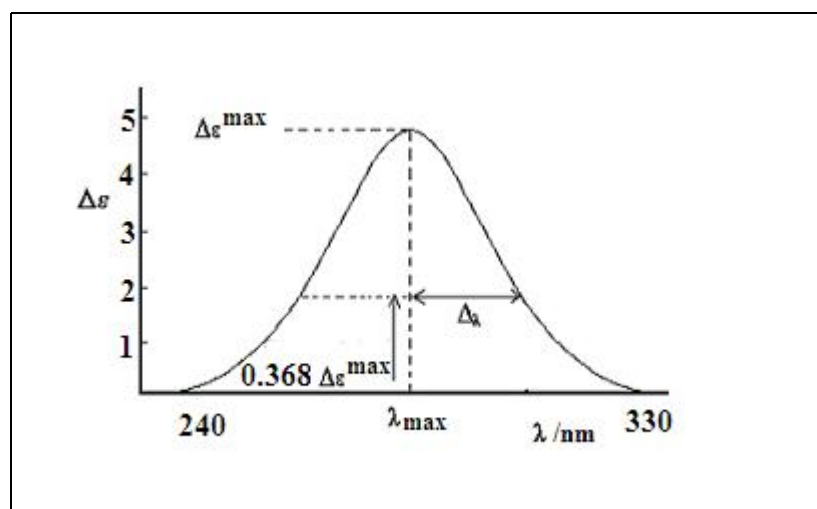


Fig. 3.3. An approximate typical positive CD band clarifying how to apply eq. 3.26.

3.2.3 Induced Circular Dichroism

Induced circular dichroism (ICD) is the CD observed in an optically inactive (achiral) chromophore due to its interaction with an optically active (chiral) moiety, *e.g.* as a result of the complexation by a chiral host. An ordered and site-specific spatial relationship between the achiral molecule and the chiral host is a necessary condition for the observation of this effect, since otherwise the variable signs of the induced CD would lead to the effective cancellation of the dichroic intensity. In principle ICD can arise through either of the two following mechanisms: (1) An electric dipole-allowed transitions can gain CD intensity due to coupling with other electronic dipole-allowed transitions in its surrounding, such as one or many chirally disposed chromophores. (2) A magnetic dipole-allowed transition can gain CD intensity due to mixing with electronic dipole-allowed transitions in the same chromophore due to the perturbation of the electronic states by the chiral surrounding.¹⁴⁸

Originally the ICD was studied to prove that such interactions existed. Later the ICD was used to obtain structural information about interacting species that was difficult to obtain otherwise. The dependence of the ICD on the geometry dependent interaction between the chromophore and the chiral host was theoretically analysed using generalized symmetry and parity arguments.^{149, 150}

3.2.4 Exciton coupling and exciton chirality

Exciton coupling is one of the most sensitive spectroscopic methods for determining molecular chirality in solution. It is easily identified in a CD spectrum and forms the basis for a highly reliable non-empiric method for assigning the absolute configuration to a given molecular species.¹⁵¹ The theoretical analysis of exciton coupling, and the resulting phenomenon of exciton chirality, is based on the coupled oscillator theory.

The origin of exciton coupling is the interaction of individual chromophore excitations into delocalized excitations. Two or more chromophores may interact under certain conditions with each other, even if there is no orbital overlap or electron exchange, when one chromophore is electronically excited. For effective interaction the chromophores should be similar, or have similar excitation energies, and there should be a fixed geometric disposition between the chromophores. The chromophores can be part of the same molecule or they can be placed on different molecules, which are in close contact. As a result of the interaction, the individual electronic transitions become delocalized over the different chromophores attaining new properties – energies and intensities – as a result.

Exciton coupling is manifest both in ordinary UV/Vis absorption spectroscopy and in CD spectroscopy. Consider two identical molecular chromophores, such as two dye molecules, arranged in-line or side-by-side, as shown in Figure 3.4, left. Interaction of the two local transition dipoles leads to two coupled states, the excitons, of higher and lower energies, respectively. In the higher state, the excitations are out-of-phase, with the result that their intensity cancels. This is the forbidden excitation and cannot be seen in the spectrum. Excitation to the lower-energy state, on the other hand, in which the excitations couple in-phase leads to a very intense state which is seen in the spectrum as a band which is red-shifted from the monomer absorption. If the two chromophors are arranged face-to-face (Figure 3.4, right), the in-phase interaction leads to an allowed, blue-shifted exciton state while the out-of-phase coupling results in a low-energy but forbidden exciton state.

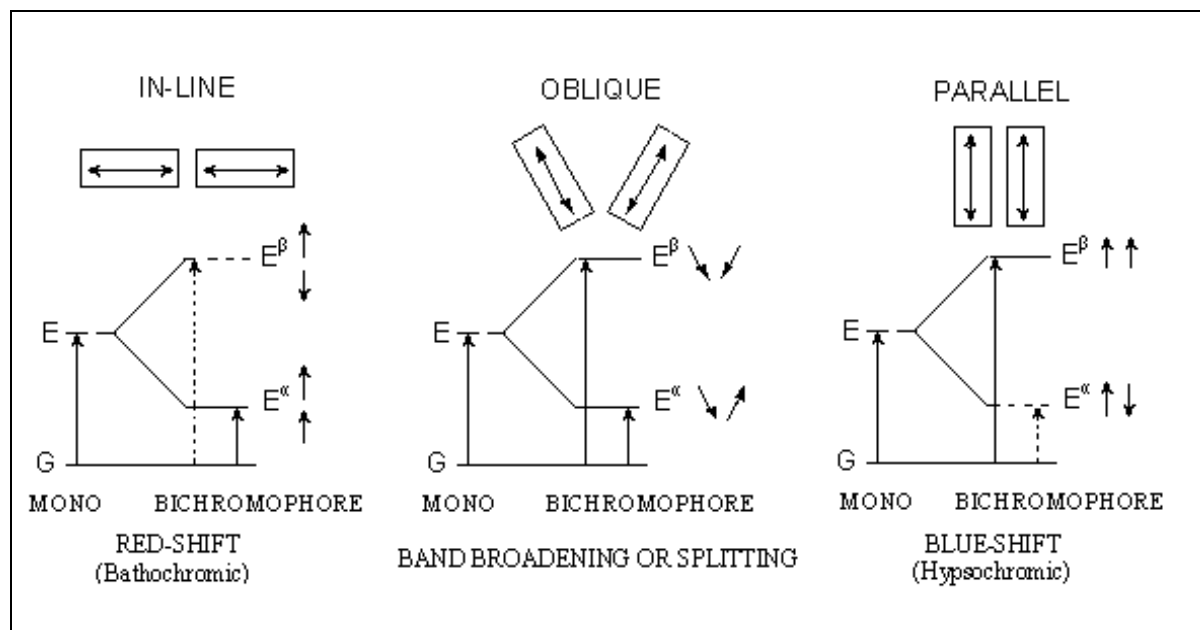


Fig. 3.4 Orientation dependence in exciton coupling between two chromophores (rectangular boxes) and their induced electric dipoles (represented by double-headed arrows). The solid arrows connecting ground (G) and excited (E) states represent allowed transitions; the dashed arrows represent forbidden transitions (adopted from ref. 152).

If the arrangement of the two chromophores is neither in-line nor parallel (Figure 3.4, center), both states are allowed and can be seen in the spectrum as two separate bands or as a broadened band depending on the interaction energy. This is the case which is realized when the chromophores are chirally disposed, whereas the cases shown in Figure 3.4 left and right correspond to J- and H-type dye aggregates, respectively.

If the two chromophores are part of a chiral molecule such as the *p*-dimethylaminobenzoate moieties of the diester shown in Figure 3.5, each of the two UV/Vis exciton bands will have a corresponding CD band. These bands resulting from two identical chromophores are called a CD or exciton “couplet”. The rotational strength associated with these bands is identical but of opposite sign. As a consequence, an exciton couplet is much easier to detect in a CD spectrum than in ordinary absorption. Also, from the relative signs of the low and the high energy component of an exciton couplet one can deduce the relative configuration of the two chromophores based on the so-called exciton chirality rule.

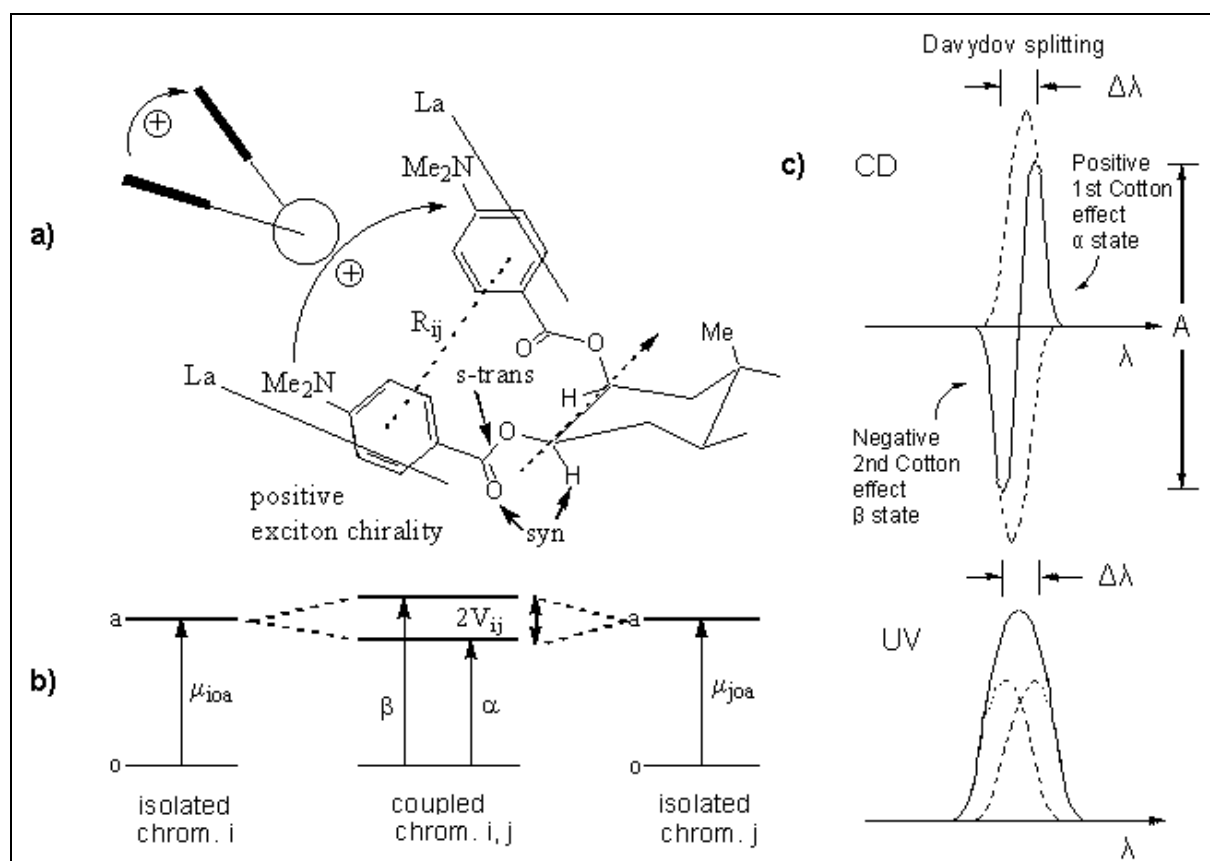


Fig. 3.5 (a) Diagrammatic representation of the exciton coupling of two identical chromophores of a steroidal 2,3-bis-p-dimethylaminobenzoate with positive chirality and interchromophoric distance R_{ij} . The conformation of the carbonyl hydrogens is *syn* to the ester carbonyl group, and the ester group is in the *s-trans* conformation. (b) Splitting of the excited states of the isolated chromophores into an α and a β state with a so-called Davydov split $2V_{ij}$. (c) The resulting exciton couplet as seen in the CD and the UV/Vis spectra. The observed CD and UV curves (solid lines) result from the summation of the CD and UV curves of the two separate exciton transitions (dotted lines) (adopted from ref. 151).

If the chirality of the transition moments is clockwise or positive, *i.e.* if the transition moment which is in front of the other has to be rotated clockwise in order to align the two moments, the low-energy couplet band has positive CD absorption and the high energy band negative absorption. Such a couplet, which is shown in Figure 3.6 left, is said to correspond to positive exciton chirality. If, on the other hand, the front chromophore has to be rotated counter-clockwise for alignment with the chromophore behind, the low and the high energy component of the exciton couplet will have negative and positive rotatory strengths, respectively. This corresponds to the case of negative exciton chirality.^{153, 154}

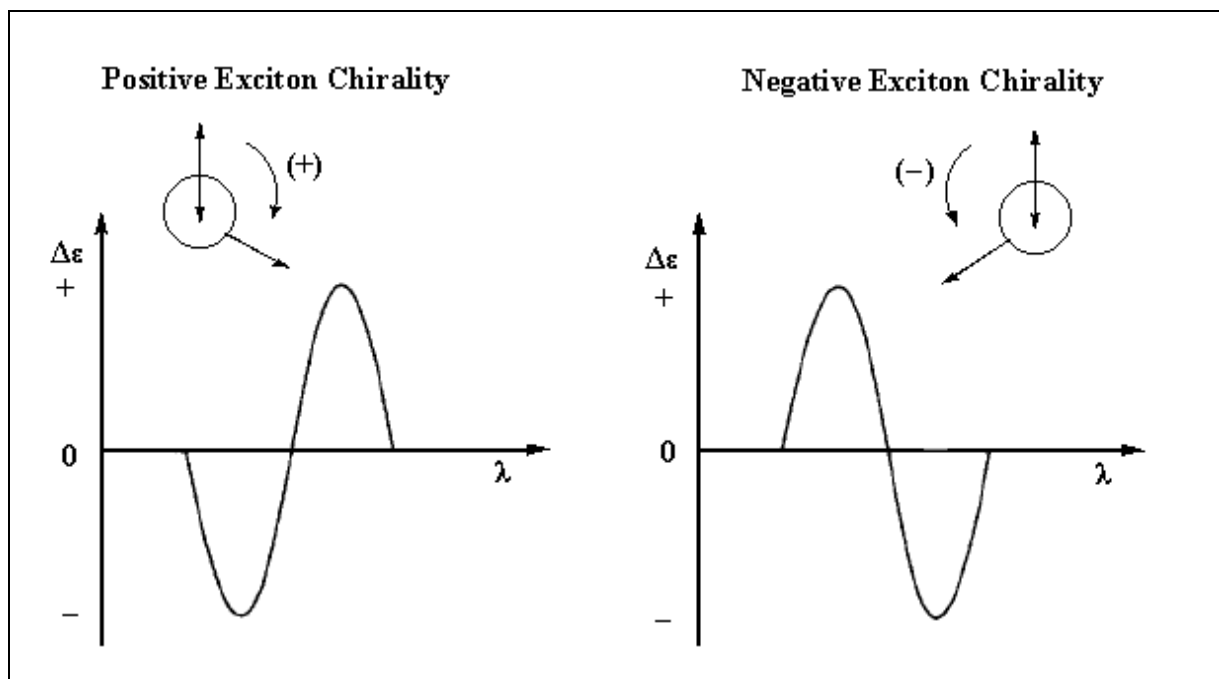


Fig. 3.6. The exciton chirality rule relating the torsion angle or helicity of two interacting electric dipole transition moments (\leftrightarrow) to the observed CD spectrum of the exciton couplet (adopted from ref.152).

3.2.5 Coupled oscillator model for the calculation of spectral properties of exciton-split chromophores

Exciton split UV/Vis and CD spectra derive from the same phenomenon, the interaction of component chromophores that results in the formation of new states, the so-called exciton states. The interaction which gives rise to these new states depends on the properties of the chromophores and also on their relative disposition. In the coupled oscillator model (“OSCI”) ^{155, 156} the excitations of the isolated chromophores i are described as oscillators of length r and charge e which give rise to an electric transition moment $\mu_{e,i}$ and a magnetic transition moment $\mu_{m,i}$ according to the following equations:

$$\mu_{e,i} = e \cdot r \quad (3.27)$$

$$\mu_{m,i} = \lambda_i \cdot \frac{\pi}{hc} r_M \times \mu_{e,i} \quad (3.28)$$

λ_i is the wavelength of the i th oscillator, c the velocity of light and r_M a vector pointing from the origin to the midpoint of the i th oscillator. Coupling of the dipoles leads to a system of coupled oscillators, with the coupling elements described by an interaction matrix. Diagonalization of this matrix leads to a set of eigenvalues k with energies ε_k and corresponding wavelengths λ_k , which represent the new exciton states of the system. From the eigenvectors of each eigenvalue the electric and magnetic moments of the coupled states are calculated according to the following equations:

$$\mu_{e,k} = \frac{1}{\sqrt{\lambda_k}} \sum_i \sqrt{\lambda_i} c_{i,k} \mu_{e,i} \quad (3.29)$$

$$\mu_{m,k} = \sqrt{\lambda_k} \sum_i \frac{1}{\sqrt{\lambda_i}} c_{i,k} \mu_{m,i} \quad (3.30)$$

In these equations, the $c_{i,k}$ stand for the coefficients of the i th oscillator in the k th eigenstate.

From the electric and magnetic moments of the coupled oscillators the rotational strength R_k for the coupled states are calculated as the scalar product:

$$R_k = \mu_{e,k} \cdot \mu_{m,k} \quad (3.31)$$

There are different ways to calculate the interaction between two electric dipoles, such as the point dipole approximation, the multipole expansion of transition charge densities or the approximation as extended dipoles. One of the options of OSCI employs the extended dipole approximation, which is easy to visualize. Consider two dipoles i and j with charges $\pm \varepsilon_{i,j}$ and $\pm \varepsilon$ which are coupled through space according to Coulomb's law (see figure 3.7).

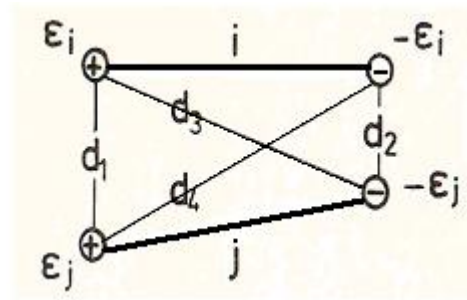


Fig. 3.7 Calculation of the interaction energy $V_{i,j}$ for an arrangement of two extended dipoles of charge ε_i and ε_j , and length i and j (adopted from ref. 156).

The interaction energy of these two dipoles is

$$V_{i,j} = \frac{\varepsilon_i \varepsilon_j}{4\pi\varepsilon_o} \left(\frac{1}{d_1} + \frac{1}{d_2} - \frac{1}{d_3} - \frac{1}{d_4} \right) \quad (3.32)$$

here ε_o is the permeability constant. One parameter which can be adjusted when using the coupled oscillator model is the length of the dipoles representing an absorption band. Since the integrated absorption intensity relates *via* the dipole strength D only to the product of length and charge of the transition moment vector, one can use different lengths of this vector and adjust the charge such that the correct value of μ_e is obtained. Since these adjustable parameters affect the interaction elements $V_{i,j}$ this methods, which will be applied later is of great value to obtain a more realistic model of the system to be described.

4. Results and Discussion

4.1 Pinacyanol chloride solutions

4.1.1 Pinacyanol chloride in aqueous solution with 7.5% v/v ethanol

Figure 4.1 shows the absorption spectra in the visible range (400-700 nm) of pinacyanol chloride in aqueous solution with 7.5 % v/v ethanol at room temperature taken at nine different concentrations ranging from $2.3 \cdot 10^{-6}$ to $2.0 \cdot 10^{-3}$ M. Ethanol has been added to increase the solubility of the dye, and thus increase the concentration range of the spectra to be studied. The amplitudes are given in terms of the apparent extinction coefficient (ϵ), which is obtained by dividing the measured absorbance, by the dye concentration and the path length of the cell.

The spectrum with the lowest dye concentration shows two main absorption bands, one centered at 600 nm ($16\,666\text{ cm}^{-1}$) and the other at 555 nm ($18\,018\text{ cm}^{-1}$). In addition, there is a weak shoulder visible at about 520 nm ($19\,230\text{ cm}^{-1}$). At this concentration the absorption at 600 nm is the most intense one and corresponds to the $0 \leftarrow 0$ vibronic transition between the electronic ground and first excited states of the molecule. Since at this low concentration there is no indication of aggregated species present the other two absorptions must correspond to

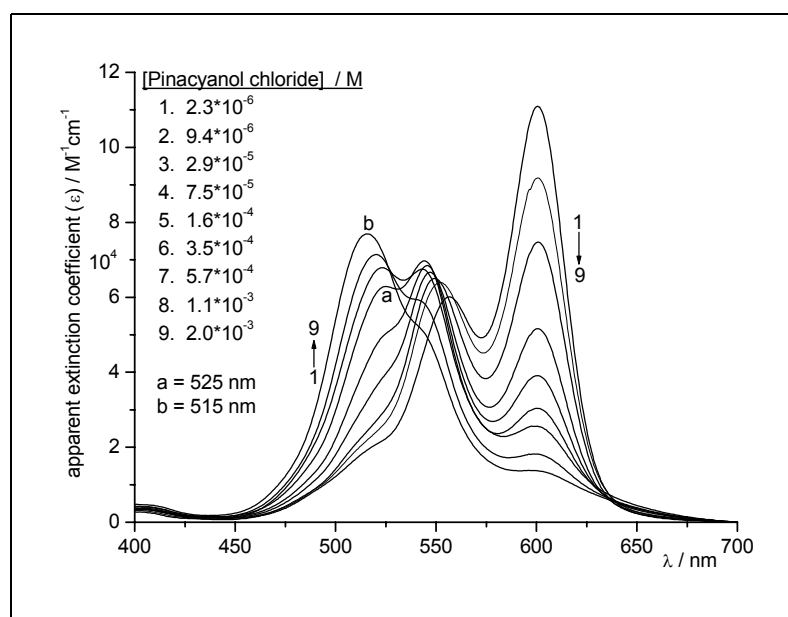


Fig. 4.1 Concentration dependent absorption spectra of pinacyanol chloride in water. 7.5 % v/v ethanol has been added to increase solubility.

monomer absorptions as well. We tentatively assign them to the $1 \leftarrow 0$ and $2 \leftarrow 0$ vibrational excitation of the ground to the first excited state. This is in line with the almost constant energy shifts of $1\,352$ and $1\,212\text{ cm}^{-1}$. Similar separations of excited state vibrational mode energies have been reported for other cyanine dyes.¹⁶

Increasing the dye concentration causes the shape of the absorption spectrum to change, leading to deviations in the Beer-Lambert law. As a result the extinction coefficient effectively becomes a function of the pinacyanol chloride concentration, because of aggregation of dye molecules in the solution. Thus the band at 555 nm suffers a blue shift to 545 nm as the pinacyanol chloride concentration is increased. This band reaches a maximum value at a concentration of $3.5 \cdot 10^{-4}\text{ M}$, together with a shoulder at 525 nm ; both bands can be assigned to the dimeric form of the dye. Continuous increase of the dye concentration causes the maximum band at 525 nm to be shifted to the lower wavelengths reaching a value of 515 nm at a concentration of $2.0 \cdot 10^{-3}\text{ M}$. This was the highest dye concentration that we could reach in our work, in which the cell we used at this high concentration had a path length of 0.01 cm , and there were difficulties caused by dye precipitation over this concentration. We attribute the two new bands at 525 nm and 515 nm to higher aggregation states of pinacyanol chloride, *viz.* the trimer and tetramer, respectively.

For the quantitative analysis of these concentration dependent spectra we have to consider the fact that the band at 555 nm which appears in the lower concentration range of pinacyanol chloride and corresponds to a vibrational overtone overlaps partially with the dimer band at 545 nm . This means that the 545 nm absorbance is not an accurate measure of the dimer concentration. In contrast the absorbance at 600 nm is a reasonable measure of the monomer concentration of pinacyanol chloride. However, Figure 4.2 shows that the extinction coefficient at 600 nm cannot be accurately calculated from the slope of a plot of absorbance against concentrations in the range of 10^{-6} M , in which most of the dye molecules are expected to be present in the monomeric form. Even at this low concentration, however, the absorbance varies nonlinearly with the concentration (Figure 4.2b). The deviation is indicative of the concentration dependent shift of the equilibrium between the monomer and dimer forms, which can be noted from the slight non-linear decrease of the absorbance at 600 nm and the increase around 555 nm . This is accompanied by a significant blue-shift of the absorption maximum due to the formation of dimer at the cost of monomer. Another effect concerns the precipitation of dye on the cell walls at very low dye concentrations. This effect leads to a significant decrease in the absorbance at 600 nm and at 555 nm , as can be seen in Figure 4.2a.

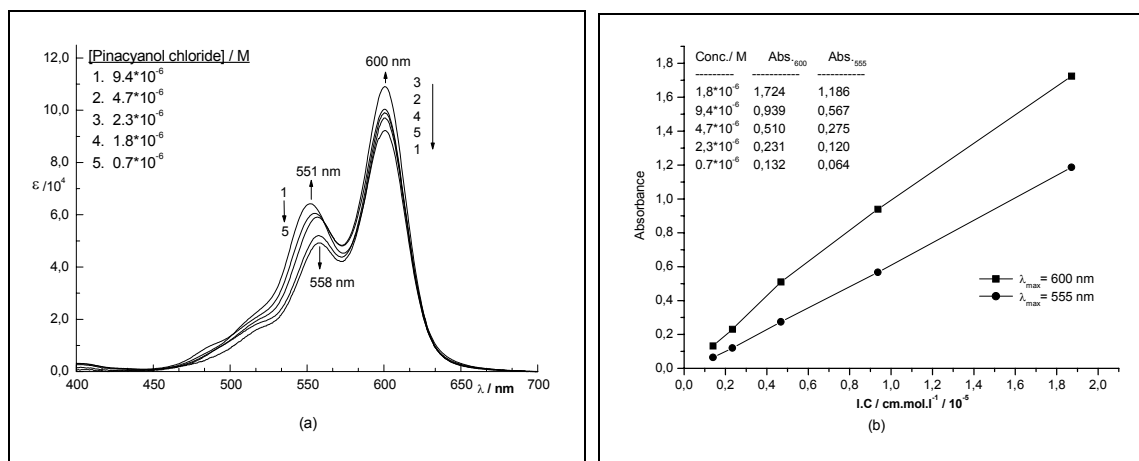


Fig. 4.2. (a) The visible absorption spectra of pinacyanol chloride in aqueous solution with 7.5 % v/v ethanol added at room temperature at low dye concentrations ($\sim 10^{-6}$ M) showing mainly the monomer vibronic bands. (b) Beer's law plot of the absorbance at 600 nm and 555 nm in Figure 4.2a.

In conclusion, it is difficult to make accurate measurements of the extinction coefficient of the monomeric form of pinacyanol chloride in aqueous dye solutions even at concentrations of 10^{-6} M or less.

4.1.2 Pinacyanol chloride spectra in ethanol

The UV/Vis spectrum of pinacyanol chloride in ethanol (100%) displays two main absorption maxima at 606 ($16\,500\text{ cm}^{-1}$) and 562.5 nm ($17\,777\text{ cm}^{-1}$) in addition to a shoulder at 520 nm. These features are independent of the concentration in the range from 10^{-6} to 10^{-4} M (Figure 4.3a). This is in contrast to the significant spectral changes that are observed in the aqueous solutions of the dye. This indicates that pinacyanol chloride in pure ethanol is present only in the form of monomeric molecules, and that no dimers or any higher aggregates are formed under these conditions. This is supported by a Beer's law plot of the two absorbance maxima at 606 and 562.5 nm, Figure 4.3a. The absence of any deviation in the plot proves that there is only one component of pinacyanol chloride in ethanol in the range of concentrations studied at room temperature.

From the linear plots displayed in Figure 4.3b, values of the extinction coefficients of monomeric pinacyanol chloride in ethanol of 175 200, 77 600, and 18 000 $\text{cm}^{-1}\text{M}^{-1}$ at 606.5, 562.5, and 521.5 nm, respectively, can be derived. The energy difference between the main peak at 606.5 nm and the second vibronic peak at 562.5 nm is 1290 cm^{-1} , and between the second vibronic peak and the vibronic shoulder at 521.5 nm is 1390 cm^{-1} . The ratio of the

absorbance intensities between 562.5 nm and 600 nm is 0.44, and between 521.5 nm and 600 nm is 0.10. These ratios will be used later in analysing the UV/Vis spectra of pinacyanol chloride in aqueous solutions.

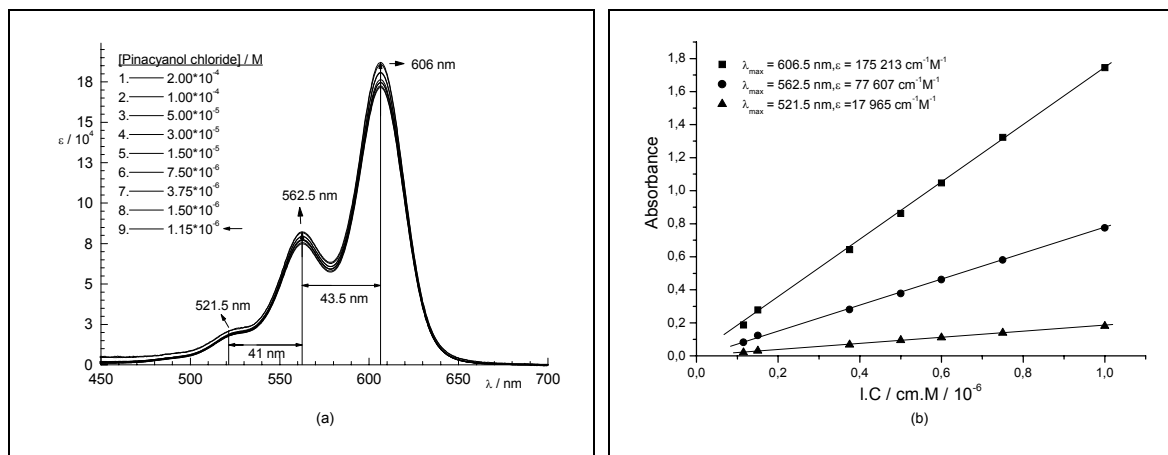


Fig. 4.3 (a) The visible absorption spectra of pinacyanol chloride in pure ethanol at room temperature and different dye concentrations (between 10^{-6} and 10^{-4} M) showing the monomer bands of absorptions (b) Beer's law plot of the absorbance at 606.5, 562.5 and 521.5 nm of Figure 4.3a.

4.1.3 Pinacyanol chloride spectra with different concentrations of ethanol

Figure 4.4a shows the visible spectra of pinacyanol chloride in aqueous solutions with different percentages of ethanol (v/v, from 0 – 100%). The dye concentration is kept constant at $1.5 \cdot 10^{-5}$ M. This concentration, used in a standard cell of 1.00 cm path length, yields reliable values of the absorbance. We note a distinct increase in the intensity of the monomer form of pinacyanol chloride and a slight red shift of the maximum wavelength as the ethanol concentration is increased, from 599.5 nm at 0% to 606.5 nm at 100%. Intensities and absorbance maxima in the 550 nm range where the monomer vibronic overtone and the dimer band overlap are more complex but reveal a distinct shift from the monomer/dimer mixture in pure water to pure monomer at 100% ethanol. Thus, there is a distinct band maximum at 546 nm in water, which results from the overlapping monomer and dimer absorbance. Increasing the ethanol content shifts the maximum to 562 nm, with an approximate isosbestic absorbance at 555 nm.

From the effect of the solvent on the λ_{\max} shift one can distinguish between the kinds of electronic transition occurring in the dye.¹⁵⁷ When a red shift is observed on decreasing the polarity of the solvent, the electronic transition is of the type n,π^* ; in contrast a blue shift is

observed when the electronic transition is of the π,π^* type. The red shift apparently arises from the reduced solvation of the non-bonded electron pair, which increases the energy of the n-type orbital. Hence the energy difference between excited and ground state is lower in a less polar environment than in a more polar one, and in consequence, the absorption maximum associated with such a transition is shifted to longer wavelength.³³ While this conclusion has been shown true for many dyes it appears doubtful that it can be applied to the case of pinacyanol. The intensity of the absorption at 606 nm is typical for a π,π^* absorption; the intensities of n, π^* absorptions are smaller by some orders of magnitude. We conclude that the red shift of λ_{\max} in the pinacyanol chloride spectrum as a result of decreasing the polarity of the solvent is due to a shift of the monomer-dimer equilibrium of the dye towards its monomeric form.

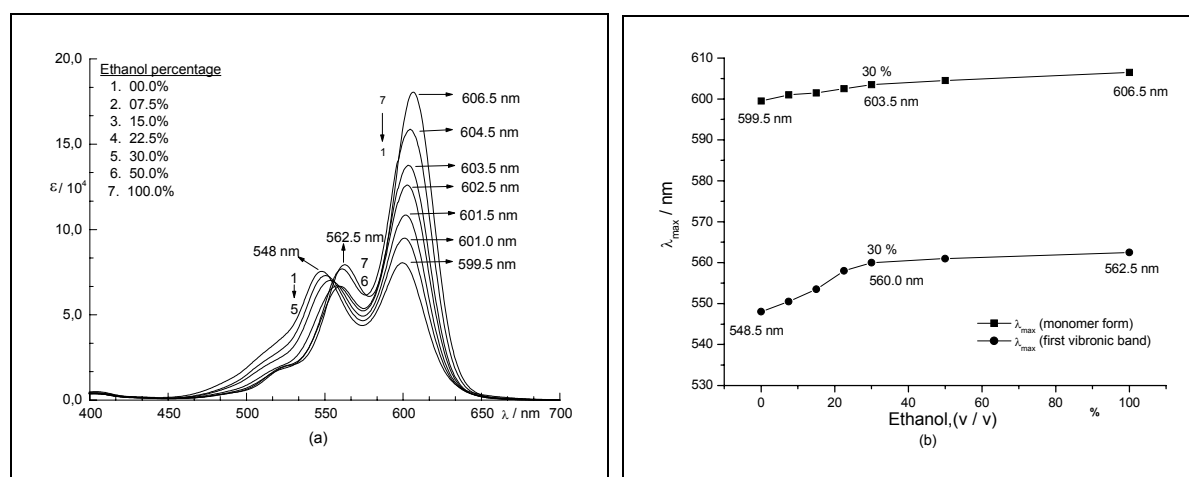


Fig. 4.4. (a) The visible absorption spectra of pinacyanol chloride ($1.5 \cdot 10^{-5}$ M) at different percentages of ethanol added to the aqueous solution. (b) The wavelength of the absorbance maxima as a function of the ethanol concentration.

4.1.4 Derivative spectra

An aqueous solution of pinacyanol chloride contains several different components with strongly overlapping absorbances as indicated by the spectra shown in Figure 4.1. There are three prominent areas of absorbance, at 600 nm, between 555 and 545 nm, and between 525 and 515 nm. One finds it difficult to determine the exact maximum wavelength for each component from these spectra directly. Derivative spectroscopy can help to identify and analyze the composition of such a mixture in a quantitative manner. The term derivative spectroscopy refers to a spectral measurement technique in which the slope of the spectrum, *i.e.* the rate of change of absorbance A with wavelength λ , is measured as a function of the

wavelength. Thus, the first-derivative spectrum is a plot of the spectral slope ($\Delta A/\Delta\lambda$) against the wavelength, in which ($\Delta A/\Delta\lambda$) is zero at the wavelength corresponding to the peak maximum of the original spectrum. The second-derivative spectrum is the first derivative of the first-derivative spectrum, *i.e.* ($\Delta^2 A/\Delta\lambda^2$), in which in contrast the second- or even higher order derivatives appear as sharpened representations of the original spectrum. The magnitude of the resolution enhancement depends on the derivative order and band shape, as well as the relative bandwidths and heights of the overlapping peaks.¹⁵⁸

Figure 4.5A represents as an example the visible spectrum of pinacyanol chloride at a concentration of $7.5 \cdot 10^{-5}$ M (spectrum #4 in Figure 4.1), while Figures 4.5B, C, and D are, respectively, the first-, second-, and fourth-derivative spectra of the same solution in the wavelength range from 400 to 700 nm. In the absorption spectrum a, b, c d, and e indicate absorptions of the monomer, dimer, and three other higher aggregates, respectively, which can be correlated with the derivative spectra. Repeating the same procedure for the other eight concentrations of pinacyanol chloride solutions shown in Figure 4.1, we obtain the maximum wavelengths for each component of pinacyanol chloride at each concentration. Figure 4.6 shows the maximum wavelengths for monomer, dimer, and the higher aggregates, which are taken from the fourth-derivative spectrum by identifying the position of the peak maxima.

In Figure 4.6 we show how the positions of the different band maxima change with the pinacaynol chloride concentration. At low concentration most of the dye is present as monomer, and the maximum wavelength is about 601 nm (averaged). At moderate concentration (10^{-4} M), there is a significant ratio of the dimer with maximum wavelength of 546 nm. At higher concentration ($3.5 \cdot 10^{-4}$ M), there is a the third peak with a maximum of about 522.5 nm, which occurs for the first time in the spectra shown in Figure 4.1. It has a maximum wavelength of above 525 nm and rises with increasing dye concentration. The other two absorption maxima in Figure 4.6 (507 and 486 nm) are attributed to higher aggregates of the dye.

It is most satisfying to see that the wavelengths of the absorption maxima of these different aggregated species is in effect independent from the dye concentration, as they should be. In our work with the peakFit program, which will be described in the next section, we took these values in account as the suggested maximum wavelengths of the pinacyanol chloride components in the quantitative analysis of the strongly overlapping band components.

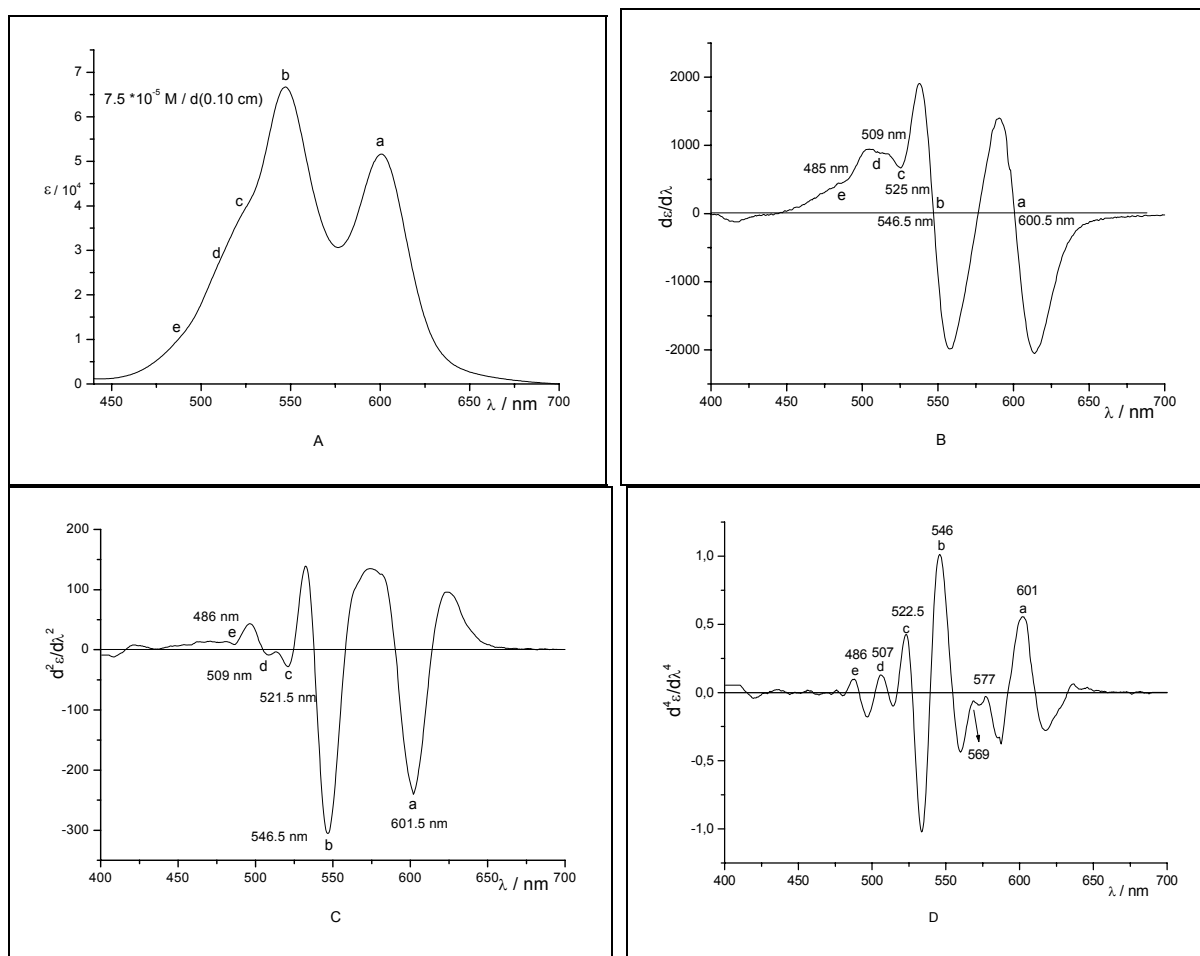


Fig. 4.5 A, B, C, and D representing the absorption and the first-, second, and fourth-derivative spectra, respectively, of a $7.5 \cdot 10^{-5}$ M pinacyanol chloride aqueous solution with 7.5 % ethanol at room temperature.

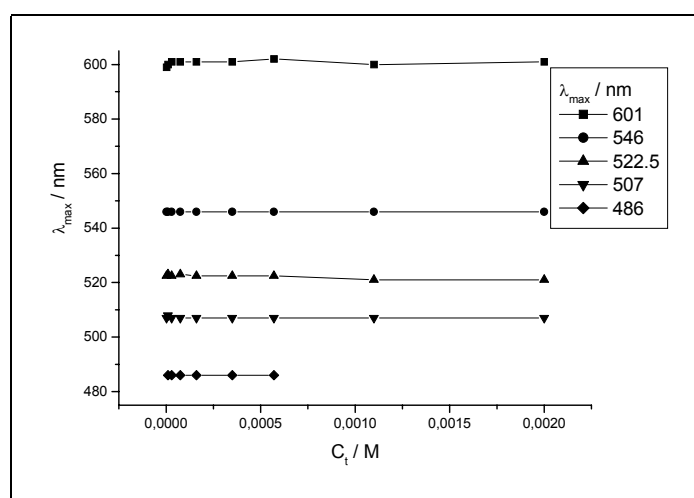


Fig. 4.6 The wavelengths of the different absorption maxima of pinacyanol chloride at different concentrations obtained from the fourth-derivative spectra of the absorbance.

4.1.5 Peak height measurements

The derivative peak amplitude D in the second-derivative spectrum of the absorbance is usually measured in the unit of the y-axis, which is $\text{cm}^{-1}\text{M}^{-1}\text{nm}^{-2}$ in our work. Figure 4.7a shows the different possibilities to obtain the intensity of a derivative peak. D_L is the long wavelength peak satellite, D_S is the short wavelength satellite, and D_B and D_Z are the peak-tangent baseline and the peak-derivative zero, respectively, which can be also used.¹⁵⁸

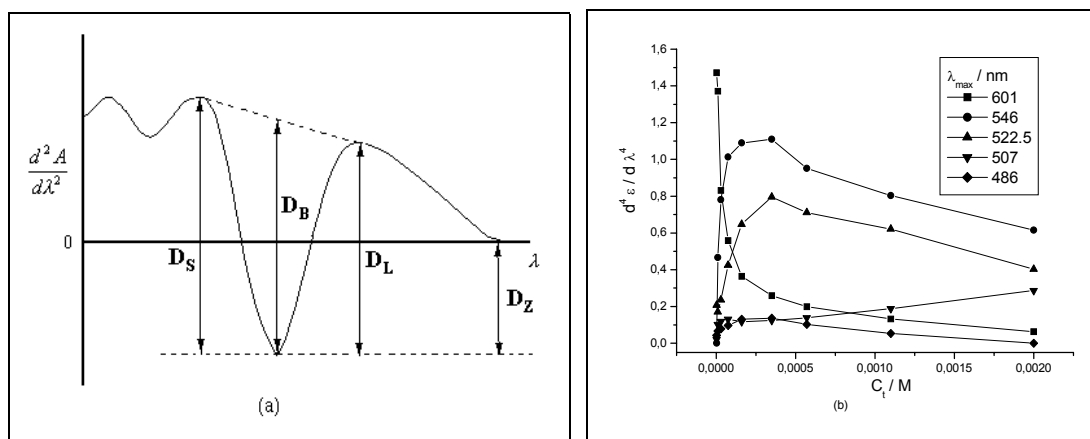


Fig. 4.7. (a) The possible ways to measure the intensity of the fourth derivative peak.¹⁵⁸ (b) The peak height of each component of pinacyanol chloride at different dye concentrations.

The peak heights of all peaks in the fourth-derivatives of the nine absorption spectra shown in Figure 4.1 were determined based on the D_Z values as shown in Figure 4.7a. The results (in units of $\text{cm}^{-1}\text{M}^{-1}\text{nm}^{-4}$) were plotted as a function of the total dye concentration to show the concentration dependence of each pinacyanol component in that range (Figure 4.7b). From this Figure, one can notice that the peak height of the monomer form at 601 nm decreases in a monotone manner as the dye concentration increases. For the dimer at 546 nm and the higher aggregates at 522.5 and 486 nm, the behaviour is different. First the peak heights increase until a dye concentration of $7.5 \cdot 10^{-5}$ M is reached, and then the peak heights start to decrease again. In contrast, the component with absorption maximum of 507 nm shows always an increase in its peak height as the dye concentration increases.

4.1.6 Analysis of the spectra using PeakFit

PeakFit v4.05 (a program acquired from Systat software Inc.) is a non-linear peak-fitting program (The analyzed data sets are directly imported from the raw ASCII data measured by

the spectrophotometer), which is capable to separate overlapping peaks of a spectrum containing different components as well as to uniquely characterize the fundamental underlying parameters for each peak component. PeakFit is unique in offering a pure analytical computation of the Voigt function, the line shape arising as a result of the convolution of the Lorentzian and Gaussian components within a spectroscopic peak. In many cases, PeakFit offers both an amplitude and area model for a given function.¹⁵⁹ Figure 4.8a shows the resolved absorption bands for the $7.5 \cdot 10^{-5}$ M pinacyanol chloride spectrum of Figure 4.1. They are, starting with long wavelengths (from the right): the monomer band at 601 nm, the first vibronic overtone at 557 nm, the dimer at 546 nm, and the higher aggregates at 522.5, 507 and 486 nm. The obtained λ_{\max} values from PeakFit are in very good agreement with the values obtained from the fourth-derivative spectra (Figure 4.6). The graph of the residuals shown in Figure 4.8b is a separate PeakFit graph activated in the Review window to display graphically the residuals of the different peaks. It depicts the difference between the experimental absorption spectrum and the spectrum calculated with PeakFit on the basis of the different components.

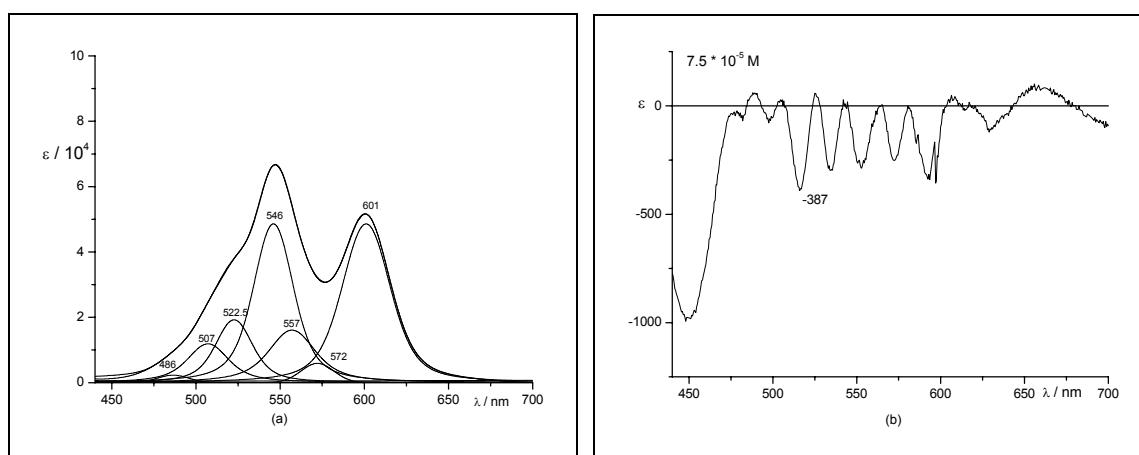


Fig. 4.8 (a) The absorption spectrum of the $7.5 \cdot 10^{-5}$ M pinacyanol chloride solution resolved into its components with PeakFit. (b) The graph of the residuals, which is the difference between the normal absorption spectrum data and the one obtained using the PeakFit data for the component.

The maximum absolute value of the residual graph shown in Figure 4.8b is $387 \text{ cm}^{-1}\text{M}^{-1}$, which is 0.6 % of the highest extinction of Figure 4.8(a). This is statistically highly acceptable according to the experimental and technical conditions. Figure 4.9 shows the peak fit results for the other eight concentrations of pinacyanol chloride presented in Figure 4.1. The percentage of residuals in their maximum values can be noted together with each of the resolved spectrum in Figure 4.9

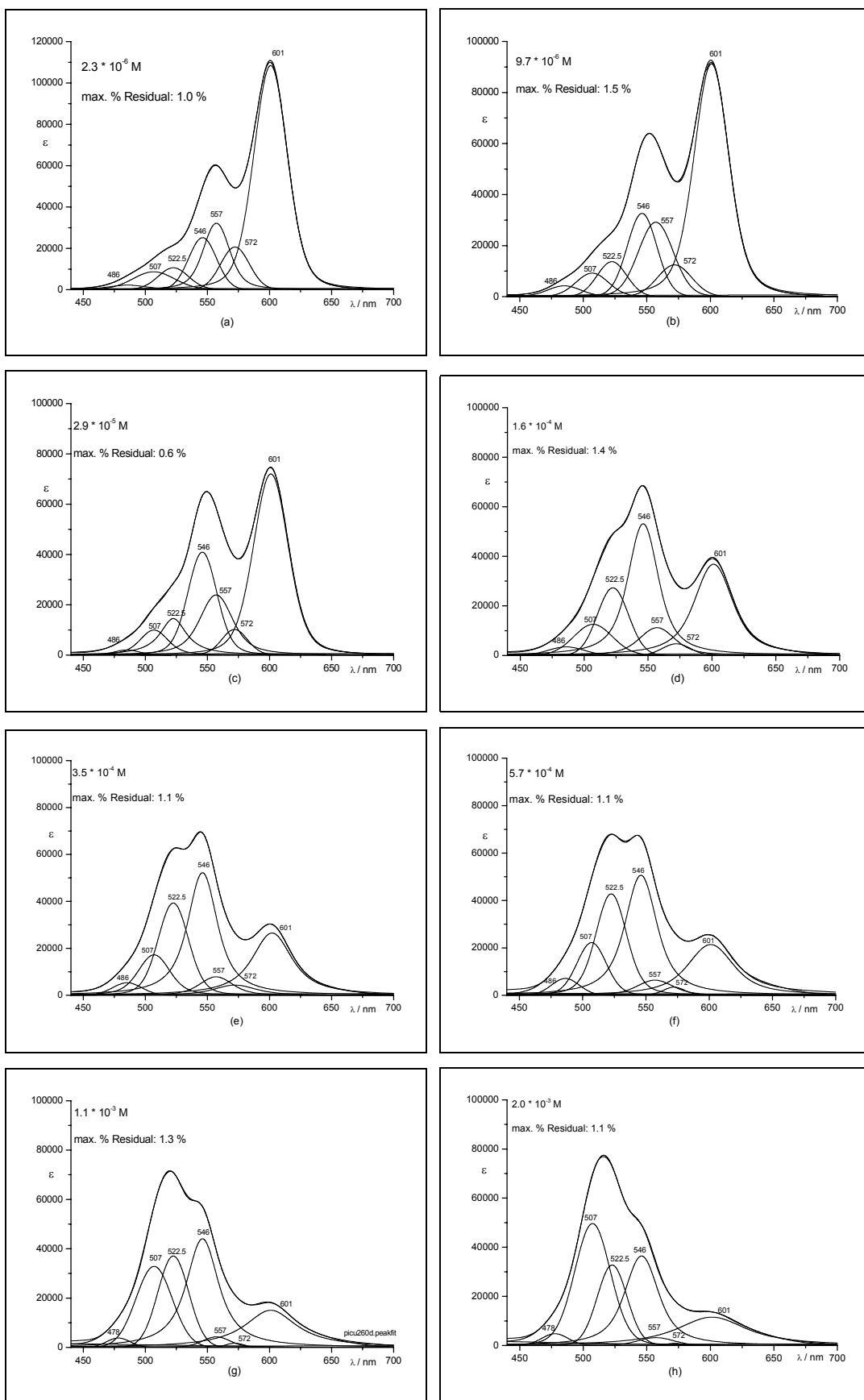


Fig. 4.9. (a – h) The absorption spectra of pinacyanol chloride, resolved into their components using PeakFit. Also shown are the percentage of residuals in their respective maximum values.

The wavelengths of the absorption maxima and their heights as obtained with PeakFit are collected for each of the different pinacyanol chloride concentrations in Figure 4.10. The position of the absorption maxima obtained with PeakFit are in good agreement with the values obtained from an analysis of the fourth-derivative spectra. The distribution of each pinacyanol component as shown in Figure 4.10b is logical with respect to the spectra in Figure 4.1 in so far as there is a continuous decrease of the monomer band height. In contrast, the dimer at 522.5 nm and the higher aggregate at 486 nm increase in the beginning and then start to decrease, but the species absorbing at 507 nm always increases. The behaviour of the vibronic overtone of the monomer is similar to the main monomer band, and their intensity ratios are constant over the range of concentrations studied.

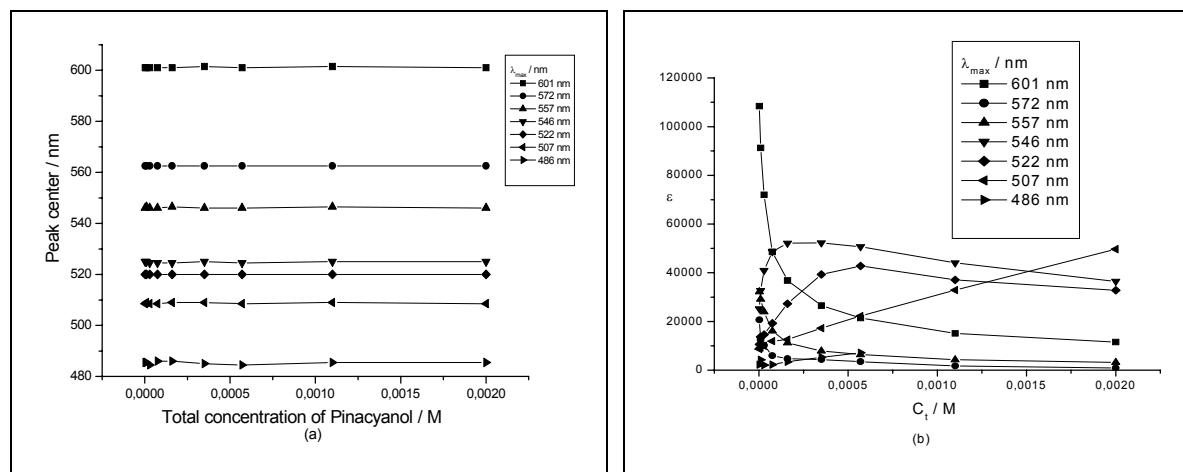


Fig. 4.10. (a) Wavelengths of absorption maxima and (b) their amplitudes for each component at different pinacyanol chloride concentrations obtained with PeakFit.

Table 4.1 summarizes the information obtained from the analysis of the spectra shown in Figure 4.1 using PeakFit. In the Table, the values of absorbances are converted to extinction coefficients and were taken directly from the PeakFit program.

Table 4.1. Absorbances of the resolved peaks of Figure 4.9.

Sol n. nr.	Total conc./M	Path length /cm	Absorbance at 601 nm	Absorbance at 557 nm	Absorbance at 546 nm	Absorbance at 522.5 nm	Absorbance at 507 nm	Absorbance at 486 nm
1.	$2.3 \cdot 10^{-6}$	2.00	0.499	0.148	0.116	0.049	0.040	0.010
2.	$9.7 \cdot 10^{-6}$	2.00	1.771	0.566	0.634	0.266	0.179	0.083
3.	$2.9 \cdot 10^{-5}$	0.50	1.045	0.347	0.594	0.211	0.145	0.030
4.	$7.5 \cdot 10^{-5}$	0.20	0.729	0.241	0.729	0.289	0.178	0.034
5.	$1.6 \cdot 10^{-4}$	0.10	0.589	0.179	0.851	0.437	0.201	0.055
6.	$3.5 \cdot 10^{-4}$	0.05	0.464	0.137	0.914	0.688	0.302	0.093
7.	$5.7 \cdot 10^{-4}$	0.01	0.122	0.036	0.289	0.244	0.127	0.041
8.	$1.1 \cdot 10^{-3}$	0.01	0.166	0.047	0.485	0.408	0.362	0.042
9.	$2.0 \cdot 10^{-3}$	0.01	0.231	0.064	0.729	0.655	0.993	0.096

Using the data of the Table we can form nine different equations with five unknown values of the extinction coefficients for pinacyanol chloride which absorb at 601, 546, 522.5, 507, and 486 nm and which may be attributed to the monomer, dimer, and three higher aggregates, respectively. The nine different equations can be formed from the following general one:

$$l C_t = C_m + 2C_d + nC_{h1} + mC_{h2} + pC_{h3} \quad (4.1)$$

$$= A_m \cdot \varepsilon_m^{-1} + 2A_d \cdot \varepsilon_d^{-1} + nA_{h1} \cdot \varepsilon_{h1}^{-1} + mA_{h2} \cdot \varepsilon_{h2}^{-1} + pA_{h3} \cdot \varepsilon_{h3}^{-1} \quad (4.2)$$

in which C_t is the total dye concentration in solution, l is the path length of absorbance, C_m , C_d , C_{h1} , C_{h2} , and C_{h3} are the concentrations of the monomer, dimer and the three higher aggregates, respectively. A 's are the absorbances and ε 's are the extinction coefficients of the different components. As an example, the equation of the solution number 1 in Table 4.1 can be written by using equation (4.2) as follows:

$$4.60 \cdot 10^{-6} = 0.499 \cdot \varepsilon_m^{-1} + 0.116 \cdot 2 \cdot \varepsilon_d^{-1} + 0.049 \cdot n \cdot \varepsilon_{h1}^{-1} + 0.040 \cdot m \cdot \varepsilon_{h2}^{-1} + 0.010 \cdot p \cdot \varepsilon_{h3}^{-1} \quad (4.3)$$

Using a 4-unknown calculator ¹⁶⁰ and ignoring the absorbance of the aggregate at 486 nm, which is justified considering its very low intensity, we obtain the following results for the first four unknowns:

$$\varepsilon_m^{-1} = 5.395 \cdot 10^{-6}; 2 \cdot \varepsilon_d^{-1} = 1.224 \cdot 10^{-5}; n \cdot \varepsilon_{h1}^{-1} = 1.480 \cdot 10^{-6}; m \cdot \varepsilon_{h2}^{-1} = 9.170 \cdot 10^{-6}$$

therefore, $\varepsilon_m = 185\,350 \text{ cm}^{-1}\text{M}^{-1}$, $\varepsilon_d = 163\,400 \text{ cm}^{-1}\text{M}^{-1}$, $\varepsilon_{h1} = 2\,027\,000 \text{ cm}^{-1}\text{M}^{-1}$ if $n = 3$, $\varepsilon_{h2} = 436\,200 \text{ cm}^{-1}\text{M}^{-1}$ if $m = 4$.

By using a 3-unknown calculator ¹⁶¹ and by again ignoring the absorbance of the aggregate at 486 nm and additionally ignoring absorption at 522.5 nm (Its ε value is unreasonable, and it behaves similar to dimer form, so that can be assumed to be a vibronic transition band of the dimer form) (see figures 4.7b and 4.10b), we obtain the following values for the three unknowns:

$$\varepsilon_m^{-1} = 5.263 \cdot 10^{-6}; 2 \cdot \varepsilon_d^{-1} = 1.304 \cdot 10^{-5}; m \cdot \varepsilon_{h2}^{-1} = 9.698 \cdot 10^{-6}$$

therefore, $\varepsilon_m = 190\,000 \text{ cm}^{-1} \text{ M}^{-1}$, $\varepsilon_d = 153\,400 \text{ cm}^{-1} \text{ M}^{-1}$, $\varepsilon_{h2} = 309\,350 \text{ cm}^{-1} \text{ M}^{-1}$ if $m = 3$.

4.1.7 Thermodynamic considerations

Not only the concentration, but also other external factors, such as the temperature, affect the equilibrium between the different aggregated species of the dye in solution. Figure 4.11 shows how increasing the temperature from 10.0 to 50.0 °C changes the equilibrium between the monomeric and the dimeric form of pinacyanol chloride in aqueous solution with 7.5 % ethanol added. At higher temperatures there is a significant increase in the concentration of the dimer; we also note that upon lowering the temperature there is a significant increase of the absorbance at higher wave numbers. We also note the formation of isosbestic points at 557 and 640 nm.

In order to evaluate ΔH° , ΔS° , and ΔG° , which represent the standard enthalpy change, the standard entropy change and the standard free energy change of the dimerization process, the temperature dependence of the equilibrium constant for the dimerization has to be studied. The concentration of the monomer and dimer, C_m and C_d , respectively, at low concentration can in good approximation be written as:

$$\frac{C_d}{C_m^2} = K_d \tag{4.4}$$

where K_d is the association constant of the dimer. Because the solution was measured at five different temperatures, five different values of K_d can be obtained and the temperature dependence be studied. The different values of C_d and C_m at each temperature have been obtained by using PeakFit as described before in section 4.1.6.

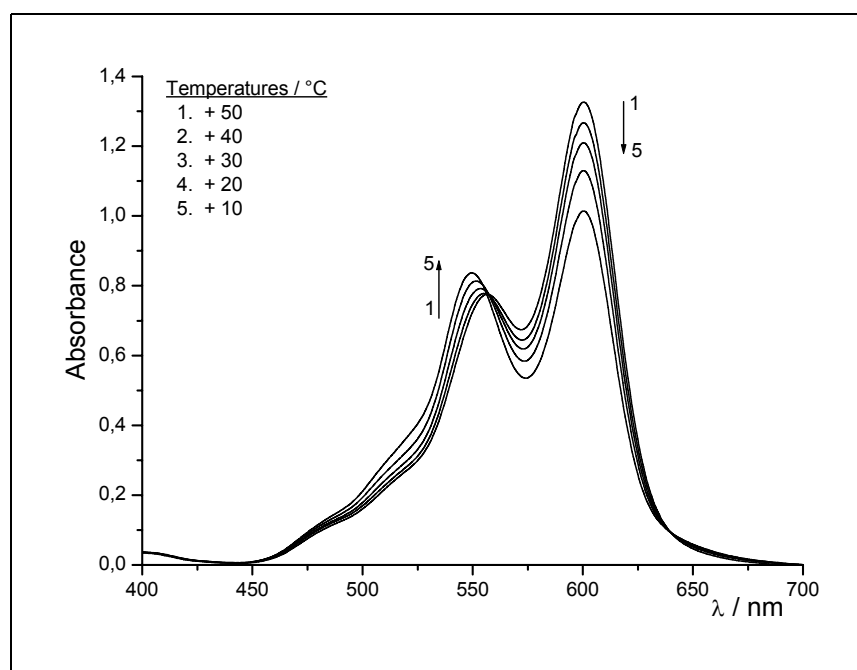


Fig. 4.11. The temperature dependence of the equilibrium between monomer and dimer forms of pinacyanol chloride ($1.5 \cdot 10^{-5} \text{ M}$) in aqueous solution with 7.5 % ethanol added.

Table 4.2 lists the absorbances and concentrations of the monomer and dimer forms, which can be calculated from the assumed values of the extinction ($190\,000$ and $153\,400 \text{ cm}^{-1} \text{ M}^{-1}$, respectively) and the calculated dimerization constant K_d at each of the five different temperatures studied. The change of density solvent within the used temperature range is not significant according to our experimental conditions. The error is less than 1% of the total dye concentration.

Table 4.2. Absorbance and concentration of the monomer and dimer forms in a pinacyanol chloride solution ($1.50 \cdot 10^{-5}$ M) at different temperatures.

Temperature / °C	Absorbance, 601 nm	Absorbance, 546 nm	[Monomer] / M	[Dimer] / M	K_d / M ⁻¹
50.0	1.240	0.198	$6.526 \cdot 10^{-6}$	$1.291 \cdot 10^{-6}$	$3.031 \cdot 10^4$
40.0	1.192	0.233	$6.274 \cdot 10^{-6}$	$1.519 \cdot 10^{-6}$	$3.859 \cdot 10^4$
30.0	1.131	0.285	$5.953 \cdot 10^{-6}$	$1.858 \cdot 10^{-6}$	$5.243 \cdot 10^4$
20.0	1.048	0.338	$5.516 \cdot 10^{-6}$	$2.203 \cdot 10^{-6}$	$7.240 \cdot 10^4$
10.0	0.931	0.389	$4.900 \cdot 10^{-6}$	$2.536 \cdot 10^{-6}$	$1.056 \cdot 10^5$

The values of ΔH° and ΔS° at 298 K were obtained by subjecting the data of Table 4.2 to a linear regression analysis according to the following thermodynamic equation:

$$2.303 R \cdot \log K_d = - \Delta H^\circ (1/T) + \Delta S^\circ \quad (4.5)$$

where ΔH° and ΔS° are obtained from the slope and intercept of equation 4.5. The value of ΔG° can be calculated according to the following thermodynamic equation:

$$\Delta G^\circ = \Delta H^\circ - 298 \Delta S^\circ \quad (4.6)$$

From the straight linear plot shown in Figure 4.12, with a correlation coefficient of 0.999, the following values are obtained: $\Delta H^\circ = - 5696 \text{ calmol}^{-1}$, $\Delta S^\circ = 2.8 \text{ calmol}^{-1}\text{K}^{-1}$ and $\Delta G^\circ = - 6540 \text{ calmol}^{-1}$. The negative value of ΔH° shows that the dimerization process of pinacyanol chloride is exothermic. The absolute value of ΔH° is less than expected for interactions in which covalent or electrostatic bonding is operative. The negative value of ΔG° indicates that the dimerization process is spontaneous. The slightly positive value of ΔS° shows that the dimerization process is accompanied by an entropy increase.

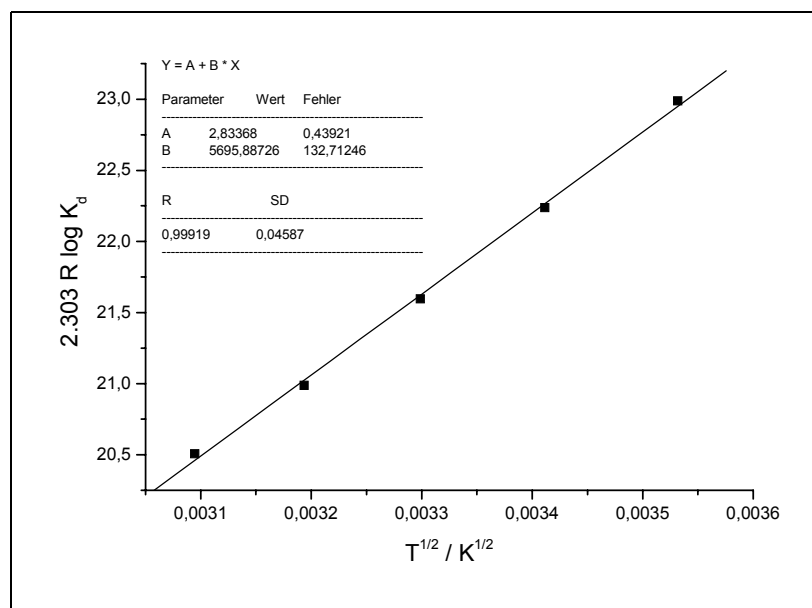


Fig. 4.12. Plot of equation 4.5 for the dimerization process of pinacyanol chloride in aqueous solution with 7.5 % ethanol added.

The values for the dimerization constant of pinacyanol chloride, obtained in this study, are in the order of 10^4 M^{-1} (Table 4.2), which is consistent with literature results. For example, West and Pearce have reported values of $2.9 \cdot 10^4 \text{ M}^{-1}$ and $6.7 \cdot 10^4 \text{ M}^{-1}$ as the dimerization constants of 3,3'-diethylthiacarbonycyanine iodide and 3,3'-diethylthiadicyanone iodide, respectively.¹⁶ Min and co-workers reported a value of $9.8 \cdot 10^4 \text{ M}^{-1}$ for 1,1'-diethyl-2,2'-carbocyanine iodide (pinacyanol iodide).¹⁶² They also reported a value of $-6.7 \text{ kcal mol}^{-1}$ for the enthalpy of dimerization, ΔH° , of pinacyanol iodide in water. Our result, $-5.7 \text{ kcal mol}^{-1}$ for pinacyanol chloride in 7.5 % ethanol/water, is not far from their value.

4.1.8 Discussion

There are two factors that contribute to the self-association of pinacyanol chloride in water without the addition of any aggregation agents. One is the so-called hydrophobic force, which minimizes the interaction between the solvent water and the hydrophobic solute by forming aggregates with lower exposed surface. In addition there are strong intermolecular or van der Waals-like attractive forces between the dye molecules that are supported by the flat geometry of dye molecules and lead to the preferred stacked structures of the aggregates. In solution

these aggregates exhibit distinct spectral changes compared to the monomeric dye molecules, which have been used here to deduce the aggregation pattern and the size of the aggregates.

In Figure 4.1, several different components with strongly overlapping absorbances at 600, 555, 545, and between 525 and 515 nm are observed in aqueous pinacyanol chloride solutions at different concentrations. By converting the spectra into the fourth derivative spectra it was possible quantitatively to analyze bands in the overlapping region with respect to their absorbance maxima and their peak heights. Figure 4.6 shows five different bands of pinacyanol chloride that have fixed absorbance maxima in the concentration range from $2.3 \cdot 10^{-6}$ to $2.3 \cdot 10^{-3}$ M. The wavelengths corresponding to these maxima are, respectively, 601, 546, 522.5, 507, and 486 nm. Only the absorption at 601 nm belongs to the monomer. The position of the vibronic overtone band has been established from the spectra in pure ethanol (Figure 4.4). This conclusion is supported by the evidence presented in Fig. 4.10b, which shows the peak heights at the absorbance maxima as a function of the concentration. Only the band corresponding to the 601 nm monomer absorption displays a monotonous decrease in height with increasing concentration.

Using as a general directive that the blueshift of an H-type aggregate increases with increasing number of monomers, we propose that the band at 546 nm corresponds to a sandwich type dimer of pinacyanol. The very similar behaviour of the 522 nm band can be interpreted in two different ways. Either this band corresponds to a vibrational overtone of the dimer band (absorbing at 546 nm), or it represents a dimer of different geometry and therefore different absorbance. The energy splitting of the two bands at 546 and 522 nm of 842 cm^{-1} is in the same range, but significantly smaller than for the monomer. However, the presence of a different dimer cannot be ruled out either. The 507 nm band shows a completely different behaviour than the ones discussed so far, since its height increases almost linearly after a certain concentration has been reached. Especially puzzling is the fact that even at the highest concentrations the band does not show any levelling, which one would expect if there were significant dissociation and aggregation into an even larger aggregate. In the absence of more information we assign this peak to a trimer or higher aggregate.

After using the PeakFit program to analyse the spectra of all the pinacyanol components in Fig. 4.1 and calculating the extinction coefficients for these components, the band at 522.5 nm yields only unreasonable extinction coefficients. From Table 4.1, and after ignoring the two bands at 522.5 and 486 nm in the calculation, values for the extinction coefficients of the monomer, dimer, and a higher aggregate at 601, 546 and 507 nm are obtained by using a 3-unknown calculator; these values are, respectively, 190 000, 153 400, and $309\,350 \text{ cm}^{-1}\text{M}^{-1}$.

From the absorbances and the cell constants given in Table 4.1 the total dye concentration was calculated according to

$$C_t = A_m / \epsilon_m \cdot l + 2 A_d / \epsilon_d \cdot l + 3A_t / \epsilon_t \cdot l \quad (4.7)$$

The calculated total dye concentrations for the nine different solutions are in good agreement with the dye concentration used to prepare the samples and feature an error of less than 1%. From the slope of the extinction coefficient of the monomer form in 100% ethanol at 606 nm against concentration (Fig. 4.3b), an extinction coefficient of 175 200 cm⁻¹M⁻¹ is obtained. The difference between this value and the value found with the PeakFit program (190 000 cm⁻¹M⁻¹) may reflect a solvent effect apart from a possible error coming from the different method that was used. The extinction coefficient of the pinacyanol dimer, which is present in high concentration in the γ -cyclodextrin cavity, was estimated from the visible spectra (see next section, Fig. 4.15a). The value is 142 000 cm⁻¹M⁻¹ which is in good agreement with the value calculated by using the PeakFit program (153 400 cm⁻¹M⁻¹).

A blue shift in the maximum wavelength of the visible absorption band of a dye indicates near vertical stack aggregation of the dye molecules and depends on the number of monomers in the aggregate. In addition to the dimer, which absorbs at 546 nm and considering the calculated extinction coefficients, we attribute the band at 507 nm to the trimeric state of the dye. Formation of higher aggregates is possible on the one hand in equilibrium with and on the other hand at the cost of dimer and trimer aggregates. Experimentally, such higher aggregates are difficult to detect due to the very low concentrations and the overlap of their bands with the intense dimer and trimer aggregates. The aggregate absorbing at 486 nm behaves like another dimer form (see figure 4.7b); increasing the total dye concentration reduces the intensity of this band, which eventually disappears completely. The new band with relatively low intensity which appears at 478 nm (Fig. 4.9) may be attributed to a higher aggregated form than the trimer.

4.2 The inclusion of pinacyanol chloride by cyclodextrins

The formation of inclusion complexes in aqueous solution between guest molecules and cyclodextrin as a host can be detected by spectrophotometric methods if, as a consequence of the inclusion process, the spectrum of the guest molecules is altered. Such alterations may include changes in the intensity of an absorption band, shifts in the absorption maxima, and the occurrence of isosbestic points. If the guest molecules, such as pinacyanol chloride, are achiral, they may exhibit induced circular dichroism (ICD) in the chiral environment of the cyclodextrin. Such changes are illustrated in the following section.

4.2.1 Interaction with γ -cyclodextrin - UV/Vis spectra

Figure 4.13a shows the effect of γ -cyclodextrin on the visible spectra of pinacyanol chloride ($2.0 \cdot 10^{-4}$ M) in aqueous solution. As shown in the preceding section, the solution of the free dye presents as a mixture of several components. The addition of γ -cyclodextrin to this mixture resulted in a decrease of the intensity of the bands at 600 and 522 nm, and an increase in the intensity of the band at 545 nm. This increase is accompanied by a red shift, reaching a value of 556 nm at higher γ -cyclodextrin concentrations. The presence of two isosbestic points at 587 and 617 nm is noted as the host concentration is increased. Figure 4.13b shows the effect of added γ -cyclodextrin on the visible spectra of pinacyanol chloride ($1.5 \cdot 10^{-5}$ M) in aqueous solution, in which the dye molecules are present mainly as monomers and dimers. In this case the addition of the cyclodextrin leads to a decrease in the intensity of

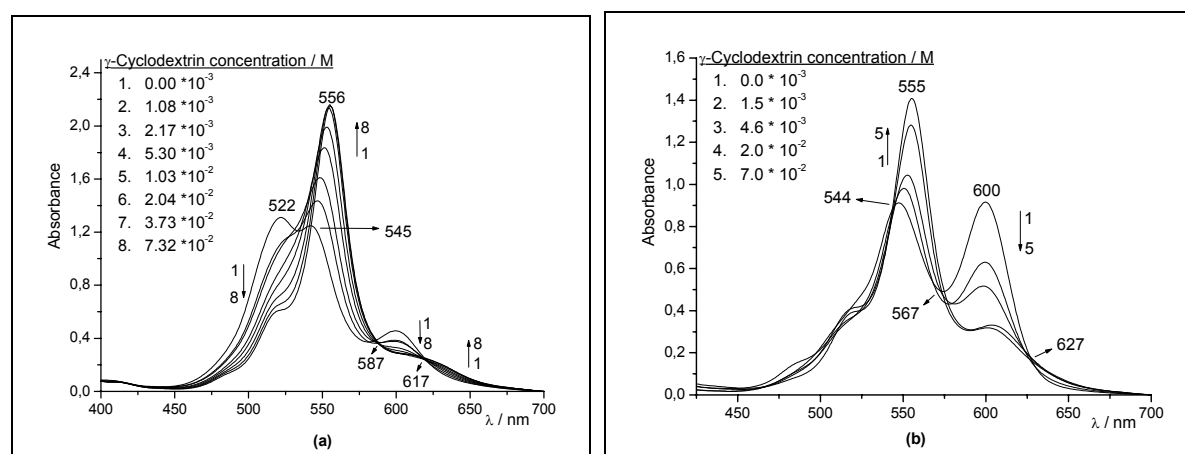


Fig. 4.13 (a) The effect of γ -cyclodextrin added to an aqueous solution of pinacyanol chloride ($2.0 \cdot 10^{-4}$ M); 0.10 cm cell at room temperature. (b) The effect of γ -cyclodextrin added to an aqueous solution of pinacyanol chloride ($1.5 \cdot 10^{-5}$ M); 1.00 cm cell at room temperature.

the band at 600 nm and increase in the intensity of the band at 545 nm, the latter accompanied by a significant shift toward lower energy. Three isosbestic points are visible and appear at 567, 627, and 544 nm.

4.2.1.1 The fourth derivative of the visible spectra

Figure 4.14a shows the fourth derivative spectra of all the spectra given in Figure 4.13a. The changes in the intensity of the absorption bands and the red shifts of the bands maxima become more clear and quantitatively can be measured, as indicated in Figure 4.13b. The intensity increase of the bands at 507, 545.5 and 572 nm, and the intensity decrease of the bands at 484, 522, and 601 nm are clearly visible in Figure 4.13b. The increase of what we have shown to be the dimer band at 545.5 nm indicates a favorable interaction between pinacyanol chloride as dimer and the γ -cyclodextrin host, probably occurring inside the cyclodextrin cavity. The intensity increase of the band at 507 nm, which we have attributed to one of the higher aggregates, probably a trimer, indicates likewise that the cyclodextrin host promotes this aggregation. However, for steric reasons this interaction must occur outside the cavity or through partial inclusion. The decrease in the intensity of the band at 522 nm, which we have attributed to the vibronic band of the dimer, may be a consequence of the different kind of interaction in the dimer or of the change of the environment from aqueous to organic nonpolar inside the cyclodextrin cavity.

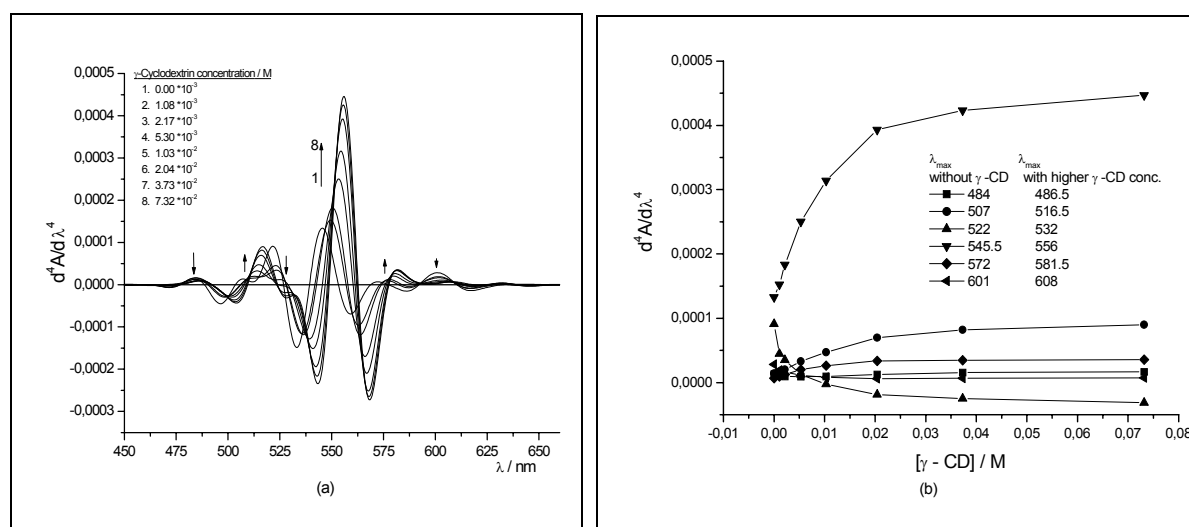


Fig. 4.14. (a) The fourth derivative of the spectra shown in Figure 4.13a. (b) The peak heights of the bands in Figure 4.14a as a function of the γ -cyclodextrin concentration.

4.2.2 Interaction with γ -cyclodextrin -Circular Dichroism spectra

Figure 4.15 depicts the visible absorption and the circular dichroism spectrum of an aqueous solution of pinacyanol chloride ($7.5 \cdot 10^{-5}$ M) with $1.0 \cdot 10^{-1}$ M γ - cyclodextrin added. The CD spectrum shows two main absorption bands at 553 (negative) and 670 nm (positive) in addition to a small positive band at 603 nm and two shoulders at 516 and 484 nm. Figure 4.16, in which the concentrations of the dye and of the cyclodextrin host are different, shows spectra, which are very similar to the ones shown in Figure 4.15. Especially the bands of the CD spectrum in Figure 4.16 have identical positions as in Figure 4.15. Again there are two main bands with opposite signs at 553 ($18\ 080\ \text{cm}^{-1}$) and 670 nm ($14\ 925\ \text{cm}^{-1}$). The mean of these two energies is $16\ 500\ \text{cm}^{-1}$ or 603 nm, which is identical to the position of the monomer absorption band. It can be safely assumed that the two bands correspond to the two exciton states of the dye in its dimeric aggregation state. The weak negative band at 516 nm ($19\ 380\ \text{cm}^{-1}$), the positive CD band at 603 ($16\ 500\ \text{cm}^{-1}$) and the positive shoulder at 726 nm ($13\ 770\ \text{cm}^{-1}$) which can be seen more clearly in Figure 4.15b, are ascribed tentatively to the trimer form of pinacyanol chloride. Again, they have an average energy of $16\ 575\ \text{cm}^{-1}$, which is identical to the energy of the monomer at 603 nm ($16\ 500\ \text{cm}^{-1}$), and the trimeric aggregates generate three exciton states.

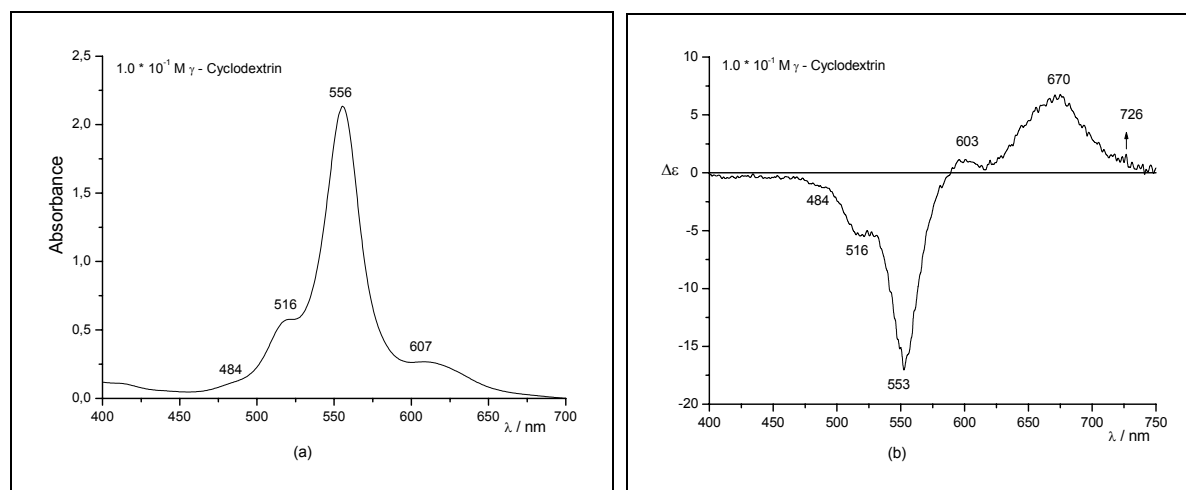


Fig. 4.15. The visible absorption spectrum (a) and the CD spectrum (b) of pinacyanol chloride ($7.5 \cdot 10^{-5}$ M) and γ -cyclodextrin ($1.0 \cdot 10^{-1}$ M) in aqueous solution; 0.20 cm cell at room temperature.

As was discussed in detail in section 3.2.4, interaction of chromophores under favourable circumstances may result in the formation of delocalised exciton states with energy separations depending on the relative orientation of the monomers. In a chiral environment the exciton states may acquire rotational strengths enabling their identification in a CD spectrum.

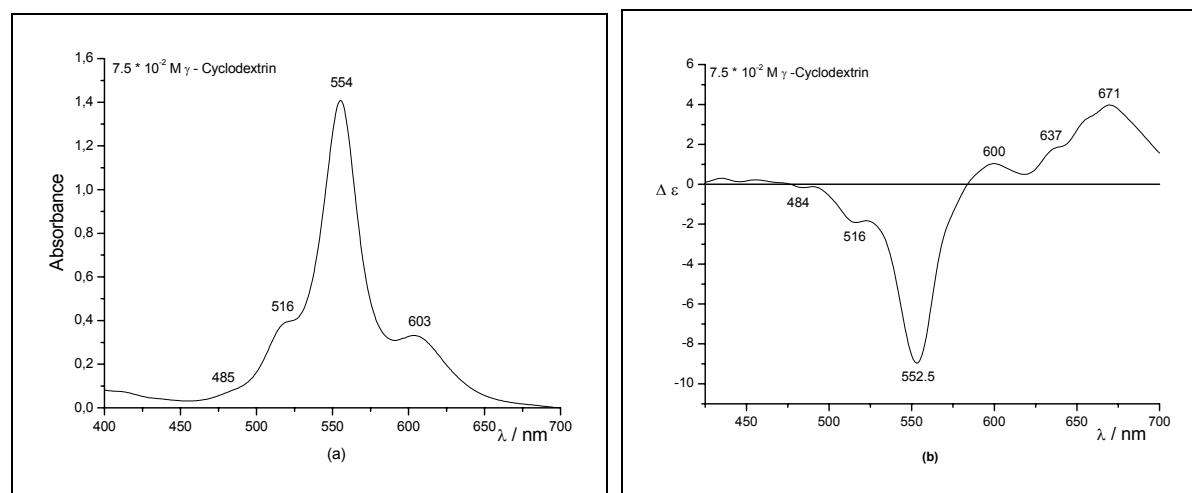


Fig. 4.16. The visible absorption spectrum (a) and the CD spectrum (b) of pinacyanol chloride ($1.5 \cdot 10^{-5}$ M) and γ -cyclodextrin ($7.5 \cdot 10^{-2}$ M) in aqueous solution; 1.00 cm cell at room temperature.

The exciton states of a dimer always have opposite signs, and they are displaced symmetrically from the absorption of the monomer; this is shown by the two bands at 552 and 671 nm. Such a dimer shows no absorbance at the monomer energy in the UV/Vis or CD spectrum. From the intensity of the exciton states in ordinary absorption one can deduce qualitatively the relative orientation of the two components of the dimer. If, as in Figures 4.15a and 4.16a, only the high-energy component of the dimer bands is visible, the two components aggregate in a face-to-face (“H-type”) manner with an acute angle between their long axes. In a trimer, the three monomer excitations split into three exciton states, of which two are again symmetrically displaced from the monomer absorption, and the third is observed at the wavelength, where the monomer absorbs.¹⁶³ This appears to be a valid interpretation of the three additional bands in Figures 4.15a and 4.16a as discussed above.

In Figure 4.15b the negative and the positive CD bands at 553 and 670 nm, respectively, have an approximately Gaussian shape, in spite of the presence of shoulders beside the bands. The rotational strengths associated with these bands were evaluated directly from the spectrum using the formula, which applies to the evaluation of approximately Gaussian

shaped curves as in equation (3.26) and Figure 3.3. The values obtained are respectively, $-2.36 \cdot 10^{-39}$ and $1.30 \cdot 10^{-39}$ cgs units for the two bands. Theoretically, the two values should be the same; their mean absolute value is $1.83 \cdot 10^{-39}$ cgs units, and this value will be used in the coupled oscillator calculations.

4.2.3 The dipole strength of pinacyanol chloride

From the visible spectrum of pinacyanol chloride in 100 % ethanol (Figure 4.17), in which the dye is present in an approximately pure monomer state, the dipole strength of the dye can be obtained according to the equations given in the section on UV/Vis spectrometry. Thus, the oscillator strength of the absorption band shown in Figure 4.17 is:

$$\begin{aligned} A_i &= \epsilon_{\max} N_{1/2} \\ &= (186\,826 \text{ M}^{-1}\text{cm}^{-1}) (872 \text{ cm}^{-1}) \\ &= 1.6 \cdot 10^8 \text{ M}^{-1}\text{cm}^{-2} \end{aligned}$$

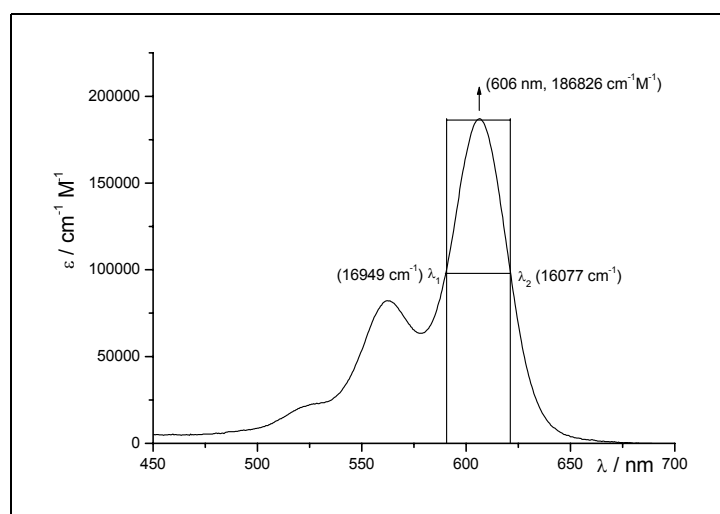


Fig. 4.17. Absorption spectrum of pinacyanol chloride ($1.15 \cdot 10^{-6}$ M) in 100 % ethanol.

From this, the oscillator strength f is calculated as:

$$f = 4.315 \cdot 10^{-9} \cdot A_i = 0.7037$$

The dipole strength D of the pinocyanol absorption band is then obtained as:

$$D = \frac{3he^2}{8\pi^2 m_e c \bar{\nu}_{\max}} f$$

$$= 1.00857 \cdot 10^{-57} \text{ m}^2 \text{C}^2$$

The electric transition moment is

$$\mu = \sqrt{D} = 3.1758 \cdot 10^{-29} \text{ Cm}$$

which, with the unit electron charge e , translates into a length of the transition moment of

$$r = \frac{3.1758 \cdot 10^{-29}}{1.6022 \cdot 10^{-19}} = 1.982 \text{ \AA}$$

4.2.4 Modelling the pinacyanol aggregation with OSCI

The blue-shifted aggregate spectra of pinacyanol chloride in aqueous solution provide strong evidence for a face-to-face one-dimensional arrangement of the dye molecules. In order to model these aggregates, calculations were performed with the OSCI program. This program needs, as input data, the data for the isolated chromophore excitations, in particular the absorption maximum (in nm) and the length and the charge of each of the dipole contributing to the aggregate. In the case of the pinacyanol aggregate these data have been obtained in the preceding section. For calculating the interaction matrix, a model of the aggregate is built in 3-dimensional space, and from the Cartesian coordinates the interaction matrix is set up using the extended dipole model for calculating the interaction potential.

As was pointed out in the section presenting the OSCI method, there is an adjustable parameter in the model in that the length and the charge of the extended dipoles can be adjusted to best fit the experimental data, with the restriction, that the product of the transition moment length and charge be constant. With this in mind, eight different parameter sets were developed and applied to 9 molecular aggregates of pinacyanol of different aggregate size. Four different combinations of transition dipole lengths and charges all leading to the same transition dipole moment of $3.175889 \cdot 10^{-29} \text{ Cm}$ were combined each with two different distances of the monomer molecular planes in the aggregate, 3.5 and 4.0 Å. Table 4.3 lists the entry data for the eight different sets to be used in the coupled oscillator program. With each of the eight data sets, nine stacked dye aggregates were calculated which differed in the numbers of monomers ranging from 2 to 20. There was no internal twist applied to the aggregates, *i.e.* they were achiral. The calculated blue shifts of the highest energy exciton states of each aggregate with each set of entry data are depicted graphically in Figure 4.18.

Table 4.3. The eight different entry sets for the OSCI program.

model #	dipole charge / 10^{-20} C	dipole length / Å	monomer distance / Å
1.	16.0219	1.9821	3.5
2.	8.01095	3.9642	3.5
3.	4.00547	7.9284	3.5
4.	2.00274	15.857	3.5
5.	16.0219	1.9821	4.0
6.	8.01095	3.9642	4.0
7.	4.00547	7.9284	4.0
8.	2.00274	15.857	4.0

Figure 4.18 shows graphically the calculated wavelength shifts of the nine aggregates calculated with the 8 different data sets. The experimentally observed wavelength shift of the dimer relative to the monomer is 55 nm. The data set that comes closest to this value is #7, which gives a blue shift of 540.6 nm. By fine-tuning the dipole length and charge to 8.50 Å and $3.7361 \cdot 10^{-20}$ C, respectively, the experimental result is reproduced quantitatively. We call this dipole, together with the distance of 4 Å and 0° angle twist the data set #7*. The maximum wavelength values belong to the points from *a* to *i* in figure 4.18 are respectively 546, 517.5, 491, 484, 479, 475, 470, and 460 nm.

With increasing aggregate size the blue-shift increases, but not in a linear manner, but approaching a limiting value instead. With an aggregate size of 20 stacked dye molecules the limit is not quite reached, but a good estimate is obtained where the infinite aggregate might absorb. The different data sets differ significantly in the predicted blue-shift of the infinite aggregate, from about 60 nm for set # 8 to more than 340 nm for set # 1. With the set which reproduces the dimer shift rather well (# 7*) the calculated wavelength shift of the very large aggregate is 125 nm which corresponds to an absorption maximum at 476 nm in surprisingly good agreement with the value found for the limiting aggregate (Figure 4.18).

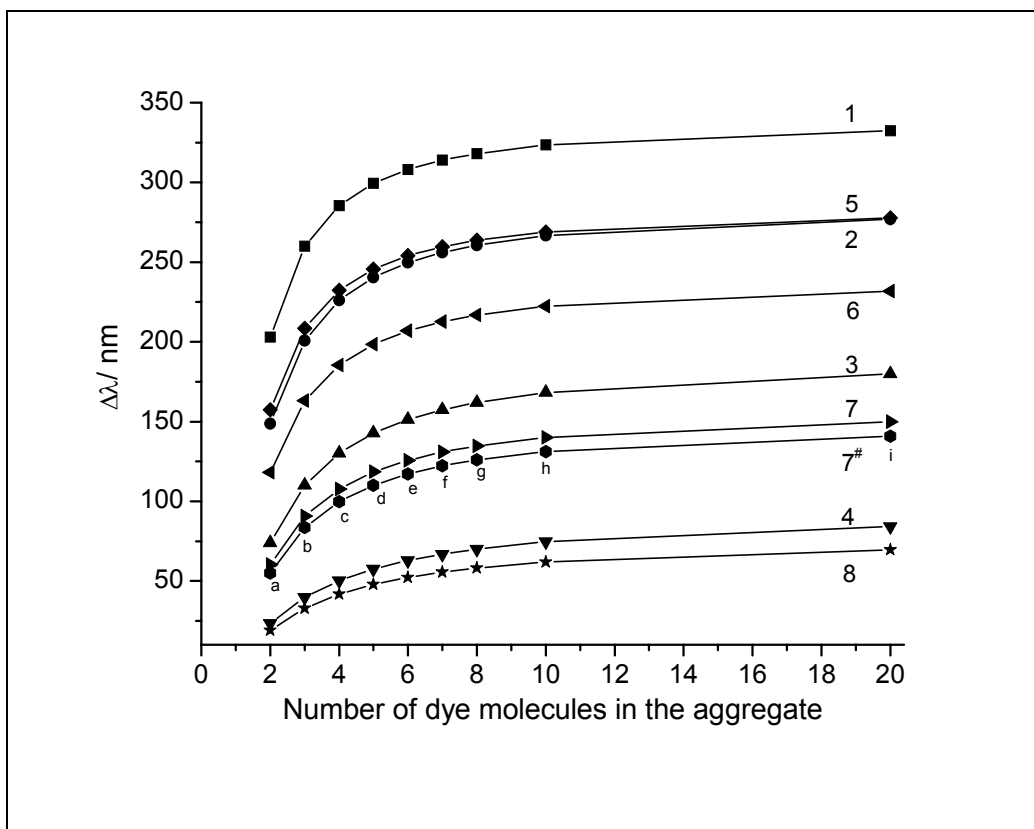


Fig. 4.18. The blue shift of pinacyanol chloride as a function of its aggregation state calculated with different values of dipole length and charge.

4.2.5 Calculating the twist angle of pinacyanol chloride in γ -cyclodextrin

The experimental value for the rotational strength of the two exciton states of the pinacyanol dimer in γ -cyclodextrin is $1.83 \cdot 10^{-39}$ cgs units. If this rotational strength is due to a twist of the two dye molecules against each other, OSCI allows to calculate the twist angle. For this, different twist angles are used as input data, together with the data derived in the preceding section, and oscillator and rotational strengths calculated on the basis of the assumed structure. Entering the data of set # 7* into OSCI and increasing the twist angle in steps of 0.3° one thus obtains the rotational strength as a function of the twist angle of the dye molecules against each other.

Figure 4.19a shows that this function is linear: the greater the twist, the greater the rotational strength. The angle, which is appropriate to the observed rotational strength from the CD spectrum, is 1.1° . Figure 4.19b is a three-dimensional representation of the two identical dipoles of pinacyanol chloride with a twisting angle of 1.1° .

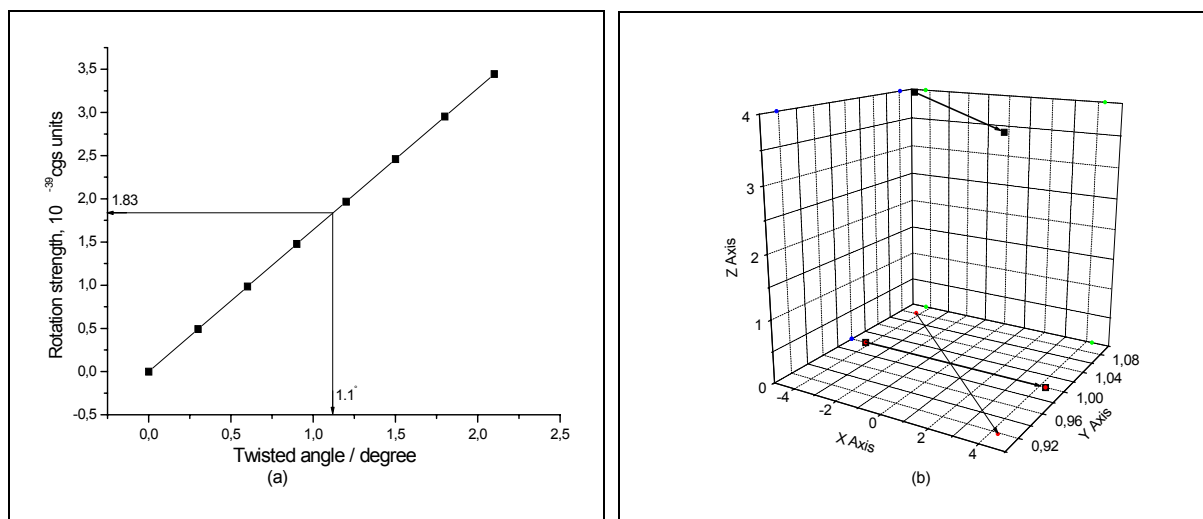


Fig. 4.19. (a) Rotational strength as a function of the twisted angle of the pinacyanol dimer (b) Three-dimensional presentation of the twisted pinacyanol dimer with a 1.1° angle of twist.

4.2.6 Discussion

The difference between the spontaneous aggregation of pinacyanol chloride in water and the aggregation promoted by γ -cyclodextrin is tremendous: instead of a complex concentration dependent equilibrium involving at least four different entities, γ -cyclodextrin promotes the formation of one major aggregate which on all accounts corresponds to a face-to-face (sandwich-type) dimer. Both the intensities of the absorption bands and the shift of the absorption maximum in addition to the formation of isosbestic points attest to this. In Figure 4.13, the increase in the intensity of the dimer band of the dye as a result of adding γ -cyclodextrin is evidence to the formation of the dimer form at the cost of other forms. The red shift of the absorption maximum due to the change of the medium from (polar) water to the non-polar microenvironment inside the cavity is an indication that the dimer forms inside γ -cyclodextrin.

In the dimer, the dye molecules are twisted slightly against each other, as evidenced by the visible CD-spectra with their oppositely signed absorption bands displaced symmetrically from the monomer absorption. The twist, and the preference of one sense of twist over the other, is a consequence of the chiral surface provided by the cyclodextrin cavity. Analysis of the CD-spectra in terms of the exciton model, and the numeric calculation of rotational strength using the extended dipole model leads to a calculated splitting, the Davydov splitting, which can be adjusted, via the electric transition moments, to agree with the experimentally

observed splitting. Modelling the pinacyanol chloride with OSCI gives a value of $\sim 1^\circ$ as the twisting angle of the dimer in the γ -cyclodextrin cavity. The positive sign of the twisting angle is deduced from the positive sign of the long wavelength CD band (positive exciton chirality).

In Fig. 4.14, the intensity of the band at 507 nm, which we have attributed to one of the higher aggregates, probably a trimer, increases with addition of cyclodextrin in the solution. This increase indicates that the cyclodextrin host promotes not only the dimerization of pinacyanol chloride, but also higher aggregation, albeit to a lesser degree. For steric reasons, this type of aggregation must occur outside the cavity or through partial inclusion. In the CD spectrum of figure 4.15b, the weak negative band at 516 nm, the positive CD band at 603 and the positive shoulder at 726 nm are ascribed tentatively to this trimer. In this type of aggregate the three monomer excitations split into three exciton states, of which two are again symmetrically displaced from the monomer absorption, and the third is observed where the monomer absorbs. The decrease in the intensity of the band at 522 nm, which we have attributed to the vibronic band of the dimer, may be a consequence of the different kind of interaction in the dimer or the change of the environment from aqueous to organic non-polar inside the cyclodextrin cavity.

4.3 Interaction of pinacyanol chloride with alginates

4.3.1 Manucol-LHF; characterization by CD

Figure 4.20 shows the CD spectrum of Manucol-LHF between 195 and 250 nm. The spectrum has been taken in aqueous solution, and the concentration is 0.80 mg/ml, corresponding to $4.0 \cdot 10^{-4}$ M, if monomeric sodium mannuronate or guluronate, $C_6H_7O_6Na$, are taken as the molecular mass unit. The spectrum shows a positive peak at 200 nm, and a negative trough at 215. From the ratio of the peak to the trough amplitude (Figure 4.20) the composition of Manucol-LHF, in terms of mannuronate and guluronate can be calculated by using the equation (2.1).⁶² The calculated values are 62.9 and 37.1 %, respectively. Therefore, Manucol-LHF that was used in the following aggregation experiments contains an excess of mannuronate over guluronate in the ratio of 1.7 : 1.

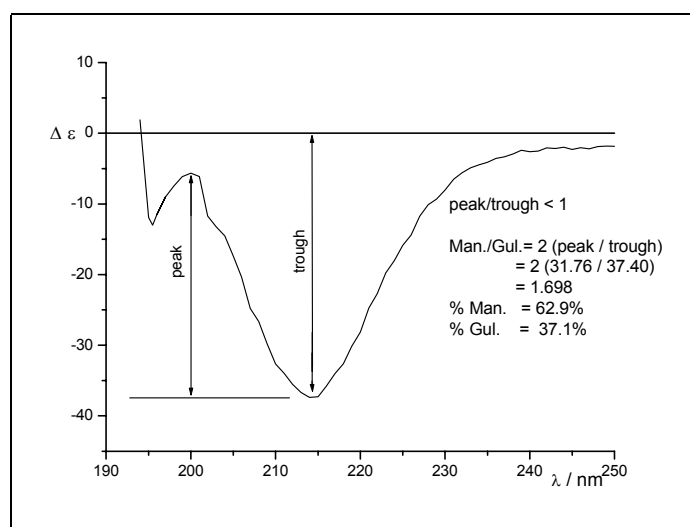


Fig. 4.20. CD-spectrum of Manucol-LHF (0.80 mg/ml); pH = 6.80, and cell width is 1.00 cm.

4.3.2 Aggregation of pinacyanol chloride with Manucol-LHF

4.3.2.1 UV/Vis and CD spectra

Ionic polymers increase the inherent tendency of many cyanine dyes to form aggregate in aqueous solution, a phenomenon that is generally called metachromasia.⁵ The effect of metachromasia can be shown in different ways; one of the most obvious is the change in absorbance, which accompanies the addition of the polymer to a dye solution. Figure 4.21 presents the UV/Vis spectra of a $1.5 \cdot 10^{-5}$ M aqueous solution of pinacyanol chloride in the

presence of different concentrations of Manucol-LHF, from $1.50 \cdot 10^{-5}$ to $3.75 \cdot 10^{-4}$ M, covering a molar concentration ratio of polysaccharide to dye from 1:1 to 25:1. The aggregating effect of the polysaccharide is easily seen. The absorption maxima of the free dye are found at 600, 546, 507 nm; there is a slight shoulder at about 485 nm. The initial effect of Manucol-LHF is to broaden the spectrum between 550 and 585 and to develop the shoulder at 485 nm into a separate band. There is, in addition to the blue-shifted bands, a red-shifted shoulder at around 630 nm. Increasing the polysaccharide concentration shifts the intensity more and more to this short wavelength band. The highest absorbance of this band is observed at a polysaccharide to dye ratio of 10:1 (curve # 6 in Figure 4.21). Increasing this ratio still further reverses this effect: the intensity of the 485 nm band starts to decrease, while the broad absorbance between 555 and 585 nm starts to increase again.

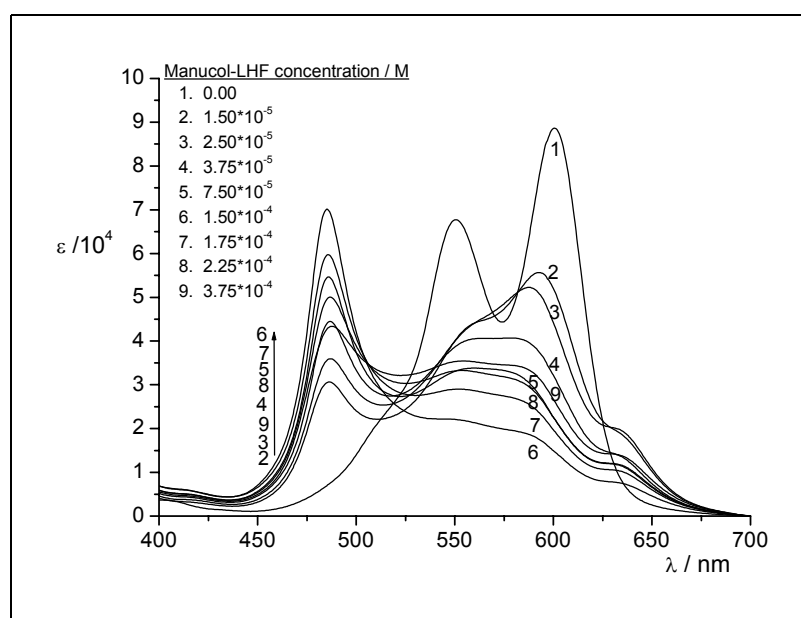


Fig. 4.21. The visible absorption spectra of an aqueous solution of $1.50 \cdot 10^{-5}$ M pinacyanol chloride in the presence of eight different concentrations of Manucol-LHF at room temperature. 7.5 % v/v ethanol have been added to increase the solubility of the dye.

Figure 4.22 shows the CD spectra of the different solutions taken under identical conditions as in Figure 4.21. In the absence of Manucol-LHF there is, as expected, no circular dichroic and only the base line is recorded. At low polysaccharide/dye ratios there is an S-shaped absorption band between 500 and 600 nm; the red-shifted shoulder at 630 nm shows as a distinct positive band in the CD. Increasing the ratio leads to a very sharp couplet with a zero-point crossing at 485 nm. This couplet reaches its maximum amplitude at a polymer to

dye ratio of 10:1, which also corresponds to the maximum absorbance of the 485 nm band in figure 4.21. Also, as is observed in the UV/Vis spectra, the intensity of the couplet decreases as the polymer to dye ratio is increased further; the couplet finally collapses and a negative band remains.

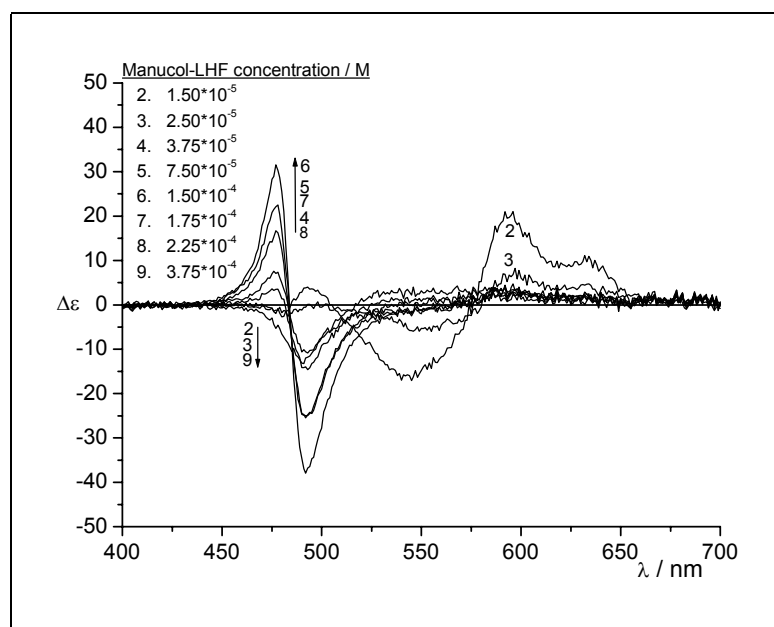


Fig. 4.22. CD spectra of an aqueous solution of $1.5 \cdot 10^{-5}$ M pinacyanol chloride in the presence of eight different concentrations of Manucol-LHF at room temperature. 7.5 % v/v ethanol have been added to increase the solubility of the dye.

4.3.2.2 Job's Method for determination of stoichiometry

Job's plot, also called the Method of Continuous Variation,¹⁶⁴ is used to determine the stoichiometry of a chemical reaction. For this, a series of solutions is prepared and submitted to a spectrometer that contains the same total number of moles of the two reactants, but differs in the molar fraction of each reactant. The reaction between pinacyanol chloride and Manucol-LHF belongs to the so-called double displacement reaction type, in that the sodium cation of the carboxylate group of Manucol-LHF is replaced by the cationic dye molecule. The maximum absorbance of the complex formed is then determined from the spectrum for the set of solutions, and also the absorbance of the monomer and the dimer aggregate of the dye. Figure 4.23a shows the plot of absorbance of the complex formed (at 485 nm) against the mole fraction of added Manucol-LHF. The two straight lines intersecting at a ratio of 0.5 of polymer to polymer plus dye show the formation of a 1:1 complex between the dye and

polysaccharide. The same ratio is also found in Figure 4.23b, in which the decrease of the absorbance at 600 nm (dye monomer) and at 550 nm (dye dimer) are plotted.

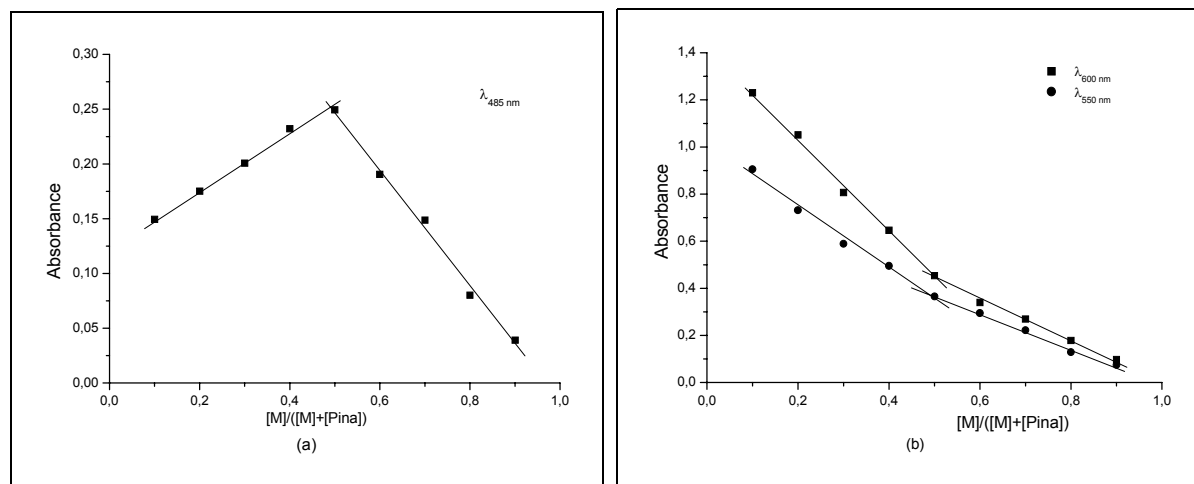


Fig. 4.23. (a) Job's plot (absorbance at 485 nm vs. Manucol-LHF mole fraction) of the interaction between Manucol-LHF and pinacyanol chloride. (b) Job's plot (absorbance at 600 and 550 nm vs. Manucol-LHF mole fraction) of the interaction between Manucol-LHF and pinacyanol chloride.

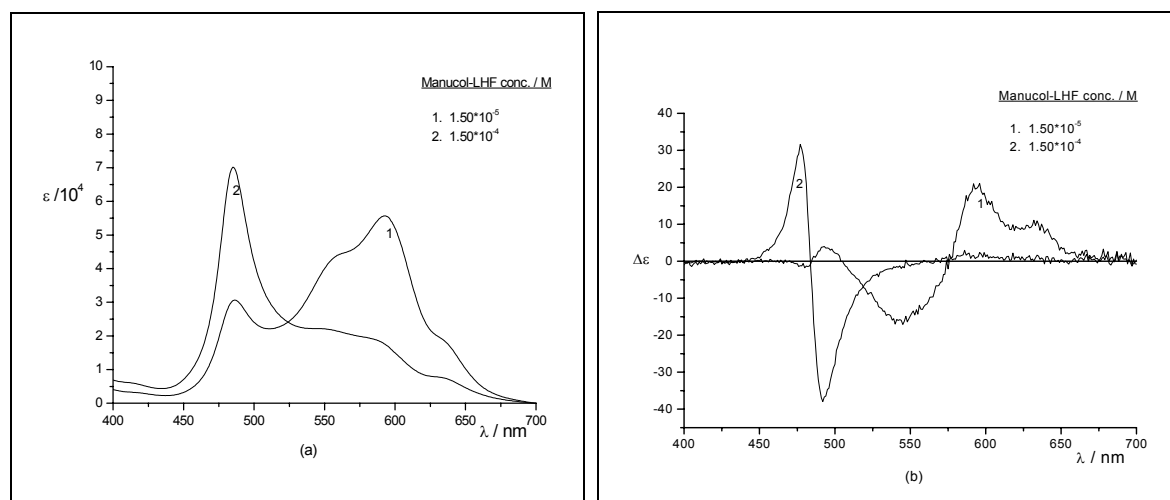


Fig. 4.24. (a) The visible absorption, (b) the CD spectra of $1.50 \cdot 10^{-5}$ M pinacyanol chloride in the presence of two different concentrations of Manucol-LHF at room temperature. 7.5% v/v ethanol added to increase solubility.

Another complex with an intense absorbance at 485 nm forms with a large excess of polysaccharide molecules. A Job plot for this high molar ratio is not practical. According to both the CD and the UV/Vis spectra the maximum concentration of this complex is reached when there are approximately ten polysaccharide monomers per 1 dye molecule. The CD and the UV/Vis spectra of these two different kinds of complexes are displayed against each other in Figures 4.24a and 4.24b.

4.3.2.3 Conductometric titration

The stoichiometry of interaction can be also determined by following the titration reaction between two ionic reactants in a conductometric cell, with one reactant present in a fixed amount and the other being gradually added.¹⁶⁴ Figure 4.25 shows the “conductometric behaviour” (equivalent conductance against square root of concentration) of pinacyanol chloride and Manuicol-LHF in a limited range of concentrations in aqueous solution. The shapes of the curves reflect the type of electrolytes. As expected the two reactants both represent weak electrolytes due to the non-linear shape in the plot of figure 4.25.

Figures 4.26a and b present the conductometric titration curves of the reactants. Both show definite breaks in their linear behaviour, corresponding to the 1:1 stoichiometry of interaction. The two reactants are not present completely as a monomer form in the solution under the experimental conditions. Manuicol-LHF is a polymer, and pinacyanol chloride is a mixture of monomers, dimers, and also of higher aggregates. The concentrations shown in the Figures are calculated on the basis of only monomers being present. The interaction between the two reactants seems to occur between pinacyanol monomers and Manuicol-LHF. Dye dimers probably do not interact directly with Manuicol-LHF due to steric considerations, and from Figure 4.21 it is obvious that the dimer concentration decreases with increasing Manuicol-LHF concentration to produce another form of aggregation. Therefore, there will be a shift in the

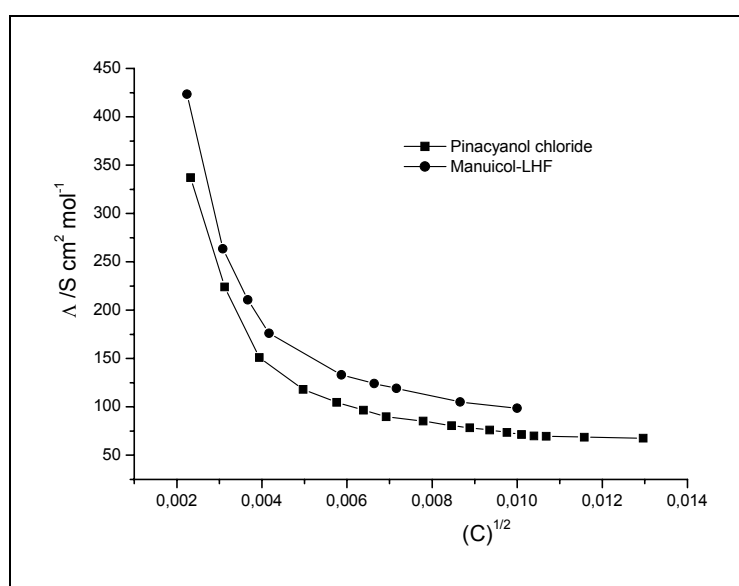


Fig. 4.25. Equivalent molar conductance of an aqueous solution of pinacyanol chloride and Manuicol-LHF, plotted against the square root of molar concentration.

equilibrium to the side of monomer form during the titration process. The initial break in the curve in Figure 4.26b may be due to the very low concentration of Manucol-LHF and the difficulties to shift the monomer-dimer equilibrium to the side of the monomer in the presence of low Manucol concentration. In Figure 4.26a the titration starts with low concentration of the dye, but now Manucol-LHF is present in excess, which will shift the equilibrium in the direction of the monomeric form of pinacyanol chloride.

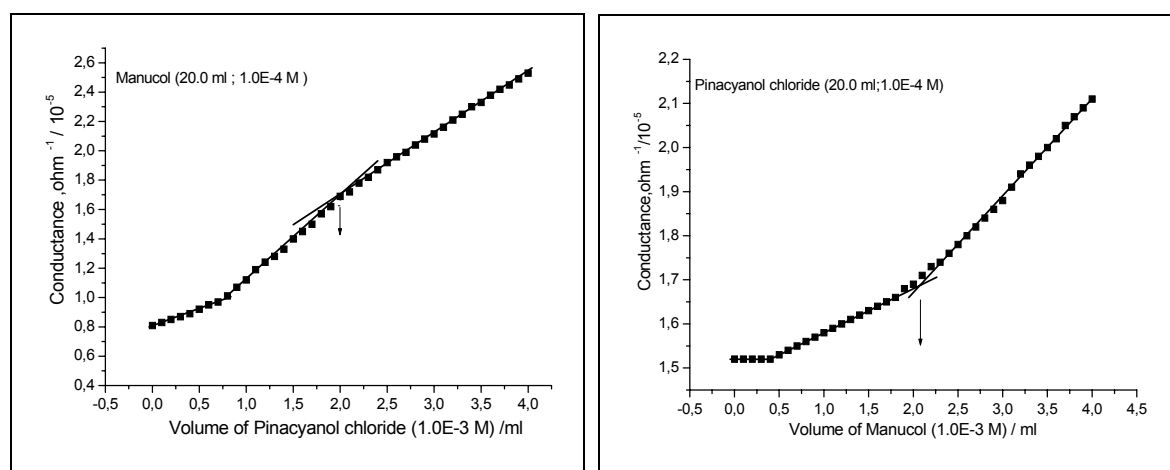


Fig. 4.26. (a) Conductometric titration of Manucol-LHF (20.0 ml, $1.0 \cdot 10^{-4}$ M) with pinacyanol chloride ($1.0 \cdot 10^{-3}$ M). (b) Conductometric titration of pinacyanol chloride (20 ml, $1.0 \cdot 10^{-4}$ M) with Manucol-LHF ($1.0 \cdot 10^{-3}$ M).

4.3.2.4 Effect of ethanol on the spectra

Ethanol increases the solubility of pinacyanol chloride in water and reduces its aggregation tendency; the effect of ethanol on pinacyanol/Manucol-LHF complexes is not known. Figure 4.27 shows what happens to the absorbance and the CD spectra of an aqueous solution of pinacyanol/Manucol-LHF (molar ratio of 1:1) when ethanol is added in different concentrations (from 0 to 42.5%). As would have been expected the monomer absorption band (Fig. 4.27a) of the monomer increases with increasing ethanol percentage in the solution; in contrast the intensity of the aggregation band at 485 nm decreases. In the CD spectra (Fig.4.27b) the S-shaped band with intersection at 580 nm has the highest intensity when the ethanol percentage is 7.5 %. When the ethanol concentrations are 22.5 and 30 % (spectra # 4 and 5) the exciton-like couplet centered at 485 nm develops, as in Figure 4.22. This indicates that ethanol can substitute for the high concentration of Manucol-LHF, in the formation of this complex. The higher ethanol concentration shifts the monomer/aggregate equilibrium away from the

monomer. This is the reason why in the other spectral investigations we employed a constant low concentration of 7.5 % ethanol. In this concentration aggregation is still significant and can be studied. However, the exciton doublet does not develop under this condition unless a high concentration of the polysaccharide is added to the dye.

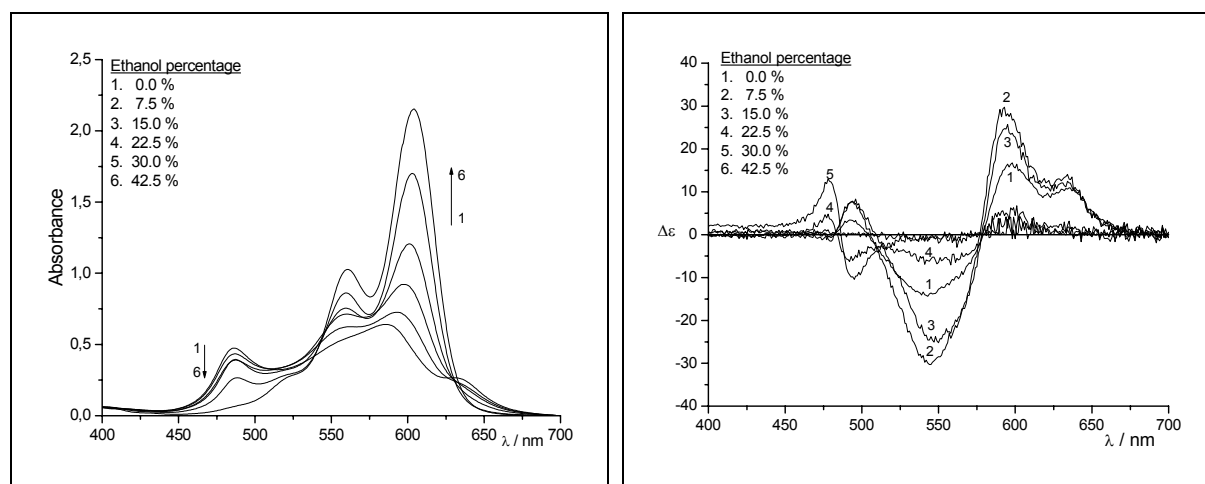


Fig. 4.27. (a) Visible absorption and (b) CD spectra of aqueous solutions of pinacyanol chloride ($1.50 \cdot 10^{-5}$ M) and Manucol-LHF ($1.50 \cdot 10^{-5}$ M) with different ethanol concentration (0.0 – 42.5%) at room temperature.

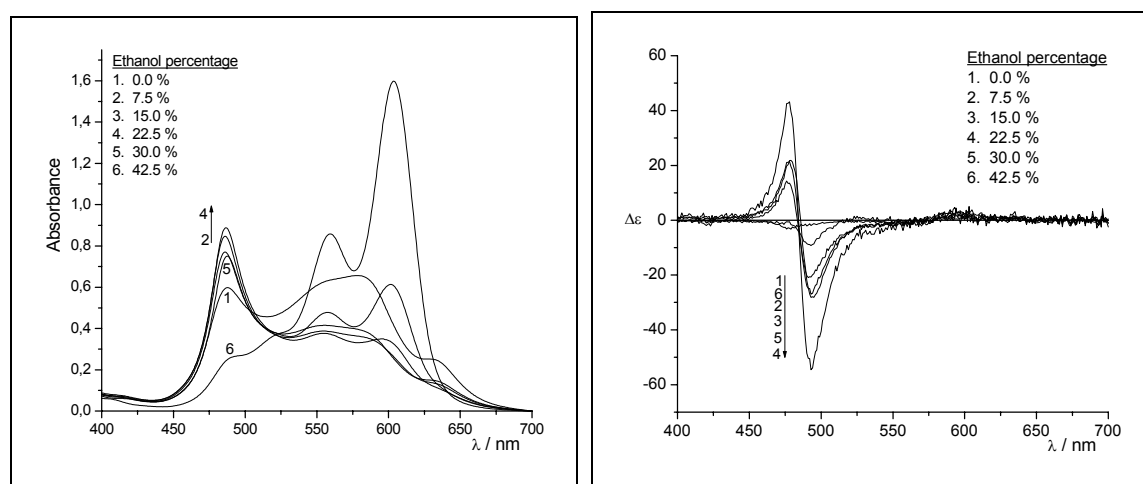


Fig. 4.28. (a) Visible absorption and (b) CD spectra of aqueous solutions of pinacyanol chloride ($1.50 \cdot 10^{-5}$ M) and Manucol-LHF ($1.50 \cdot 10^{-4}$ M) with different ethanol concentration (0.0 – 42.5%) at room temperature.

Addition of ethanol has quite different consequences, when the molar ratio of dye to polysaccharide is not 1:1, as in Figure 4.27, but 1:10 (Figure 4.28). While the change in the absorbance is more subtle, there are drastic changes in the CD, which exhibits the strong

exciton couplet at 485 nm. The amplitude of the couplet has a clear maximum, when the ethanol concentration is 22.5 %. With 42.5 % ethanol there remains a negative CD band only that in position and shape is similar found at the identical 1:10 ratio pinacyanol/Manucol-LHF but with an ethanol concentration of only 7.5 %.

4.3.2.5 Temperature effect on the spectra

All the factors, which affect the aggregation behaviour of pinacyanol dye, can be expected to affect the dye/polysaccharide interaction as well. Figure 4.29 shows how the absorbance and the CD spectra of pinacyanol/Manucol-LHF in a molar ratio of 1:1 in aqueous solution change as the temperature is changed, from 10 to 50 °C. Increasing the temperature shifts the intensity towards the 485 nm band, and away from the absorptions at longer wavelengths, indicating that the dye aggregates under the influence of higher temperature in the presence of Manucol-LHF. The CD spectra, however, give a different picture. The absorbance at 485 nm is almost unchanged, while the 600 nm band increases somewhat as the temperature is raised. In conclusion, the spectral changes do not indicate a strong dependence of the solution composition on the temperature (in contrast to the pure dye spectra which change strongly in the same temperature range).

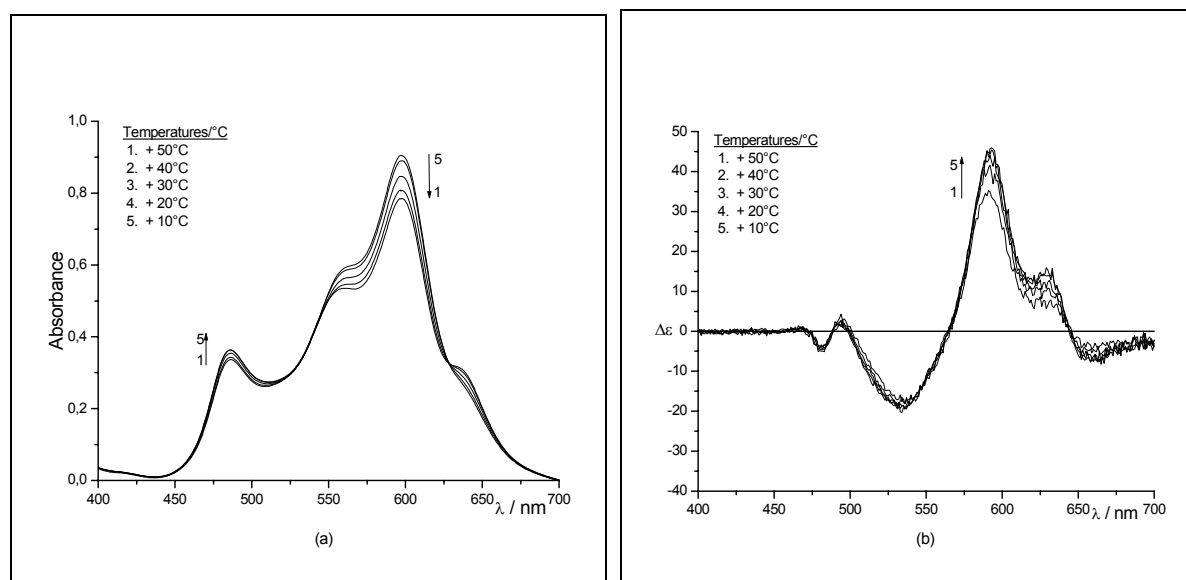


Fig. 4.29. (a) Visible absorption and (b) CD spectra of aqueous solutions of pinacyanol chloride ($1.50 \cdot 10^{-5}$ M) and Manucol-LHF ($1.50 \cdot 10^{-5}$ M) with 7.5 % ethanol at different temperatures (10 to 50 °C).

4.3.2.6 Effect of pH on the spectra

Figures 4.30 and 4.31 show how the visible absorption and CD spectra of a pinacyanol/Manucol-LHF, 1:10, solution changes with changing the pH values of the solvent by using buffer and HCL solution, respectively. Buffers were prepared according to tables suitable for spectrophotometry.¹⁶⁵ The pH of pinacyanol/polysaccharide solutions before adding the buffer or HCL is about 8.3. At this pH value the 485 nm absorption band and the excitonic doublet in the CD spectra are at an optimum in their intensities, but strongly dependent on any change of the pH value. In Figure 4.30, the spectral shapes of the buffered solutions (# 2 to 7) are almost the same, but they appear completely different from the unbuffered one (# 1) They are similar to the visible spectrum when the Manucol-LHF concentration is $1.5 \cdot 10^{-5}$ M (see Figure 4.21). In Figure 4.31, the intensity of the absorption band at 485 and the excitonic doublet in CD spectra decrease gradually as HCl is added; from 6.45 there is no significant change in the spectra, which are similar to the buffered solutions in Figure 4.30.

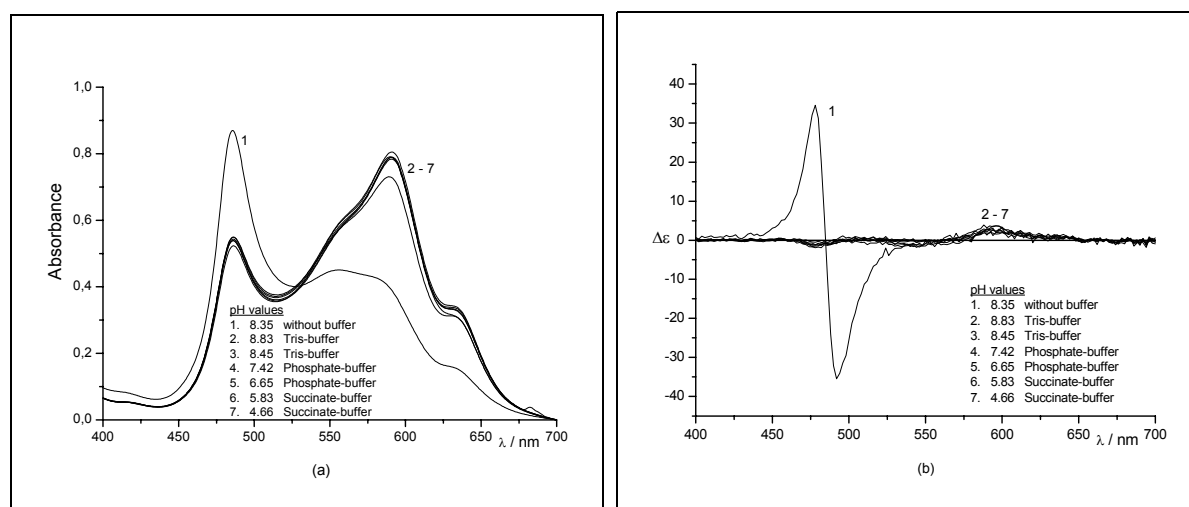


Fig. 4.30. (a) The visible absorption and (b) the CD spectra of aqueous solutions of pinacyanol chloride ($1.50 \cdot 10^{-5}$ M) and Manucol-LHF ($1.50 \cdot 10^{-4}$ M) at different pH values (8.83 to 4.66) using buffered solutions.

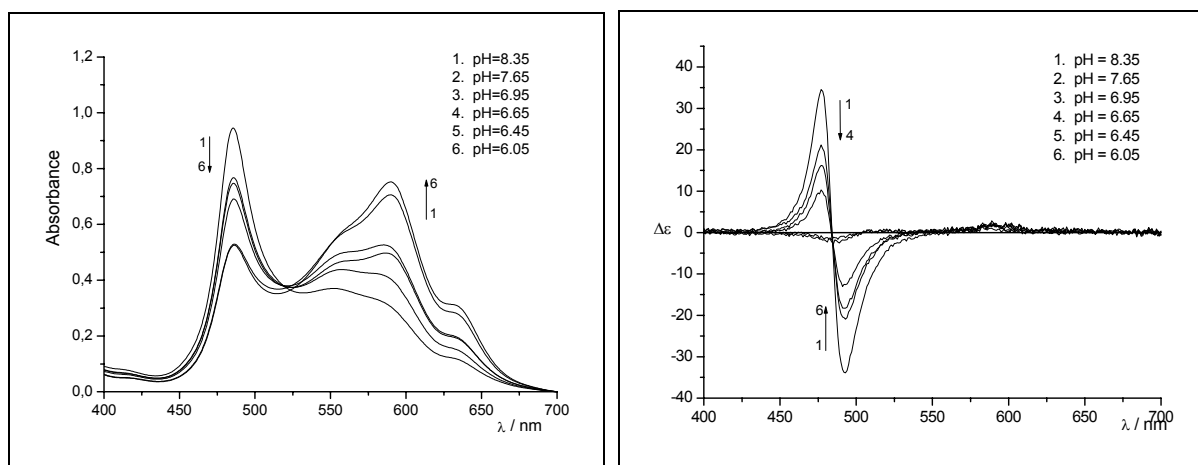


Fig. 4.31. (a) The visible absorption and (b) the CD spectra of aqueous solutions of pinacyanol chloride ($1.50 \cdot 10^{-5}$ M) and Manucol-LHF ($1.50 \cdot 10^{-4}$ M) at different pH values (8.35 to 6.05) using HCl solutions.

4.3.2.7 Effect of divalent cations on the spectra

The formation of the 1:1 complex is practically not affected by addition by Ca^{2+} (spectra not shown). In the case of the 1:10 complex things are completely different. Figure 4.32 shows how the visible absorption and CD spectra change with the addition of CaCl_2 solution. The intense 485 nm absorbance and the excitonic couplet band at the same position in the CD break down gradually, as the salt is added reaching at $1.4 \cdot 10^{-5}$ M a shape similar to the spectra when the Manucol-LHF concentration is $1.5 \cdot 10^{-5}$ M (see Figure 4.21)

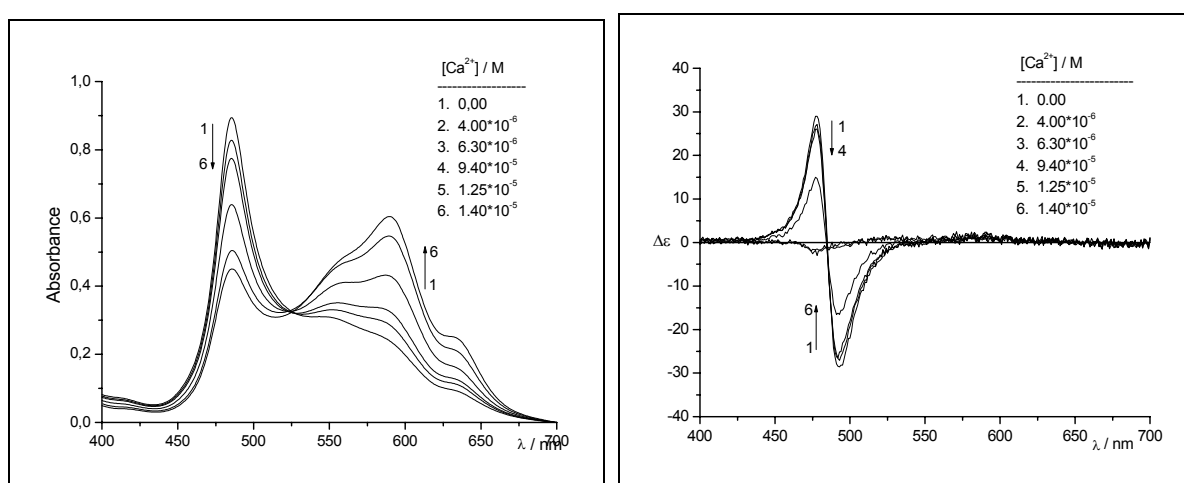


Fig. 4.32. The visible absorption (left) and CD spectra (right) of aqueous solutions of pinacyanol chloride ($1.50 \cdot 10^{-5}$ M) and Manucol-LHF ($1.50 \cdot 10^{-4}$ M) with different Ca^{2+} concentrations ($4.00 \cdot 10^{-6}$ to $1.40 \cdot 10^{-5}$ M).

For more precise quantitative data, Figures 4.33 and 4.34 show titration curves of the visible absorbance and the CD spectra as three different divalent cations, Ca^{2+} , Mg^{2+} , and Mn^{2+} , are added to the dye/Manucol-LHF solution. The plot of the absorbance at 485.5 nm against the cation concentration shows that the effect of Ca^{2+} is stronger than the two other cations. It also shows that significant spectral change do not occur any longer when the concentrations of the Ca^{2+} , Mg^{2+} , and Mn^{2+} cations have reached values of, respectively 1.41, 1.75, and $1.81 \cdot 10^{-5}$ M. The visible spectra at these limiting cation concentrations are also similar to the spectrum when Manucol-LHF concentration is $1.5 \cdot 10^{-5}$ M, as in Figure 4.21.

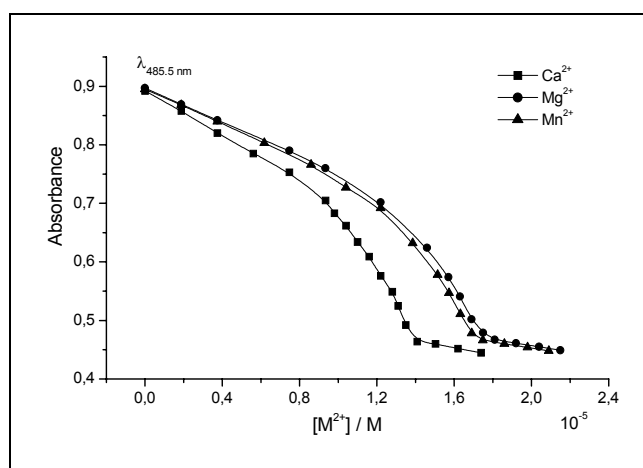


Fig. 4.33. The absorbance of aqueous solutions of pinacyanol chloride ($1.50 \cdot 10^{-5}$ M) and Manucol-LHF ($1.50 \cdot 10^{-4}$ M) at $\lambda_{\text{max}} = 485.5$ nm with different concentrations of Ca^{2+} , Mg^{2+} , and Mn^{2+} .

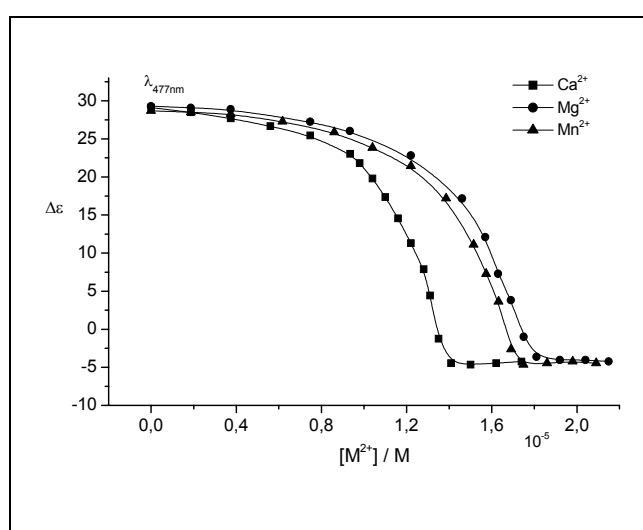


Fig. 4.34. CD absorbance of aqueous solutions of pinacyanol chloride ($1.50 \cdot 10^{-5}$ M) and Manucol-LHF ($1.50 \cdot 10^{-4}$ M) at $\lambda = 477$ nm with different concentrations of Ca^{2+} , Mg^{2+} , and Mn^{2+} .

4.3.3 Mannuronate rich alginate; characterization by CD

Figure 4.35 shows the CD spectrum of mannuronate rich alginate (prepared from Manucol-LB) in aqueous solution between 250 and 195 nm, at a concentration of 0.80 mg/ml or $4.0 \cdot 10^{-4}$ M. In the same way as described in section (2.2.3.4) the spectrum was analysed to obtain the concentration of mannuronate and guluronate in the sample. The values found were 83.3 and 16.7 %, respectively. In mannuronate rich alginate according to this method the ratio of mannuronate to guluronate units therefore is 5:1.

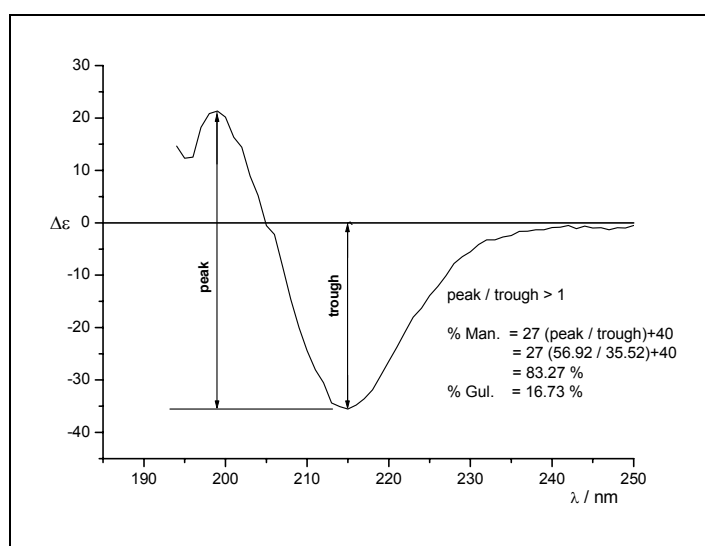


Fig. 4.35. CD-spectrum of mannuronate rich alginate (0.80 mg/ml) at pH = 7.05, in a 1.00 cm cell.

4.3.4 Aggregation of pinacyanol chloride with mannuronate rich alginate

The complexing properties of mannuronate rich alginate are distinctly different from those of Manucol-LHF. With a polysaccharide/dye ratio of 10:1 (Fig 4.21) the absorbance at 485 nm is less than the maximum absorbance at 600 nm; in the CD the intensity of the exciton-like couplet bands is very small. This is in stark contrast to the spectra obtained with Manucol-LHF.

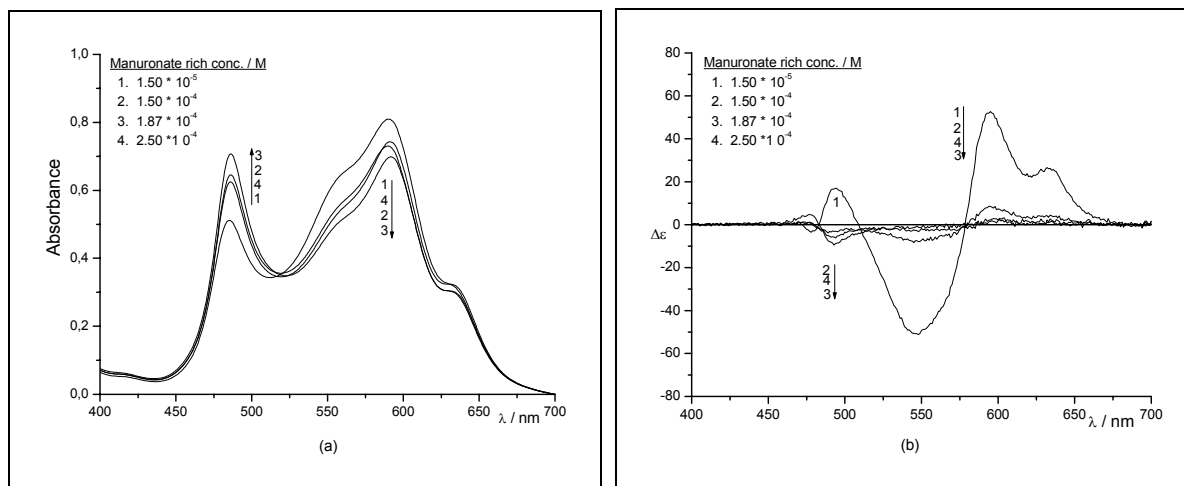


Fig. 4.36. The visible absorption (a) and the CD spectra (b) of aqueous solutions of $1.50 \cdot 10^{-5}$ M pinacyanol chloride with 7.5 % v/v ethanol in the presence of four different concentrations of mannuronate rich alginate at room temperature.

4.3.5 Guluronate rich alginate; characterization by CD

Figure 4.37 shows the CD spectrum of guluronate rich (prepared from Manucol-LB), in aqueous solution between 250 and 195 nm at a concentration of 0.80 mg/ml or $4.0 \cdot 10^{-4}$ M. Analysis of this spectrum yields a guluronate to mannuronate ratio of 2.8 : 1.

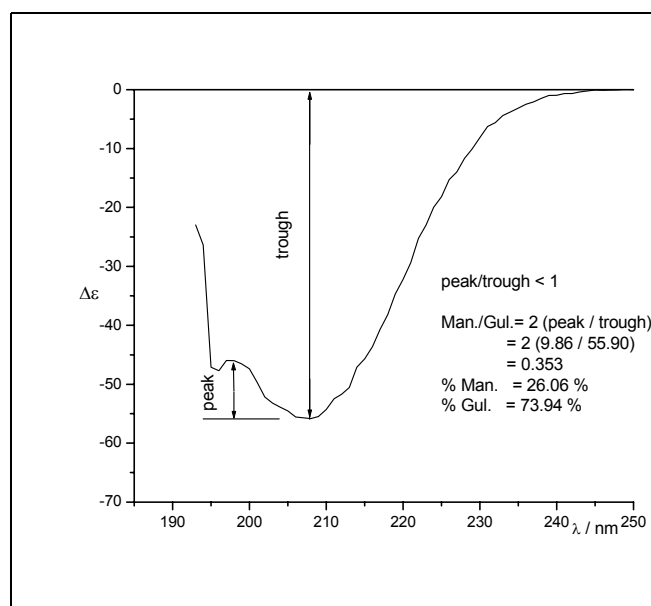


Fig. 4.37. CD-spectrum of guluronate rich alginate (0.80 mg/ml) at pH = 6.85 in a 1.00 cm cell.

4.3.6 Aggregation of pinacyanol chloride with guluronate rich alginate

This polysaccharide strongly favors the formation of the 485 nm complex at a 10:1 molar ratio, as shown in Figure 4.38 and similar to Manucol-LHF at the same experimental conditions.

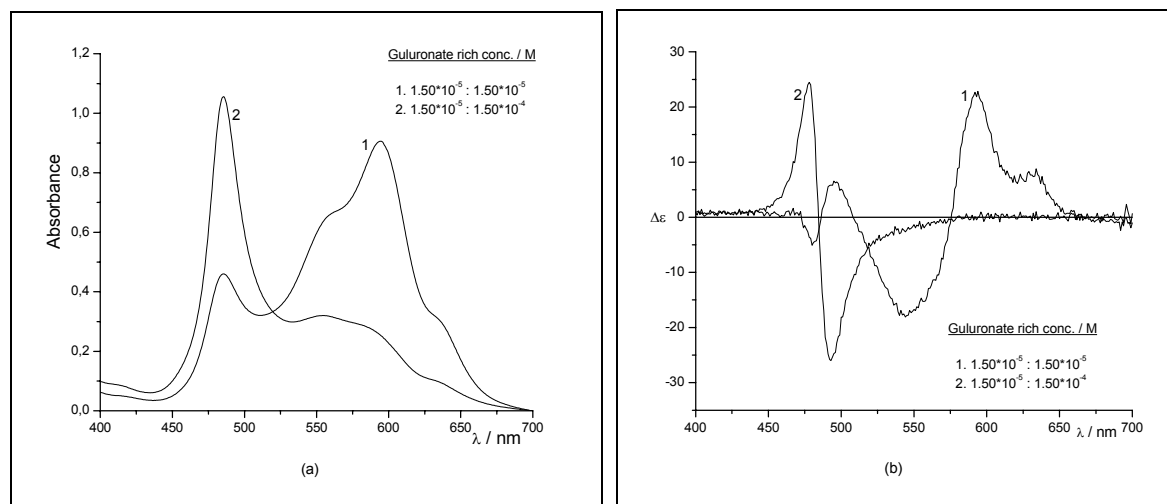


Fig. 4.38. The visible absorption (a) and the CD spectra (b) of aqueous solutions of $1.50 \cdot 10^{-5}$ M pinacyanol chloride with 7.5 % v/v ethanol in the presence of equimolar amounts or a tenfold excess of Guluronate rich alginate at room temperature.

4.3.7 SG81- Alginate; characterization by CD

SG81-Alginate is an anionic bacterial polysaccharide, in which some of the 2- and/or 3-positions of the D-mannuronate residues are O-acetylated ($-\text{COCH}_3$). Figure 4.39 shows the CD spectrum of SG81-Alginate in aqueous solution between 250 and 195 nm, from which according to the method used before the relative percentage of mannuronate and guluronate units was calculated. We found a ratio of 2.8:1, *i.e.* SG81-Alginate contains more mannuronate than guluronate.

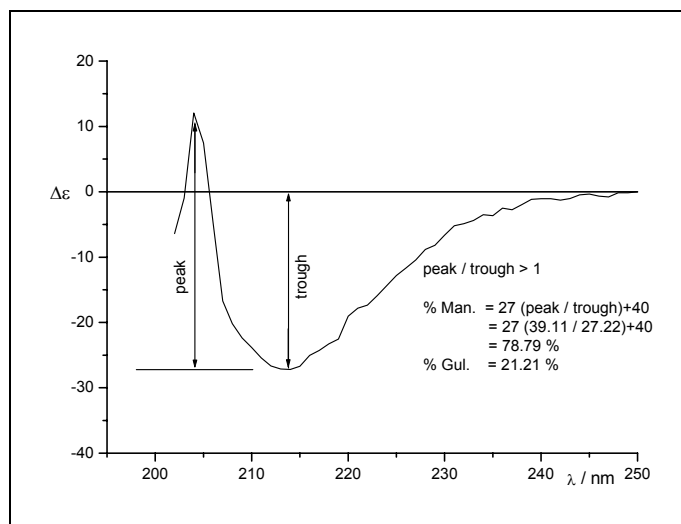


Fig. 4.39. CD-spectrum of SG81-Alginate (0.80 mg/ml) at pH = 7.05 in a 1.00 cm cell.

4.3.8 Aggregation of pinacyanol chloride with SG81- Alginate

Like mannuronate rich alginate, SG81-Alginate does not favour the formation of the complex that is formed with Manucol-LHF when the polymer/dye ratio is 10:1. Figure 4.40 shows the visible and the CD spectra of the interaction between SG81-Alginate and pinacyanol chloride. With increasing alginate/dye ratio above 1:1, the intensity of the visible band at 485 slightly increases, with an optimal absorbance at a ratio of 10:1 (Figure 4.40a). The CD spectra shows a strong S-shaped band structure centered at 570 nm, but no exciton-like couplet at 485 nm.

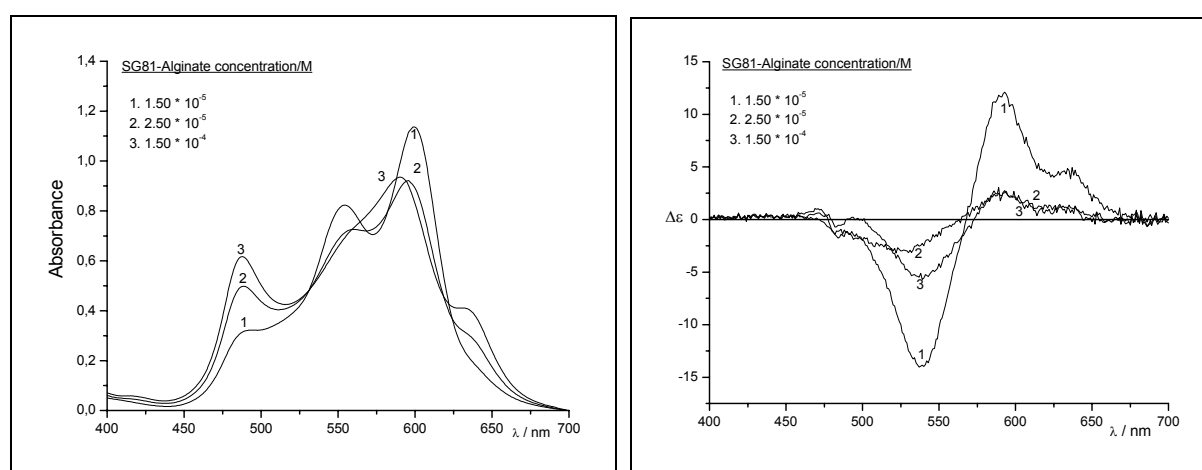


Fig. 4.40. The visible absorption (left) and the CD spectra (right) of aqueous solutions of $1.50 \cdot 10^{-5}$ M pinacyanol chloride with 7.5 % v/v ethanol in the presence of three different concentrations of SG81-Alginate at room temperature.

4.3.9 Discussion

Solutions containing chiral alginates and achiral pinacyanol chloride become optically active in the spectral region of the dye. This, and the appearance of aggregate bands in the absorption spectra, is indicative of complex formation between the alginates and the dye. Complexation is mediated by electric charges, negative on the alginates due to the ionised carboxylate groups and positive on the cyanine dye. This ionic coupling makes the dye chiral and causes the absorption bands to become optically active. Coupling with the dye molecules may also induce conformational changes in the chiral moiety.

The measured visible absorption and CD spectra of the different alginates show two kinds of spectra from which the presence of two different types of complexes can be deduced. Their formation depends on the alginate concentration if the dye concentration is held fixed. The first type of complex is formed when the alginate and pinacyanol chloride are present in the solution in a 1:1 stoichiometry. This ratio is also found from Job's plots and conductometric titrations. This experimental result agrees with the fact that the reactants are oppositely charged, with one unit charge on each unit of reactant. Assuming ionic coupling to be the cause of complexation, one might suppose that monomeric dye cations interact with the anionic sites of alginate to form an aggregate with a blue-shifted band within the visible range of spectra at the cost of the monomer. (The hypochromic shift of the absorbance in this case does not indicate aggregation, but results from localization of the positive charge as a result of ionic coupling). However, the visible spectra are not that simple, displaying multiple bands instead. The presence of many different bands at this 1:1 ratio indicate that only some of the carboxylic groups are occupied by dye molecules, and excess dye remains in solution or aggregates with dye molecules which are coupled directly to the alginate matrix. The S-shaped absorption band in the CD spectra between 500 and 600 nm indicates that these dye aggregates assume chiral conformations.

The second type of spectra is obtained when Manucol-LHF or guluronate rich alginate and pinacyanol chloride are present in a 10:1 stoichiometry in aqueous solution with 7.5 % ethanol added. The highly intense blue-shifted metachromatic band at 485 nm (figure 4.21), in addition to a lower broad band between 500 and 600 nm, are the characteristic features of this type, which appears to represent a more regular or uniform kind of aggregation than the type discussed above. The appearance of sharp-banded spectra at this high polysaccharide/dye ratio is due to the absence of excess dye aggregation and to the fact that only a fraction of the anionic sites of the polysaccharide are occupied by dye molecules. Thus, the very irregular way of bonding between alginate and the dye in the case of 1:1 stoichiometry changes to a

more regular one at a ratio of 10:1. This phenomenon occurs only with Manucol-LHF or guluronate rich alginate. From this we conclude that at high polysaccharide/dye ratio the dye prefers to interact with the more rigid 2-fold screw helical alternating sequence of guluronate residues (-G-G-G-G-) rather than the 3-fold left-handed helix mannuronate residues (-M-M-M-M-) or the disordered conformation (-M-G-M-G-) (see figure 2.14 in section 2.2.3.2).

Figure 4.41 represents a qualitative interpretation of the spectra, in which the dye molecules are bound by ionic coupling to guluronate residues. The presence of two different conformations in equilibrium with each other is deduced from the isosbestic point at about 520 nm for the two main different spectra and the other intermediate spectra.

Upon addition of divalent cations (section 4.3.2.7) the conformation of the second complex formed at the 10:1 ratio is destroyed and is changed to the 1:1 type, possibly because of competition between the cations and the dye molecules for the anionic binding sites of the polysaccharide: there is evidence that guluronate blocks are better disposed to chelate the divalent ions due to their spatial arrangement between adjacent blocks which is suitable to complex these cations at the cost of the dye molecules.

The very intense exciton couplet seen in Figures 4.21 and 4.22 centered at the sharp 485 nm absorption band of the UV/Vis spectra can be explained by applying exciton theory to the case of two interacting chromophores. Chromophores may interact under certain conditions with each other, even if there is no orbital overlap or electron exchange, when one chromophore is electronically excited. For effective interaction the chromophores should be similar, or have similar excitation energies, and there should be a fixed geometric disposition between the chromophores. Interaction leads to two absorption bands of energies and intensities depending on the geometric disposition, and to two oppositely signed CD-bands, one positive at 477 nm, one negative at 491 nm (see Fig. 4.42). The sharp visible band at 485 nm corresponds to the absorbance of the exciton state, which is allowed and thus has high intensity.

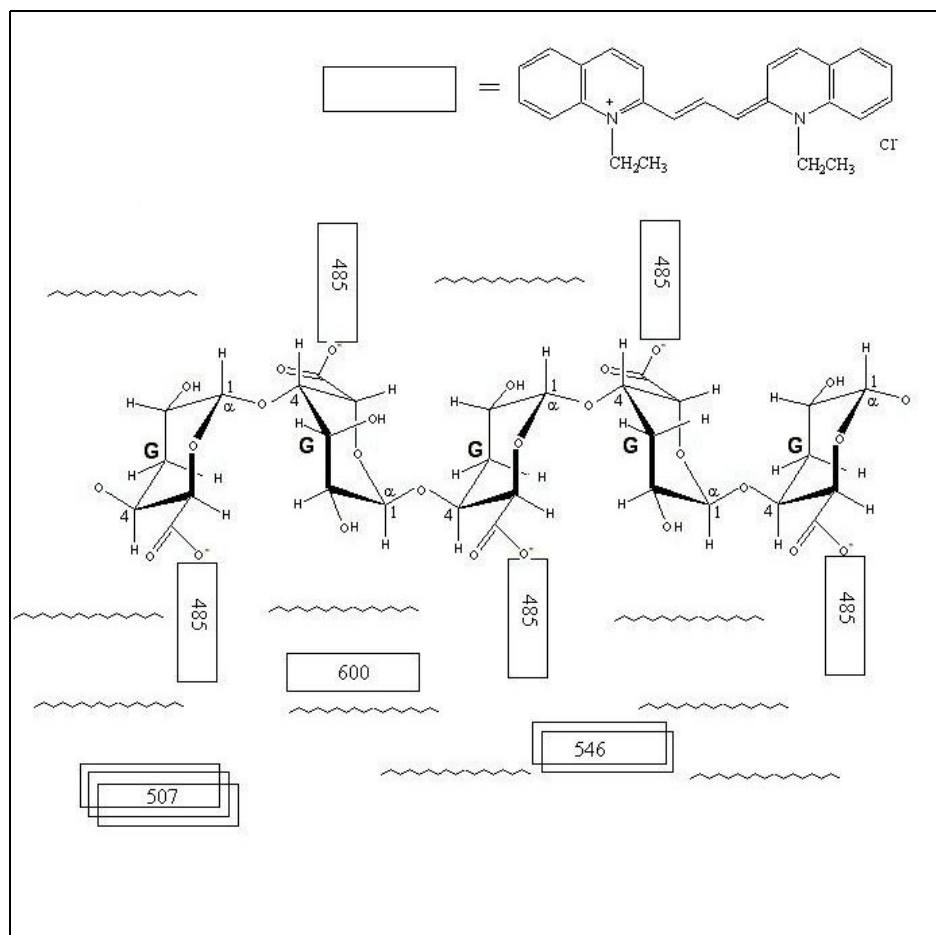


Fig. 4.41. Dye aggregates and ionic coupling of pinacyanol to gulonate residues in alginate. Numbers indicate the wavelengths of the absorption maxima in the UV/Vis spectra.

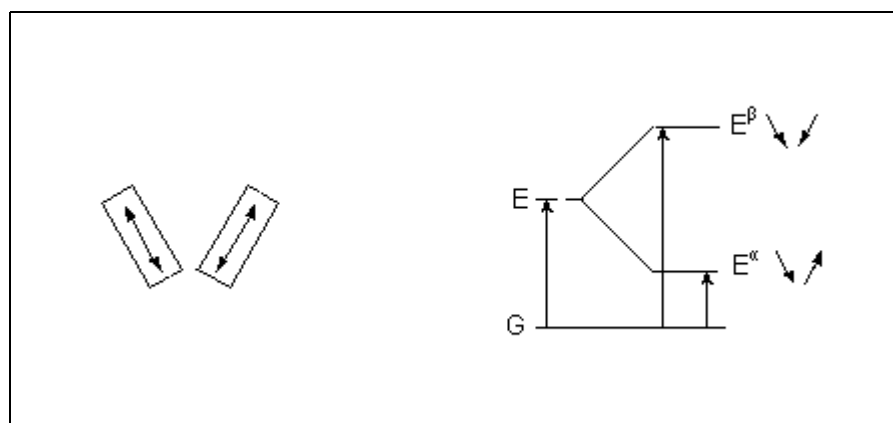


Fig. 4.42. Schematic representation of the exciton coupling for the interaction between pinacyanol chloride and alginate. At this acute angle between the dye monomers α -type coupling leads to low-intensity red-shifted absorbance, and β -type coupling to high-intensity blue-shifted absorbance.

4.4 Complex formation of Pinacyanol chloride with Aerosol-OT

4.4.1 UV/Vis and CD spectra in aqueous solutions

Figure 4.43 shows the visible spectra of pinacyanol chloride in aqueous solution ($1.0 \cdot 10^{-5}$ M) in the presence of Aerosol-OT ranging in molar concentrations from $0.5 \cdot 10^{-5}$ to $3.0 \cdot 10^{-3}$ M. This covers a molar concentration range of Aerosol-OT/dye from 0.5:1 to 300:1, respectively. The spectra reveal that the intensities of the absorption maxima of free pinacyanol chloride depend significantly on the Aerosol-OT concentrations in the solution: as the surfactant to dye ratio increases, the intensities of the bands at 600, 546 nm decrease, and the formation of a new broad blue-shifted band is visible, with intensity and maximum wavelength depending on the Aerosol-OT to dye ratio. When the ratio is between 0.5:1 and 2:1, the maximum of this new band lies between 490 and 499 nm, with an additional shoulder at about 465 nm (spectrum # 3 in Figure 4.43). When the ratio is 20:1 (spectrum # 4) the band intensity starts to decrease and the maximum is red-shifted to 477 nm, in addition to a shoulder over 499 nm. The maximum intensity of the blue-shifted band, with a wavelength of 468 nm, is reached at a surfactant/dye ratio of 50:1 (spectrum # 5); under these conditions, the absorbances of the free dye reach their lowest intensities. At even higher Aerosol-OT/dye ratios the intensity of the 468 nm band starts to decrease again, as the intensities of the free dye increase (spectrum # 6). In conclusion, Aerosol-OT induces the formation of one metachromatic band in pinacyanol, at 468 nm, and possibly another one at 495 nm.

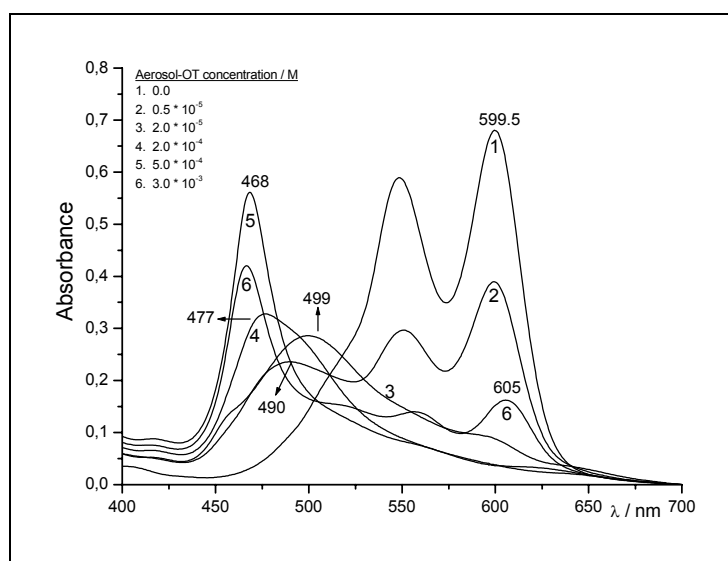


Fig. 4.43. The visible absorption spectra of aqueous solutions of $1.0 \cdot 10^{-5}$ M pinacyanol chloride in the presence of five different concentrations of Aerosol-OT at room temperature.

Figure 4.44 shows the CD spectra of aqueous Aerosol-OT/dye solutions taken under identical conditions as in Figure 4.43. The metachromatic band at 468 nm in Figure 4.43 corresponds in the CD to a negative band at 468 nm and a positive band at about 500 nm. This broad couplet reaches its maximum amplitude in spectrum # 5, which corresponds to the maximum of the visible absorbance of this band. When the Aerosol-OT/dye ratio is further increased (spectrum # 6) the couplet breaks down and is reduced to two weak negative bands – just as the absorbance of the band is reduced, though not so drastically. There is a clear isosbestic point in the CD spectra, at about 483 nm, and there is no indication of CD absorption corresponding to free dye molecules.

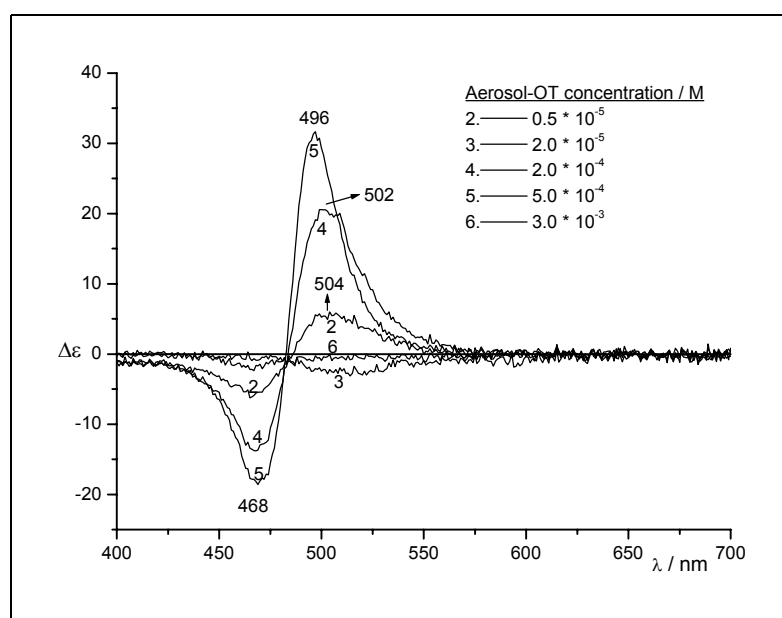


Fig. 4.44. CD spectra of aqueous solutions of $1.0 \cdot 10^{-5}$ M pinacyanol chloride in the presence of five different concentrations of Aerosol-OT at room temperature.

The reported value of the critical micelle concentration (cmc) for Aerosol-OT at room temperature is $2.4 \cdot 10^{-3}$ M.¹⁴³ All the spectra shown in Figures 4.43 and 4.44 correspond to surfactant concentrations below the cmc, except for the highest concentration. (This assumes that the value of the cmc is not significantly changed in the presence of pinacyanol in very low concentration). We note that the CD couplet reaches its highest amplitude as the surfactant concentration approaches the cmc; upon exceeding this value (spectrum # 6 in Figure 4.44) the couplet breaks down completely.

4.4.2 Effect of ethanol on the surfactant spectra

Ethanol is known to affect the aggregation behaviour of dyes, and it will affect the aggregation behaviour of the surfactant, including its cmc. With the caution in mind that we don't know the values of the cmc in ethanol/water mixtures we present the following spectra only as qualitative pictures of the events taking place in surfactant/dye mixtures with varying concentrations of ethanol.

Figure 4.45 shows the effect of ethanol (from 0 to 22.5%) added to an aqueous solution of a 1:50 ratio of pinacyanol chloride and Aerosol-OT. Except for an initial weak increase the metachromatic band at 465 nm is seen to decrease strongly in intensity as ethanol is added to the solution. The concomitant red-shift of the band maximum can be assumed to be due to the overlap with the developing bands at the low-energy side of the spectrum. We also note the strong increase of the monomer dye absorption at 600 and the dimer absorption at 555 nm. There is, even at the highest ethanol concentration, a significant residual absorption at around 480 nm, which indicates the presence of a higher dye aggregate.

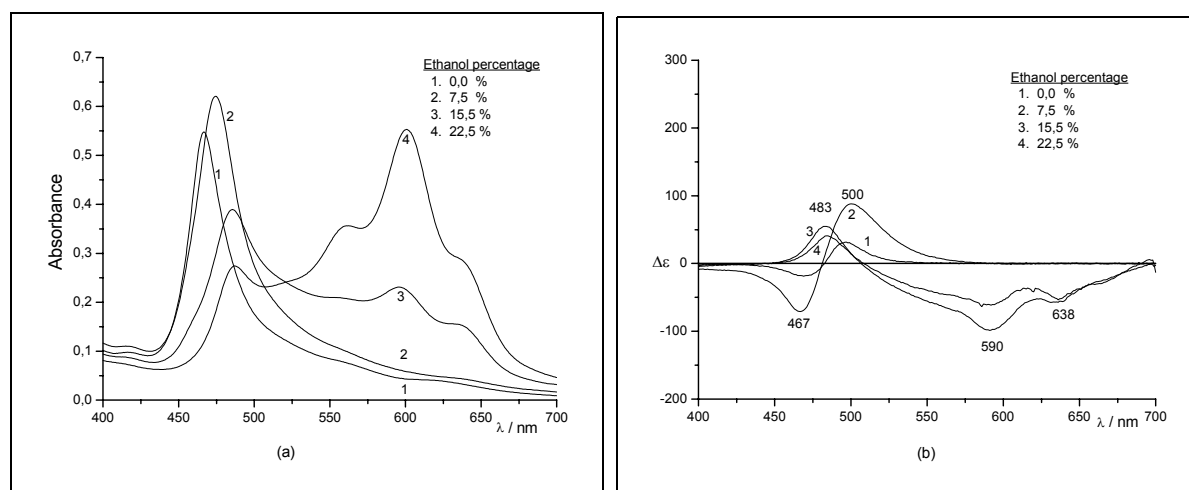


Fig. 4.45. (a) The visible absorption and (b) the CD spectra of aqueous solutions of pinacyanol chloride ($1.0 \cdot 10^{-5}$ M) and Aerosol-OT ($5.0 \cdot 10^{-4}$ M) with different ethanol concentrations (0 to 22.5 %) at room temperature.

In the corresponding CD spectra (Figure 4.45b) the couplet, which dominated the metachromatic spectra shown in Figure 4.44, is present at ethanol concentrations below 10%. It reaches its largest amplitude at 7.5 % ethanol content. The amplitude is about five-fold

compared to the spectra without ethanol. Increasing the ethanol concentration, however, has the opposite effect: the couplet breaks down, just as the metachromatic band in the visible absorption. The residual band at 480 nm, which is seen under these conditions in the visible spectrum, displays a positive absorption in the CD.

We conclude that ethanol in low concentrations promotes formation of the strongly CD active aggregate resulting from the interaction between the dye and the surfactant. At higher ethanol concentrations the dye becomes mostly dissolved in monomeric form, but a part of it remains aggregated, though in a different form.

4.4.3 Temperature effect

Figure 4.46 shows how the visible absorption and the CD spectra of a pinacyanol/Aerosol-OT solution react to changes of the temperature. The conditions were chosen such that the formation of the metachromatic band at 468 nm was most favourable.

At lower temperature (10 °C), the intensity of the absorption band has its largest value; we also note a slight blue-shift of the band maximum to 476.5 nm. The absorbance of the monomeric dye at 600 nm is minimal. Increasing the temperature has two effects: the intensity of the blue-shifted band decreases, and the band is shifted to the red. At the same time most of the absorbance is shifted into a broad band reaching from 500 to 650 nm, in which peaks corresponding to monomeric dye and to other aggregated species are clearly visible.

The CD spectra reflect this somewhat unstructured behaviour. The bisignate CD band at low temperature collapses into one positive band at 460 nm when a temperature of 45 °C is reached, and the broad band shows weak negative CD absorption. Both the visible absorption and the CD spectra taken at 45 °C are similar in shape to the spectrum # 3 in Figure 4.45, indicating that excess ethanol and excess heat affect the aggregating behaviour of pinacyanol in the presence of Aerosol-OT in a similar way.

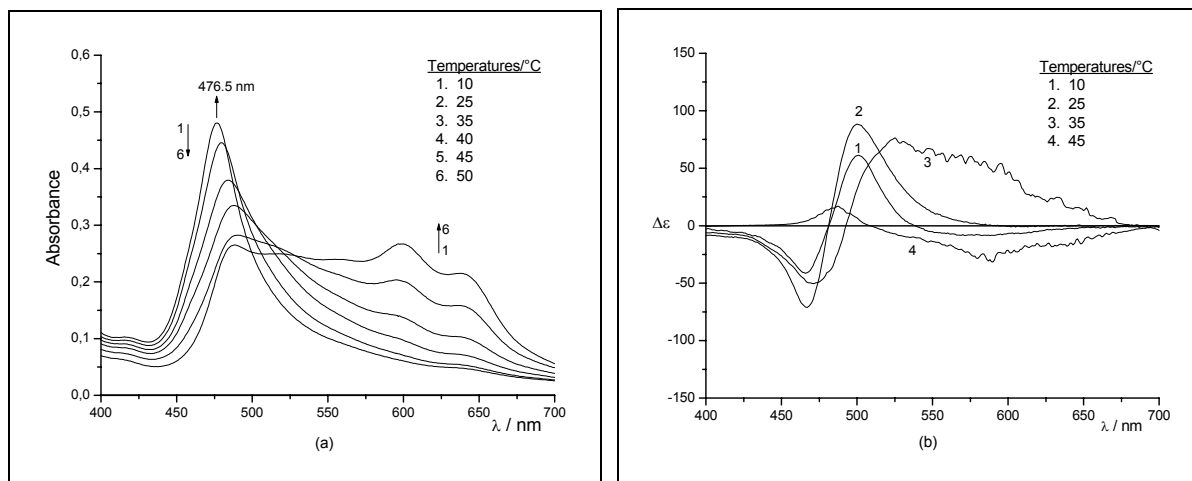


Fig. 4.46.(a) and (b) The visible absorption (a) and the CD spectra (b) of aqueous solutions of pinacyanol chloride ($1.0 \cdot 10^{-5}$ M) and Aerosol-OT ($5.0 \cdot 10^{-4}$ M) with 7.5 % v/v ethanol at different temperatures (10 to 50 C°).

4.4.4 Discussion

Aerosol-OT induces very strong blue-shifted metachromasia in pinacyanol chloride solutions at concentrations below the cmc (Figure 4.43). The reported value for the cmc of Aerosol-OT at room temperature is $2.4 \cdot 10^{-3}$ M,¹⁶⁶ which would correspond to a surfactant/dye ratio of 240 when the pinacyanol concentration is $1.5 \cdot 10^{-5}$ M. In the Figure, there is a progressive blue shift of the metachromatic band and increasing intensity as the surfactant/dye ratio is increased to 50, at which ratio the wavelength of 468 nm is reached. Above the cmc (ratio 300:1), the intensity of the metachromatic band decreases with a slight shift of 2 nm to 466 nm and appearance of weak absorbances in the region of the monomer and dimer bands. It is obvious that Aerosol-OT induces a sharp and single absorption band with pinacyanol, indicating that the dye cations aggregate systematically with reasonable distances between each other, and they are not overcrowded because there are no multiple bands.

Conductometric titrations show a 1:1 stoichiometry interaction between pinacyanol chloride and Aerosol-OT.¹⁴³ At this ratio there is a metachromatic band at 495 nm and a shoulder at 465 nm. Metachromasy with a sharp and single band and significant blue shift sets in when excess Aerosol-OT is present in the solution (Figure 4.43). The question arises whether pinacyanol binds at alternating anionic groups of aggregated Aerosol-OT, and whether these aggregates are already present in the solution before pinacyanol chloride is added. The cmc tells us that Aerosol-OT is present in monomeric form when the

surfactant/dye ratio is less than 300:1. Therefore the presence of cationic dye molecules in the solution induces the formation of Aerosol-OT aggregates, which can easily interact with the anionic Aerosol-OT molecules. Ionic coupling yields larger molecular structures, which become salt-like macromolecules and have the capability to aggregate in solution. The enhancement of this aggregation depends directly on the Aerosol-OT/dye ratio.

The presence of intense and sharp positive and negative bands in the CD spectra (Figure 4.44) indicates exciton splitting, reflecting strong dye-dye interaction with an optimum when the ratio is 50:1. Regardless of the interaction of Aerosol-OT with dyes, the cmc of the free excess Aerosol-OT in the solution should not change significantly; however, the new structure may behave different from the free excess Aerosol-OT itself. This conclusion is clear from the spectral shape of the UV/Vis band at a ratio of 300:1, in which Aerosol-OT is present in a concentration above the cmc, and the absorbance is very similar to the one observed when the ratio is 50:1 (obviously, the band can represent only the Aerosol-OT bonded to the dye which is equal at least to the concentration of the dye presents in the solution). From this we see that the aggregation of the dye induced by Aerosol-OT at low concentration is similar to the geometry induced by the surfactant at or above its cmc.

There is no easy explanation why the aggregate at the 300:1 ratio loses its optical activity. Pal and Pal ¹⁴³ argue that some of the amphiphilic dye molecules enter the micelles with the cationic charged portion of the dye facing the sulfonate groups at the surface, and that the dye cations within the micelles also aggregate, exhibiting metachromasia with different maximum wavelength. These aggregates do not exhibit optical activity because the micelle of Aerosol-OT are not chiral. This mode of aggregation may be present in the case of the 300:1 ratio because of the absence of a circular dichroism band (see Figure 4.44).

5 Summary / Zusammenfassung

5.1 Summary

A quantitative study of the aggregation behaviour of the cationic cyanine dye pinacyanol chloride in aqueous solution and in the presence of various organic matrices (anionic alginates, anionic Aerosol-OT and γ -cyclodextrin) is presented based on UV/Visible absorption and Circular Dichroism (CD) spectroscopy. The spectral data have been analysed using derivative spectra and a program ("PeakFit") to model the mixtures of different absorbing species with strongly overlapping absorption bands. The structures of the aggregates have been analysed and discussed in terms of qualitative ("H"- vs. "J"-type aggregation) and quantitative arguments based on a program ("OSCI") for the calculation of oscillator and rotatory strengths assuming an exciton-like delocalisation of molecular excitations through the entire aggregate.

Before attempting to describe the complexation of pinacyanol with macromolecular matrices and hosts a detailed analysis of the self-aggregation of the dye as a function of a wide range of concentrations was performed. The wavelengths of maximum absorbance of the different species as a function of solvent polarity and concentration were determined by converting the absorbance spectra into fourth derivative spectra. Using a peak-fitting procedure the overlapping bands were separated and analyzed. Bands with maxima at 601, 546, 523, and 507 nm could be attributed, respectively, to the monomer, a sandwich-type dimer, a vibronic overtone of the dimer, and a higher aggregate, most probably a stacked trimeric form of the dye. Extinction coefficients of the monomer, dimer and trimer were calculated from data taken from the spectral fitting. Thermodynamical data for the monomer/dimer equilibrium were obtained using the calculated extinction coefficients.

Aggregation of pinacyanol chloride is strongly enhanced in the presence of charged macromolecules and through inclusion by cyclodextrins. The reaction between pinacyanol and γ -cyclodextrin was studied using both visible and circular dichroism spectroscopy. Two types of interaction were detected: both the intensities of the dimer band at 546 nm and of the trimer band at 507 nm were found to increase with the ratio of cyclodextrin to dye. Both aggregates were shown to be optically active due to the chiral environment of the host (Induced circular dichroism, ICD). The CD spectra with two and three oppositely signed excitonic bands, respectively, support the structural assignment. From the integrated band intensity of the monomer absorbance the electric transition dipole moment of pinacyanol was

obtained and used to calculate the excited state properties of different pinacyanol aggregates. Applying eight different parameter sets aggregates of pinacyanol chloride ranging in size from two to twenty dye molecules were considered. The calculated energy splitting was adjusted, via the transition dipole length, to the experimentally observed band shift. Rotational strengths associated with the CD absorptions were calculated and used to obtain an estimate of the inherent twist of the dimer aggregate inside the γ -cyclodextrin cavity.

The interaction between pinacyanol chloride and different alginates yields profound changes in the visible absorbance and circular dichroism spectra. Two different types of aggregates were found depending on the type of alginate used and the relative concentrations. With Manucol-LHF and at high pinacyanol concentrations the formation of a 1:1 complex was deduced from an analysis of Job's method and conductometric titrations. Another complex formed at 1:10 dye/alginate ratios and only in the presence of Manucol-LHF or guluronate rich alginate. The two aggregates which display strongly different visible and CD spectral characteristics are in dynamic equilibrium according to the presence of isosbestic points in the visible region. The effect of temperature, pH, solvent, and divalent cations on the spectra was studied. The complex formed at low dye/alginate ratio was damaged by addition of hydrochloric acid and divalent cations; however, at low concentration of these agents the spectra indicated conversion of the complex into the 1:1 aggregate. Models for the two complexes are proposed taking into account the preference of guluronate binding sites for chelating ions.

Different structures are proposed for the complexes formed from the reaction between the cationic pinacyanol and the anionic surfactant Aerosol-OT. UV/Vis and CD spectra provide tools to study the concentration and solvent dependence of the interaction. Aggregation spectra are dominated by a literature-known strongly blue-shifted, sharp and single visible metachromatic band, which appears at Aerosol-OT concentrations much below the cmc of the surfactant. Above the cmc the spectra indicate dissociation into monomer and dimer species, and the system becomes completely devoid of chirality. Two different CD spectra with a distinct isosbestic point are observed for complexes with different surfactant to dye ratios. Both the addition of ethanol and increasing the temperature retards the metachromatic process.

5.2 Zusammenfassung

Das Aggregationsverhalten des kationischen Cyaninfarbstoffs Pinacyanolchlorid in wässriger Lösung und in Gegenwart verschiedener organischer Matrixmoleküle (anionische Alginat, anionisches Aerosol-OT und γ -Cyclodextrin) wurde durch Messung der UV/Vis-Absorptions- und der Circular dichroismus-(CD)-Spektren untersucht. Zur quantitativen Auswertung der Spektren wurden höhere Ableitungen und ein Programm zur Anpassung von Spektren mit stark überlappenden Banden („PeakFit“) eingesetzt. Die Strukturen der Aggregate wurden analysiert und nach qualitativen Gesichtspunkten („H“- vs. „J“-Aggregation) diskutiert. Die quantitative Diskussion erfolgte auf der Basis eines Programms (OSCI) zur Berechnung der Oszillator- und Rotationsstärken von Aggregatspektren mit excitonartiger Delokalisierung elektronisch angeregter Zustände.

Vor der Diskussion der Farbstoffkomplexe mit makromolekularen Matrizen und Wirtmolekülen wurde eine detaillierte Analyse der Selbstaggregation des Farbstoffs in einem weiten Konzentrationsbereich durchgeführt. Die Wellenlängen der Absorptionsmaxima der verschiedenen Spezies in Abhängigkeit von der Lösemittelpolarität und der Konzentration wurden durch Überführung in die 4. Ableitungsspektren ermittelt. Gemeinsam mit der PeakFit-Prozedur wurden die überlappenden Banden getrennt und analysiert. Die Banden mit Maxima bei 601, 546, 523 und 507 nm wurden dem monomeren Farbstoff, einem Sandwich-Dimer und dessen vibronischem Oberton sowie einem höheren Aggregat, wahrscheinlich einem gestapelten Trimer, zugeordnet. Die Extinktionskoeffizienten der drei Spezies wurden aus der Spektrenanpassung ermittelt; mit Hilfe dieser Werte wurden die thermodynamischen Parameter des Monomer-Dimer-Gleichgewichts berechnet.

Die Aggregation von Pinacyanolchlorid wird durch geladene Makromoleküle und durch Einschluß in Cyclodextrine stark begünstigt. Die Reaktion zwischen Pinacyanol und γ -Cyclodextrin wurde sowohl UV/Vis- als auch CD-spektroskopisch untersucht. Zwei unterschiedliche Wechselwirkungen wurden entdeckt. Sowohl die Intensität der Dimerbande bei 546 nm als auch die der Trimerbande bei 507 nm nehmen zu, wenn das Verhältnis Cyclodextrin zu Farbstoff erhöht wird. Beide Aggregate sind optisch aktiv als Folge der chiralen Umgebung (Induzierter Circular dichroismus, ICD). Die CD-Spektren mit zwei bzw. drei Excitonbanden mit entgegengesetzten Vorzeichen unterstützen die Strukturzuordnung. Aus der integrierten Intensität der Monomerabsorption wurde das elektrische Übergangsmoment von Pinacyanol ermittelt und zur Berechnung der Spektren verschiedener Farbstoffaggregate benutzt. Acht verschiedene Parametersätze wurden verwendet, um

Pinacyanolaggregate zu berechnen, die in der Größe vom Dimeren bis zum Eikosameren reichen. Die berechnete Energieaufspaltung wurde über die Länge des Übergangsmoments dem Experiment angepasst. Rotationsstärken wurden berechnet und benutzt, um eine Abschätzung des Verdrillungswinkels des Dimeren innerhalb des γ -Cyclodextrins zu erhalten.

Die Wechselwirkung zwischen Pinacyanolchlorid und verschiedenen Alginaten macht sich durch tiefgreifende Veränderungen der Absorptions- und CD-Spektren bemerkbar. Zwei unterschiedliche Arten von Aggregaten wurden gefunden, abhängig vom Konzentrationsverhältnis Alginat zu Farbstoff und davon, welches Alginat eingesetzt wurde. Mit Manucol-LHF und hohen Pinacyanolkonzentrationen wird ein 1:1-Komplex gebildet; dies bestätigen die Spektrenauswertung nach der Methode von Job und konduktometrische Titrations. Ein anderer Komplex entsteht bei einem Verhältnis von 1:10 von Farbstoff zu Alginat, aber nur in Gegenwart von Manucol-LHF oder guluronatreichem Alginat. Die beiden Aggregate, die sich in ihren UV/Vis- und CD-Spektren deutlich unterscheiden, stehen ausweislich isosbestischer Punkte in einem dynamischen Gleichgewicht. Der Einfluß der Temperatur, des pH, des Lösemittels und der Zugabe zweifach geladener Kationen wurde untersucht. Der bei niedrigem Farbstoff/Alginatverhältnis gebildete Komplex wird durch Chlorwasserstoff und durch zweiwertige Ionen zerstört; bei niedrigen Konzentrationen dieser Agentien erfolgt Übergang in das 1:1-Aggregat. Strukturmodelle für die beiden Komplexe werden entwickelt unter Berücksichtigung der bekannten bevorzugten Bildung chelatisierender Ionen durch Guluronat.

Unterschiedliche Strukturen werden für die Komplexe diskutiert, die bei der Reaktion des kationischen Farbstoffs mit dem anionischen Surfactant Aerosol-OT entstehen. UV/Vis- und CD-Spektren bieten auch hier die Möglichkeit, die Konzentrations- und Lösemittelabhängigkeit der Wechselwirkung zu untersuchen. Die Aggregatspektren werden beherrscht von einer literaturbekannten stark blau-verschobenen, scharfen Metachromasie-Bande, die bei Konzentrationen des Aerosol-OT weit unterhalb der kritischen Micellkonzentration (cmc) auftritt. Oberhalb der cmc deuten die Spektren auf Dissoziation in Monomere und Dimere hin, die keine optische Aktivität mehr zeigen. Unterschiedliche CD-Spektren mit einem ausgezeichneten isosbestischen Punkt werden für Komplexe mit unterschiedlichem Verhältnis von Surfactant zu Farbstoff beobachtet. Sowohl Zugabe von Ethanol wie auch Erhöhung der Temperatur drängen die Metachromasie zurück.

6 Experimental

6.1 Material and solvents used

Pinacyanol chloride: 1,1'-diethyl-2,2'-carbocyanine chloride was purchased from Sigma and was used without additional purification.

Manucol-LHF: algin alginate was supplied by Kelco company. This sodium alginate has a molecular mass of 88 000 g/mol and consists thus of approximately 445 monomers. The ratio of mannuronate to guluronate in the sample is 65-70: 30-35.

Mannuronate rich alginate: algin alginate was treated and extracted from Manucol-LB.¹⁶⁷ Manucol-LB has a molecular mass of 60 000 g/mol and consists thus of approximately 300 monomers. The ratio of mannuronate to guluronate in the sample is the same as in Manucol-LHF.

Guluronate rich alginate: was treated and extracted also from Manucol-LB.¹⁶⁷

SG81-Alginate: bacterial alginate was treated by a complex purification process from the bio film of the *Pseudomonas aeruginosa* SG81.¹⁶⁸ The ratio of mannuronate: guluronate in the sample is 67: 33.

γ -Cyclodextrin: The Sample is a gift from Wacker-Chemie GMBH, München and was used as received.

AOT (Aerosol-OT): The sample was purchased from Merck and was used without additional purification.

The following solid compounds, which were used to prepare the buffer solutions, were purchased from Merck:

Tris (hydroxymethyl)-aminomethane ($C_4H_{11}NO_3$)

Disodium hydrogen phosphate dihydrate ($Na_2HPO_4 \cdot 2H_2O$)

Potassium dihydrogen phosphate (KH_2PO_4)

Succinic acid ($C_4H_6O_4$).

Ethanol: for spectroscopy from Merck.

Water: Three times distilled.

6.2 Instruments used

Balance: Analytical balance, Model SARTORIUS 2474, d = 0,01 mg.

UV/Vis-spectrometer: PERKIN-ELMER, Model LAMBDA 5 connected to a personal computer for data collection as ASCII format.

CD- spectrometer: AVIV circular dichroism spectrometer model 62DS connected to a personal computer for data collection as ASCII format.

CD-cryostat system: OXFORD INSTRUMENTS, Variable Temperature liquid Nitrogen cryostat, DN 1714 (static).

Conductometer: WTW/LF 42. The conductivity cell had a cell constant of 0.73 cm^{-1} .

pH-meter: Knick-mV. The electrode was calibrated each time with buffer 4 and 9 before use.

6.3 Glassware, tool and Methods

Stoppered quartz cells were used with different optical path lengths (0.01 – 2.00 cm) as appropriate.

Micropipettes were used with different types of capacities; 100, 50, and 10 μl as appropriate.

Preparation of the test solutions. The solutions needed for studying the formation of complexes between Pinacyanol chloride and the different types of host macromolecules were prepared by using a fixed volume (4.00 ml) using a stoppered rolled rim glasses regarding the size of measuring cell (to maintain the same conditions and precision for all test samples) by using the appropriate Micropipettes. Always the host solutions were added first into a rolled rim glass of 10 cm^3 capacity, followed by adding the required amount of the dye solution. The standard solutions of the dye and the host were prepared by using volumetric flask of 25 ml. Each standard solution when prepared was used only in the same day, *i.e* all of the spectra in one figure were prepared from the same fresh standard solution. Special care was taken to assure thermal equilibrium for each test solution by waiting to get a constant read of the temperature and a reproducible absorbance at the required temperature.

The wavelength range, sensitivity scale, scan rate were selected to give the optimum signal-noise ratios.

7 References

- ¹ H. Zollinger, Color chemistry. Syntheses, Properties and Applications of Organic Dyes and Pigments; 2nd ed., VCH, Weinheim (1991).
- ² T. P. Causgrove, S. Yang, W. S. Struve, *J. Phys. Chem.*, **92**, 6121 (1988).
- ³ J. M. Lanzafame, A. A. Muentzer, D. V. Brumbaugh, *Chem. Phys.* **210**, 79 (1996).
- ⁴ (a) B. Nordén and M. Kubista, Polarized Spectroscopy of Ordered Systems, B. Samori and E. W. Thulstrup, Eds, Kluwer Acad. Publ., Dordrecht, Holland, Vol. **242** (1988). (b) J. L. Seifert, R. E. Conner, S. A. Kushon, M. Wang, and B. A. Armitage, *J. Am. Chem. Soc.* **21**, 2987 (1999).
- ⁵ M. Pal and N. Mandel, *Biopolymers*, **29**, 1541 (1990).
- ⁶ V. Buss in: "Sixth International Symposium on Cyclodextrins", A. Hedges, Ed., Paris, p.160 (1992).
- ⁷ D. J. Owen, D. VanDerveer, and G. B. Schuster, *J. Am. Chem. Soc.* **120**, 1705 (1998).
- ⁸ J. Tanaka, T. Masashi, and M. Hayakawa, *Bull. Chem. Soc. Jpn.* **53**, 3109 (1980).
- ⁹ H. Yoshioka and K. Nakatsu, *Chem. Phys. Lett.* **11**, 255 (1971).
- ¹⁰ L. G. S. Brooker, F. L. White, R. H. Sprague, S. G. J. Dent and G. VanZandt, *Chem. Rev.* **41**, 325 (1947).
- ¹¹ P. M. Henrichs and S. Gross, *J. Am. Chem. Soc.* **98**, 7169 (1976).
- ¹² W. West, S. Pearce, and F. Grum, *J. Phys. Chem.* **71**, 1316 (1967).
- ¹³ W. Grahn, *Tetrahedron*, **32**, 1931 (1976).
- ¹⁴ S. E. Sheppard and A. L. Geddes, *J. Am. Chem. Soc.* **66**, 2003 (1944).
- ¹⁵ V. L. Levschin and E. G. Baranova, *J. Chim. Phys.* **55**, 869 (1958).
- ¹⁶ W. West and S. Pearce, *J. Phys. Chem.* **69**, 1894 (1965).
- ¹⁷ D. L. Akins and J. W. Macklin, *J. Phys. Chem.* **93**, 5999 (1989).
- ¹⁸ T. Tani, J-Aggregates, T. Kobayashi, Ed., World Scientific, Singapore (1996).
- ¹⁹ A. Mishra, R. K. Behera, P. K. Behera, B. K. Mishra, and G. B. Behera, *Chem. Rev.* **100**, 1973 (2000).
- ²⁰ E. G. McRae and M. Kasha, *J. Chem. Phys.* **28**, 721 (1958).
- ²¹ M. Kasha, H. R. Rawis, and M. A. El-Bayoumi, *Pure Appl. Chem.* **11**, 371 (1965).
- ²² G. S. Levinson, W. T. Simpson, and W. Curtius, *J. Am. Chem. Soc.* **79**, 4314 (1957).
- ²³ T. Katoh, Y. Inagaki, and R. Okazaki, *Bull. Chem. Soc. Jpn.* **70**, 2279 (1997).
- ²⁴ W. J. Harrison, D. L. Mateer, and G. J. T. Tiddy, *J. Phys. Chem.* **100**, 2310 (1996).
- ²⁵ O. Valdes - Aguilera and D. C. Neckers, *Acc. Chem. Res.* **22**, 171 (1989)

- ²⁶ E. S. Emerson, M. A. Conlin, A. E. Rosenoff, K. S. Norland, H. Rodriguez, D. Chin, and G. R. Bird, *J. Phys. Chem.* **71**, 2396 (1967).
- ²⁷ A. P. Marchetti, C. D. Salzberg, and E. I. P. Walker, *J. Chem. Phys.* **64**, 4693 (1976).
- ²⁸ H. Hermel, U. DeRossi, *Int. J. Biol. Macromol.* **21**, 263 (1997).
- ²⁹ L. Strekowski, M. Lipowska, and G. Potonay, *J. Org. Chem.* **57**, 4578 (1992).
- ³⁰ P. Kaschny and F. M. Goni, *Eur. J. Biochem.* **207**, 1085 (1992).
- ³¹ S. E. Sheppard and A. L. Geddes, *J. Chem. Phys.* **13**, 63 (1945).
- ³² P. Mukerjee and K. J. Mysels, *J. Am. Chem. Soc.* **59**, 2937 (1955).
- ³³ R. Sabaté, L. Freire, and J. Estelrich, *J. Chem. Educ.* **78**, 343 (2001).
- ³⁴ S. Barazzouk, H. Lee, S. Hotchandani, and P. V. Kamat, *J. Phys. Chem. B*, **104**, 3616 (2000).
- ³⁵ H. Kuhn, *J. Chem. Phys.* **17**, 1198 (1949).
- ³⁶ G. M. Shalhoub, *J. Chem. Educ.* **74**, 1317 (1997).
- ³⁷ R. S. Moog, *J. Chem. Educ.* **68**, 506 (1991).
- ³⁸ J. F. Kennedy and C. A. White, in *Carbohydrate Chemistry*, John F. Kennedy, Ed., Clarendon Press, Oxford, p. 33ff (1988).
- ³⁹ G. O. Aspinall, Ed., *The Polysaccharides*, Vol. I, Academic Press, New York London (1982).
- ⁴⁰ M. Chaplin, Food Research Center, South Bank University in: <http://www.sbu.ac.uk/water/hypol.html>
- ⁴¹ G. P. Moss, Symbols for Specifying the Conformation of Polysaccharide Chains, <http://www.chem.qmul.ac.uk/iupac/misc/psac.html>
- ⁴² A. B. Steiner and W.H McNeely, *Adv. Chem. Ser.* **11**, 68 (1954) in: ref. 39 p.264.
- ⁴³ P. A. J. Gorin and J. F. T. Spencer, *Can. J. Chem.* **44**, 993 (1966).
- ⁴⁴ I. W. Cottrell and P. Kovacs (1980) in ref. 38 p.601
- ⁴⁵ J. G. Lewis, N. F. Stanley and G. G. Guist (1990) in: <http://www.uct.ac.za/depts/botany/pstgrd/enrico/seaweed/alginica.html>
- ⁴⁶ A. Haug, B. Larsen, and O. Smidsrød, *Acta Chem. Scand.* **20**, 183 (1966).
- ⁴⁷ G. O. Aspinall, Ed., *The Polysaccharides*, Vol. II, Academic Press, New York London (1983).
- ⁴⁸ V. J. Chapman, and D. J. Chapman (1980) in: <http://www.uct.ac.za/depts/botany/pstgrd/enrico/seaweed/alginica.html>
- ⁴⁹ D. A. Rees and J. W. B. Samuel, *J. Chem. Soc. C*, 2295 (1967).
- ⁵⁰ I. W. Sutherland, *Pure Appl. Chem.* **69**, 1911 (1997).

- ⁵¹ M. Chaplin, Food Research Center, South Bank University in:
<http://www.sbu.ac.uk/water/hyalg.html>
- ⁵² M. Yalpani, Polysaccharides. Synthesis, Modifications and Structure/ Property Relations, Elsevier, Amsterdam, p. 11 (1988).
- ⁵³ R. Seale, E. R. Morris, and D. A. Rees, Carbohydr. Res. **110**, 101 (1982).
- ⁵⁴ O. Smidsrød and A. Hang, Acta Chem. Scand. **26**, 2063 (1972).
- ⁵⁵ O. Smidsrød and A. Hang, Acta Chem. Scand. **26**, 79 (1972).
- ⁵⁶ I. Braccini and S. Perez, Biomacromolecules, **2**, 1089 (2001).
- ⁵⁷ G. T. Grant, E. R. Morris, D. A. Rees, P.J. Smith, and D. Thom, FEBS Lett. **32**,195 (1973).
- ⁵⁸ J. Wingender, T. Neu, and H.-C. Flemming, Eds., Microbial Extracellular Polymeric Substances, Springer-Verlag Berlin Heidelberg New York (1999).
- ⁵⁹ B. Thu, G. Skjåk-Bræk, F. Micali, F. Vittur, and R. Rizzo, Carbohydr. Res. **297**, 101 (1997).
- ⁶⁰ G. D. Fasman, Circular Dichroism and the Conformational Analysis of Biomolecules, Plenum Press, New York London (1996).
- ⁶¹ A. J. Stipanovic and E. S. Stevens : in Solution Properties of Polysaccharides”, D. A. Brant, Ed., American Chemical Society Symposium Series, No. 150, American Chemical Society, Washington (1981), p.303 in Ref. 52.
- ⁶² E. R. Morris, D. A. Rees, and D. Thom, Carbohydr. Res. **81**, 305 (1980).
- ⁶³ G. Klöck, A. Pfeffermann, C. Ryser, P. Gröhn, B. Kuttler, H.-J. Hahn, and U. Zimmermann, Biomaterial. **18**, 707 (1997).
- ⁶⁴ M. Hatano, Induced Circular Dichroism in Biopolymer – Dye Systems, in Advances in Polymer Science 77, S. O. Kamura, Ed., Springer-Verlag, Berlin Heidelberg NewYork Tokyo (1986).
- ⁶⁵ A. R. Engle, N. Purdie, and J. A. Hyatt, Carbohydr. Res. **265**, 181 (1994).
- ⁶⁶ G. R. Seely and R.L. Hart, Biopolymers **18**, 2745 (1979).
- ⁶⁷ A. Valliers, Compt. Rend. **112**, 536 (1891).
- ⁶⁸ F. Schardinger, Z. Unters. Nahr. u. Genussm. **6**, 865 (1903).
- ⁶⁹ F. Schardinger, Zentralbl. Bakteriol. Parasitenk. Abt. **2**. 29,772 (1911).
- ⁷⁰ K. Freudenberg, G. Blomquist, L. Ewald, and K. Soff, Ber. Dtsch. Chem. Ges. **69**,1258 (1936).
- ⁷¹ K. Freudenberg, F. Cramer, Z. Naturforsch. **3b**, 464 (1948).
- ⁷² D. French, Adv. Carbohydr. Chem. **12**,189 (1957).

- ⁷³ F. Cramer, Chem. Ber. **84**, 851 (1951).
- ⁷⁴ T. Nagai, in "Proceedings of the First International Symposium on Cyclodextrins", J. Szejtli, Ed., Reidel: Dordrecht, p. 15 (1981).
- ⁷⁵ J. Szejtli, Cyclodextrin Technology, Kluwer Academic Publisher: Dordrecht, p. 450 (1988).
- ⁷⁶ J. H. T. Luong and A.L.Nguyen, J. Chromatogr. A, **792**, 431 (1997).
- ⁷⁷ J. Jindrich in: <http://prfdec.natur.cuni.cz/~jindrich/CD/sbcdcon2.gif>
- ⁷⁸ B. Siegel and R. Breslow, J. Am. Chem. Soc. **97**, 6869 (1975).
- ⁷⁹ J. Szejtli, J. incl. Phenom. **1**, 104 (1983).
- ⁸⁰ F. Cramer and H. Hettler, Naturw. **54**, 625 (1967).
- ⁸¹ F. Cramer, W. Saenger, and H. C. H. Spartz, J. Am. Chem. Soc. **89**, 14 (1967).
- ⁸² Y. Matsui and K. Mochida, Bull. Chem. Soc. Jpn. **51**, 673 (1978).
- ⁸³ V. Buss and Ch. Reichardt, J. Chem. Soc., Chem. Commun. 1636 (1992).
- ⁸⁴ K. M. Tawarah and S. J. Khouri, Dyes and pigments, **45**, 229 (2000).
- ⁸⁵ H. Mwakibete, D. M. Bloor, E. J. Wyn-Jones, Inclusion Phenom Mol Recognit Chem. **10**, 497 (1991).
- ⁸⁶ R. P. Rohbach, L. J. Rodriguez, and E. M. Eyring, J. Phys. Chem. **81**, 944 (1977).
- ⁸⁷ R. I. Gelb, L. M. Schwartz, Inclusion Phenom Mol Recognit Chem. **7**, 465, (1989).
- ⁸⁸ A. Buvari, J. Szejtli, L. J. Barcza, J. Inclusion Phenom. **1**, 151 (1983).
- ⁸⁹ R. L. Schiller, J. H. Coates, SFJ. Lincoln, Chem. Soc. Faraday Trans, I. **80**, 1257 (1984).
- ⁹⁰ K. Connors, D. Pendergast, J. Am. Chem. Soc. **106**, 7607 (1984).
- ⁹¹ H. Hirai, N. Toshima, and S. Uenoyama, Bull. Chem. Soc. Jpn. **58**, 1156 (1985).
- ⁹² J. W. Park, H. J. Song, J. Phys. Chem. **93**, 6454 (1989).
- ⁹³ S. J. Hamai, J. Phys. Chem. **93**, 2074 (1989).
- ⁹⁴ R. J. Bergereon, D. M. Pillor, G. Gibeily and W. P. Roberts, Bioorg. Chem. **7**, 263 (1978).
- ⁹⁵ H. Harata, Bull. Chem. Soc. Jpn. **49**, 2066 (1976).
- ⁹⁶ T. Tabushi, Y. Kiyosuke, T. Sugimoto and K. Yamamura, J. Am. Chem. Soc. **100**, 916 (1978).
- ⁹⁷ P. C. Manor and W. Saenger, J. Am. Chem. Soc. **96**, 3690 (1974).
- ⁹⁸ R. I. Gelb, L. M. Schwartz., B. Cardelino, H. S. Fuhrman, R. F. Johnson and D. A. Laufer, J. Am. Chem. Soc. **103**, 1750 (1981).
- ⁹⁹ Ref. 74, p. 141.

- ¹⁰⁰ J. F. Wojcik and R.P. Rohrbach, *J. Phys. Chem.* **79**, 2251 (1975).
- ¹⁰¹ K. M. Tawarah and A. A. Wazwaz, *J. Chem Soc. Faraday Trans.* **89**,1729 (1993).
- ¹⁰² K. Harata and H. Uedaira, *Bull. Chem. Soc. Jpn.* **48**, 375 (1975).
- ¹⁰³ C. H. Tung, Z. Zhen and H. J. Xu, *J. Photochem.* **32**, 311 (1986).
- ¹⁰⁴ P. V. Demarco and A. L. Thakkar, *J. Chem. Soc. , Chem. Commun.* **2**, (1970).
- ¹⁰⁵ R. L. Vanetten, G. A. Glowes, J. S. Sebastian and M. L. Bender, *J. Am. Chem. Soc.* **98**, 7855 (1967).
- ¹⁰⁶ K. Harata, *Bull. Chem. Soc. Jpn.* **50**, 1416 (1977).
- ¹⁰⁷ D. W. Griffiths and M. L. Bender, *Adv. Catal.* **23**, 209 (1973).
- ¹⁰⁸ J. Szejtli *Chem. Rev.* **98**, 1743 (1998).
- ¹⁰⁹ J. E. Davies, W. Kemula, H. M. Powell and N. O. Smith. *J. Incl. Phenom.* **1**, 34 (1983).
- ¹¹⁰ J. Szejtli, *J. Incl. Phenom.* **1**, 104 (1983).
- ¹¹¹ D. W. Armstrong, W. Li and J. Pitha, *Anal. Chem.* **62**, 214 (1990).
- ¹¹² H. Nishi and S. Terabe, *J. Chromatogr. A*, **694**, 245 (1995).
- ¹¹³ S. A. C. Wren and R. C. J. Rowe, *Chromatography*, **603**, 235 (1992).
- ¹¹⁴ S. G. Penn, E. T. Bergström, D. M. Goodall and J. S. Loran, *Anal. Chem.*, **66**, 2866 (1994).
- ¹¹⁵ M. J. Kodaka, *J. Phys. Chem.* **95**, 2110 (1991).
- ¹¹⁶ G. Marconi, S. Monti, B. Mayer and Köhler, *J. Phys. Chem.* **99**, 3943 (1995).
- ¹¹⁷ R. P. Rohrbach and J. F. Wojcik, *Carbohydr. Res.* **92**, 177 (1981).
- ¹¹⁸ N. Yoshida, Seiyama and M. Fujimoto, *J. Incl. Phenom.* **2**, 573 (1984).
- ¹¹⁹ R. J. Clarke, J. H. Coates and S. F. Lincoln, *J. Chem. Soc. Faraday Trans. I.* **80**, 3119 (1984).
- ¹²⁰ P. C. Hiemenz, *Principles of Colloid and Surface Chemistry*, 2nd Ed., Marcel Dekker, Inc., New York Basel (1986).
- ¹²¹ M. J. Rosen, *Surfactants and Interfacial Phenomena*, 2nd Ed., John Wiley & sons, New York (1989).
- ¹²² J. L. Lynn and B. H. Bory in: *Concise Encyclopaedia of Chemical Technology*, R. Kirk, Ed., Wiley, New York, p. 1949 (1999).
- ¹²³ E. Pramauro and E. Pelizzetti, *Surfactants in Analytical Chemistry: Applications of Organized Amphiphilic Media*, Elsevier, Amsterdam (1996).
- ¹²⁴ L. L. Schramm, *Surfactants: Fundamentals and Applications in Petroleum Industry*, Cambridge University Press, Cambridge (2000).
- ¹²⁵ C. A. Bunton, L. Robinson, J. Schaak, and M. F. Stam, *J. Org. Chem.* **36**, 2346 (1971).

- ¹²⁶ F. M. Menger and C. A. Littau, *J. Am. Chem. Soc.* **113**, 1451 (1991).
- ¹²⁷ F. M. Menger and J. S. Keiper, *Angew. Chem.* **112**, 1980 (2000).
- ¹²⁸ G. H. Escamilla and G. R. Newkome, *Angew. Chem.* **106**, 2013 (1994).
- ¹²⁹ T. Kunitake, *Angew. Chem.* **104**, 692 (1992).
- ¹³⁰ (a) J. N. Israelachvili, D. J. Mitchel, and B. W. Ninham, *J. Chem. Soc., Faraday Trans. II.* **72**, 1525 (1976). (b) <http://www.ub.rug.nl/eldoc/dis/science/r.t.buwalda/>
- ¹³¹ W. C. Preston, *J. Phys. Colloid Chem.* **52**, 84 (1948).
- ¹³² P. C. T. V. S. Lobanov, A. R. Katritzky, D. O. Shah, and M. Karelson, *Langmuir*, **12**, 1462 (1996).
- ¹³³ S. E. Sheppard and A. L. Geddes, *J. Chem. Phys.* **13**, 63 (1945).
- ¹³⁴ P. Mukerjee and K. J. Mysels, *J. Am. Chem. Soc.* **59**, 2937 (1955).
- ¹³⁵ J. K. Weil and A.J. Stirton, *J. Phys. Chem.* **60**, 899 (1956).
- ¹³⁶ E. L. Colichman, *J. Am. Chem. Soc.* **73**, 3385 (1951).
- ¹³⁷ N. J. Turro, P. – L. Kuo, P. Somasundaran, and K. Wong, *J. Phys. Chem.* **90**, 288 (1986).
- ¹³⁸ C. F. Hiskey and T. A. Downey, *J. Phys. Chem.* **58**, 835 (1954).
- ¹³⁹ R. T. Buwalda, J. M. Jonker and J. B. F. N. Engberts, *Langmuir* **15**, 1083 (1999).
- ¹⁴⁰ G. J. Wang and J. B. F. N. Engbert, *Langmuir* **10**, 2583 (1994).
- ¹⁴¹ R. K. Dutta and S. N. Bhat, *Bull. Chem. Soc. Jpn.* **66**, 2457 (1993).
- ¹⁴² F. Quadrifoglio and V. Crezenzi, *J. Colloid Interf. Sci.* **35**, 447 (1971).
- ¹⁴³ M. K. Pal and P. K. Pal, *J. Phys. Chem.* **94**, 2557 (1990).
- ¹⁴⁴ P. Mukherjee and K.J. Mysels, *J. Am. Chem. Soc.* **77**, 2937, (1955).
- ¹⁴⁵ M. Fischer and J. Georges, *Spectrochim. Acta. A* **53**, 1419 (1997).
- ¹⁴⁶ P. Bilski, R. N. Hott, and C. F. Chignell, *J. Photochem. Photobiol. Chem. A* **110**, 67 (1997).
- ¹⁴⁷ P. Pal, H. Zeng, G. Durocher, D. Girard, R. Giasson, L. Blanchard, L. Gaboury, and L. Villeneuve, *J. Photochem. Photobiol. Chem. A* **98**, 65 (1996).
- ¹⁴⁸ K. Vickery and B. Nordén, *Encyclopaedia of Spectroscopy and Spectrometry*, J. C. Lindon, G. E. Tranter, and J. L. Holmes, Eds., Academic Press: London, p. 869 (2000).
- ¹⁴⁹ P. Pančoška, L. Bednarova, and V. Kapsa, *Chem. Phys. Lett.* **191**, 603 (1992).
- ¹⁵⁰ M. Hatano, Induced Circular Dichroism in Biopolymer – Dye systems, in *Advances in Polymer Science* **77**, S. O. Kamura, Ed., Springer Verlag: Berlin Heidelberg New York Tokyo 1986.

- ¹⁵¹ N. Berova, N. Harada, and K. Nakanishi, *Encyclopaedia of Spectroscopy and Spectrometry*, J. C. Lindon, G. E. Tranter, and J. L. Holmes, Eds., Academic Press: London, p. 470 (2000).
- ¹⁵² D. A. Lightner and J. E. Gurst, *Organic Conformational Analysis and Stereochemistry From Circular Dichroism Spectroscopy*, Wiley: New York (2000).
- ¹⁵³ N. Harada and K. Nakanishi, *Circular Dichroic Spectroscopy: Exciton Coupling in Organic Stereochemistry*, University Science Books: Mill Valley, CA (1983).
- ¹⁵⁴ N. Berova and K. Nakanishi in *Circular Dichroism - Principles and Applications*, N. Berova, K. Nakanishi, and R. Woody, Eds., Wiley-VCH: New York, p. 337 (2000).
- ¹⁵⁵ V. Czikkely, H. D. Försterling, and H. Kuhn, *Chem. Phys. Lett.* **6**, 11 (1970).
- ¹⁵⁶ H. J. Nolte and V. Buss, *Chem. Phys. Lett.* **19**, 395 (1973).
- ¹⁵⁷ D. A. Skoog, *Principles of Instrumental Analysis*, 3rd. ed. Philadelphia [u.a.] : Saunders College Publ. (1985).
- ¹⁵⁸ M. Thomas, *Ultraviolet and visible Spectroscopy*, 2nd Ed., John Wiley & Sons: Chichester (1996).
- ¹⁵⁹ Information inside the program: PeakFit Program version 4.05, Systat software Inc.
- ¹⁶⁰ 4-unknown calculator program: <http://www.1728.com/unknwn4.htm>
- ¹⁶¹ 3-unknown calculator program: <http://www.1728.com/unknwn3.htm>
- ¹⁶² H. Min, J. Park, J. Ju, and D. Kim, *Bull. Korean Chem. Soc.*, **19**, 650 (1998).
- ¹⁶³ C. Roos and V. Buss, *J. Incl. Phenom.* **27**, 49 (1997).
- ¹⁶⁴ K. A. Connors, *Binding Constants: The Measurements of Molecular Complex Stability*, John Wiley, New York (1987).
- ¹⁶⁵ D. D. Perrin and D. Boyd, *Buffers for pH and metal ion control*, Chapman and Hall, London, P 44-47 (1979).
- ¹⁶⁶ E. F. Williams, N. T. Woodbery, and J. K. Dixon, *J. Colloid Interface Sci.* **12**, 459 (1957) in ref.143.
- ¹⁶⁷ A. Haug, B. Larsen, and O. Smidsrød, *Carbohydr. Res.* **32**, 217 (1974), modified by N. Schürks, Duisburg University.
- ¹⁶⁸ Purification (modified by S. Grobe) in: *Bedeutung des extrazellulären Polysaccharids Alginat für die Resistenz aquatischer Stämme von *Pseudomonas aeruginosa* gegenüber Chlor*. Dissertation, Universität Bonn (1995).

CURRICULUM VITAE

Name Sa'ib Al-khouri
Date of Birth 01.04.1963
Place of Birth Bishra (Irbid-Jordan)
Personal Status Married (three children)

School Education

1969-1979 Bishra elementary & secondary school (Jordan)
1979-1981 Irbid secondary school (Jordan)

University Education

1981-1985 B.Sc. study in chemistry at Yarmouk University (Irbid-Jordan)
1988-1990 M.Sc. study in physical chemistry at Yarmouk University.
During my study I worked on the inclusion process between Azo-dyes and Cyclodextrins solutions.
Sep 1999 Commencement of my Ph.D. studies in the department of theoretical chemistry at the Gerhard-Mercator-University Duisburg, Germany, under the supervision of Prof. Dr. V. Buss.

Employment and Training

1985-1987 Military service (Army and ministry of education as teacher in a secondary school)
1991- 1999 Research and teaching assistant in the department of chemistry at Yarmouk University (Jordan). During my work I taught many Laboratories courses, mainly physical chemistry laboratory.
Mar1999-Aug1999 Intensive course of German language / Bonn, Germany.